AD-A073 654 SYRACUSE UNIV NY DEPT OF MECHANICAL AND AEROSPACE E--ETC F/G 20/13
THERMAL STRESS ANALYSIS OF GLASS SEALS IN MICROELECTRONIC PACKA--ETC(U)
JUL 79 K KOKINI, R W PERKINS, C LIBOVE F30602-78-C-0083

UNCLASSIFIED MAE-1233-T2 RADC-TR-79-201 NL

1 OF 2

AD A073654

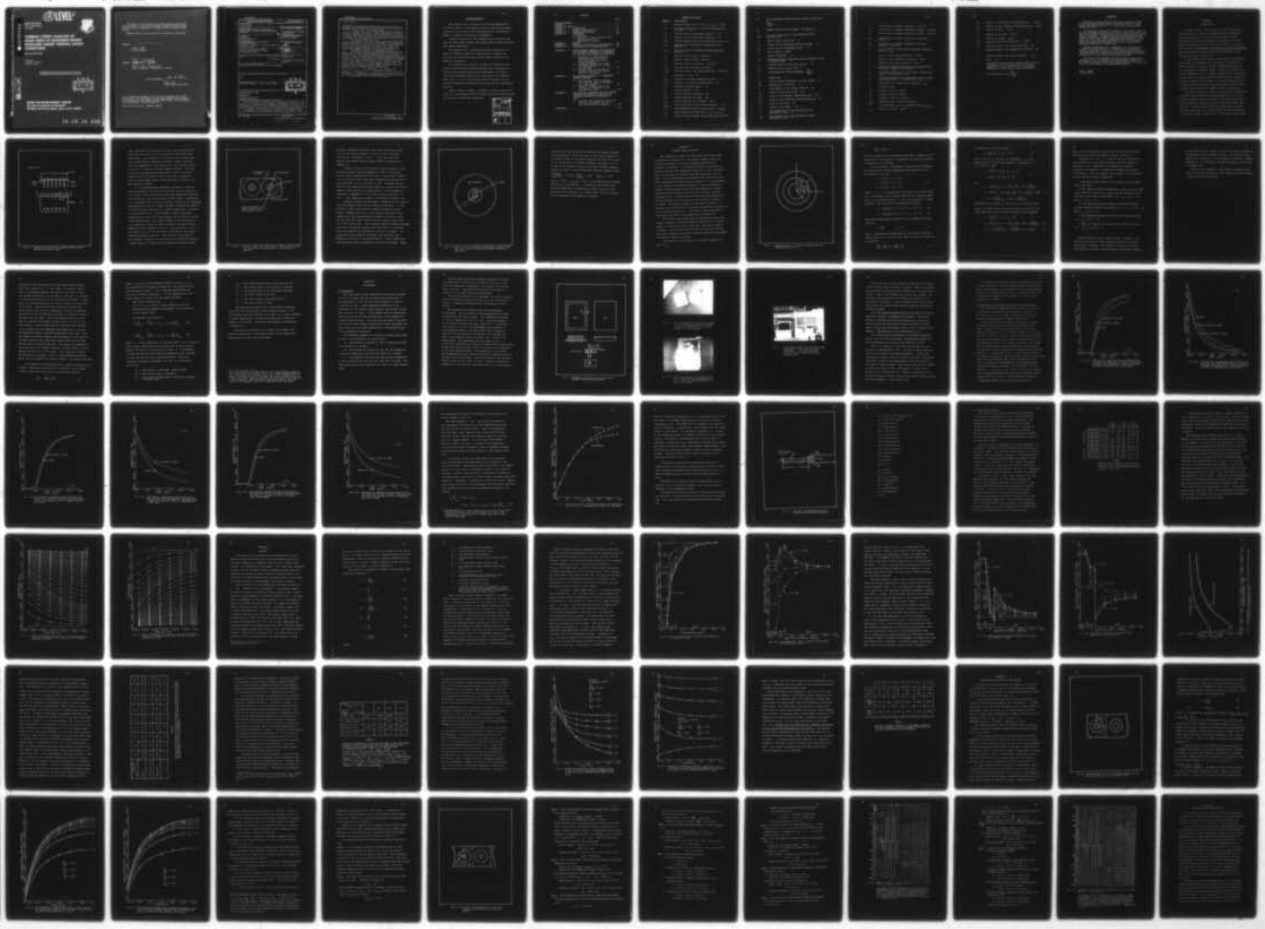

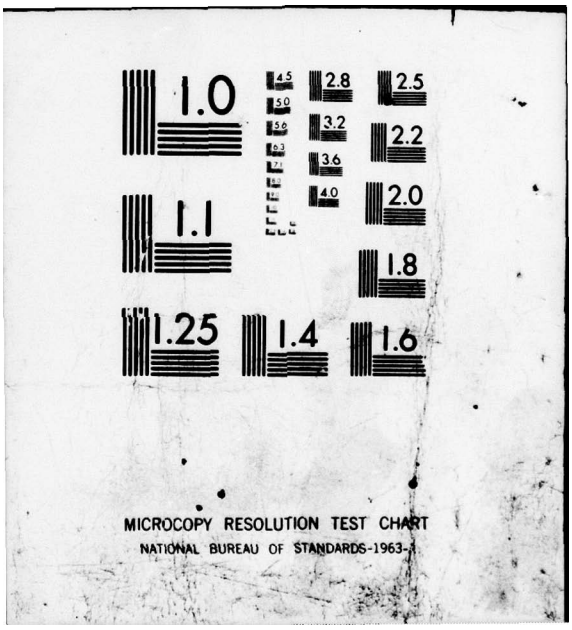
1.0
1.1
1.25
1.4
1.6
1.8
2.0
2.2
2.5
2.8
3.2
3.6
4.0
4.5
5.0
5.6
MICROCOPY RESOLUTION TEST CHART
NATIONAL BUREAU OF STANDARDS-1963-A

(12) LEVEL II

RADC-TR-79-201
Final Technical Report
July 1979

THERMAL STRESS ANALYSIS OF GLASS SEALS IN MICROELECTRONIC PACKAGES UNDER THERMAL SHOCK CONDITIONS

Syracuse University

Klod Kokini
Richard W. Perkins
Charles Libove

ROME AIR DEVELOPMENT CENTER
Air Force Systems Command
Griffiss Air Force Base, New York 13441

THERMAL STRESS ANALYSIS OF GLASS SEALS IN MICROELECTRONIC PACKAGES UNDER THERMAL SHOCK CON

This report has been reviewed by the RADC Information Office (OI) and is releasable to the National Technical Information Service (NTIS). At NTIS it will be releasable to the general public, including foreign nations.

RADC-TR-79-201 has been reviewed and is approved for publication.

APPROVED: Peter F. Manno

PETER F. MANNO
Project Engineer

APPROVED: David C. Luke

DAVID C. LUKE, Lt Colonel, USAF
Chief, Reliability & Compatibility Division

FOR THE COMMANDER: John P. Huss

JOHN P. HUSS
Acting Chief, Plans Office

If your address has changed or if you wish to be removed from the RADC mailing list, or if the addressee is no longer employed by your organization, please notify RADC (RBRM), Griffiss AFB NY 13441. This will assist us in maintaining a current mailing list.

Do not return this copy. Retain or destroy.

UNCLASSIFIED

SECURITY CLASSIFICATION OF THIS PAGE (When Data Entered)

REPORT DOCUMENTATION PAGE

READ INSTRUCTIONS BEFORE COMPLETING FORM

1. REPORT NUMBER: RADC-TR-79-201
2. GOVT ACCESSION NO.:
3. RECIPIENT'S CATALOG NUMBER:
4. TITLE (and Subtitle): THERMAL STRESS ANALYSIS OF GLASS SEALS IN MICROELECTRONIC PACKAGES UNDER THERMAL SHOCK CONDITIONS
5. TYPE OF REPORT & PERIOD COVERED: Final Technical Report
6. PERFORMING ORG. REPORT NUMBER: MAE-1233-T2
7. AUTHOR(s): Klod Kokini, Richard W. Perkins, Charles Libove
8. CONTRACT OR GRANT NUMBER(s): F30602-78-C-0083
9. PERFORMING ORGANIZATION NAME AND ADDRESS: Syracuse University, Department of Mechanical & Aerospace Engineering, Syracuse NY 13210
10. PROGRAM ELEMENT, PROJECT, TASK AREA & WORK UNIT NUMBERS: 611028, 23064P2, J4
11. CONTROLLING OFFICE NAME AND ADDRESS: Rome Air Development Center (RBRM), Griffiss AFB NY 13441
12. REPORT DATE: Jul 1979
13. NUMBER OF PAGES: 117
14. MONITORING AGENCY NAME & ADDRESS (if different from Controlling Office): Same — 116 p.
15. SECURITY CLASS. (of this report): UNCLASSIFIED
15a. DECLASSIFICATION/DOWNGRADING SCHEDULE: N/A

16. DISTRIBUTION STATEMENT (of this Report)
Approved for public release, distribution unlimited.

17. DISTRIBUTION STATEMENT (of the abstract entered in Block 20, if different from Report)
Same

18. SUPPLEMENTARY NOTES
RADC Project Engineer: Peter F. Manno (RBRM)

19. KEY WORDS (Continue on reverse side if necessary and identify by block number)
Microelectronic package
thermal shock
glass seal
transient thermal stress
lead-glass interface

20. ABSTRACT (Continue on reverse side if necessary and identify by block number)
In order to ensure the reliability of microelectronic packages which are used in the Armed Services, these packages are subjected to various tests which simulate the environments which the packages may experience in service. The test methods which are in use are described in MIL-STD-883B. The present study concerns a detailed investigation of the Thermal Shock Test (Method 1011.2).

A mathematical model is developed for predicting the transient thermal stresses that occur in a typical annular lead-through glass seal of a (Cont'd)

DD FORM 1 JAN 73 1473

UNCLASSIFIED

SECURITY CLASSIFICATION OF THIS PAGE (When Data Entered)

400 224

Item 20 (Cont'd)

microelectronic package during a thermal shock test. In this model, an approximate model is adopted where the lead, the glass seal and a part of the base are represented by 3 concentric cylinders.

In order to carry out the thermal stress analysis a temperature analysis is performed to determine the unfiorm temperature of the lead, the uniform temperature of the base and the radial temperature distribution in the seal. This temperature model takes into account the entire amount of the base material and lead material in the package and therefore is somewhat different than the thermal stress model.

The temperature model can be used to determine the approximate temperature distribution in the three cylinder model if the effective heat transfer coefficient that determines the rate of heat transfer between the lead and the fluid and between the base and the fluid is known. The effective heat transfer coefficient is evaluated using experimentally obtained time-temperature histories for the lead and the base.

The analysis is applied to a commercially used microelectronic package. The transient thermal stresses developed in the seal during the thermal shock test level A of MIL-STD-883B are computed and presented in the form of graphs. The analysis is then applied to packages with different geometries. The results thus obtained are non-dimensionalized and presented in the form of graphs. These graphs can be used to determine the thermal stresses in any package for which the ratio of the material properties (Young's modulus, coefficient of thermal expansion, Poisson's ratio, heat transfer property ratios) of the sealing material to those of the metal are equal to the corresponding material property ratios ($\bar{h}L(A_b/N)/k_{se}(L-L_o)^2 = 96.459$, $\rho_m c_m/\rho_{se} c_{se} = 1.681$, $E_m/E_{se} = 2.439$, $\alpha_m/\alpha_{se} = 1.269$, $\nu_m/\nu_{se} = 1.364$) of the experimental package used in this investigation. The present study is of general use to designers and screeners of microelectronic packages since the same combination of materials as the ones of the experimental package is used in most packages.

ACKNOWLEDGEMENTS

The present report is based on the thesis submitted by the first author to the Graduate School of Syracuse University in partial fulfillment of the requirements for the degree of Master of Science in Mechanical Engineering.

Financial support for this research was provided by the Rome Air Development Center under Grant Number F30602-78-C-0083, Task Number PRN-8-5165.

The authors wish to express particular appreciation to Robert W. Thomas of RADC for identifying the problem that initiated the study and also to Peter Manno of RADC for his helpful discussions.

The authors would also like to thank the Isotronics and *Tekform microelectronic* package manufacturing companies for donating the packages used during experiments, the Bendix Electrical Components Division for contributing the pressure bomb, and J. C. Gioia from General Electric Company for his valuable suggestions concerning the sealing of the experimental packages.

Special thanks to Robert P. McEvoy for helping during the writing of the manuscript and to Cynthia Porter and Kathy Curtice for carefully typing this manuscript.

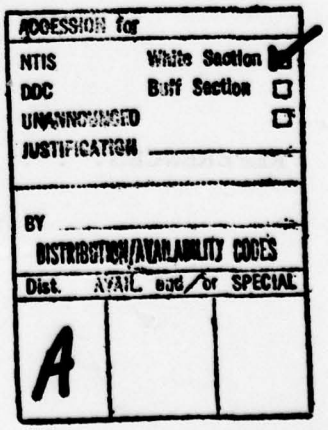

CONTENTS

SYMBOLS AND UNITS

SYMBOL	DESCRIPTION
a	Thermal diffusivity of glass $(k_g/\rho_g c_g)$ in^2/sec
A_o	Outside surface area of the lead emerging from the base in^2
A_1	Surface area of glass-base interface in^2
A_2	Surface area of lead-glass interface in^2
A_b	Outside surface area of the base and the lid in^2
c_{ch}	Specific heat of chromel thermocouple wire Btu/lb-°F
c_{co}	Specific heat of constantan thermocouple wire Btu/lb-°F
c_g	Specific heat of glass Btu/lb-°F
c_k	Specific heat of Kovar Btu/lb-°F
c_m	Specific heat of any metal Btu/lb-°F
c_s	Specific heat of solder Btu/lb-°F
c_{se}	Specific heat of any sealing material Btu/lb°F
d	Diameter of lead in
d_{ch}	Diameter of chromel thermocouple wire in
d_{co}	Diameter of constantan thermocouple in
d_s	Diameter of solder sphere in
E	Young's modulus psi
E_g	Young's modulus for glass psi
E_k	Young's modulus for Kovar psi
E_m	Young's modulus for any metal psi
E_{se}	Young's modulus for any sealing material psi
E^*	Non-dimensional Young's modulus ratio (E_k/E_g)
E_r	Least square error defined by $\sum_{i=1}^{n} (y_i - y_{ei})^2$
$\bar{h}$	Effective heat transfer coefficient Btu/hr-ft^2-°F

$\bar{h}^*$	Non-dimensional effective heat transfer coefficient, $\frac{\bar{h}A_o}{c_k \rho_k V_\ell} \tau_r$
k_g	Thermal conductivity of glass Btu/sec-in-°F
k_{se}	Thermal conductivity of any sealing material Btu/sec-in-°F
L	Total length of the lead in
L_o	Length of the lead emerging from the base in
L_w	Length of the thermocouple wires in
N	Total number of leads
r	Radial coordinate in
r_o	Outside radius of the third outside cylinder in the 3-cylinder model in
r_1	Outside radius of the glass annulus in
r_2	Radius of the circular lead in
r*	Non-dimensional radial parameter, $\frac{\bar{h}A_o}{k_g A_2} r$
T	Temperature °F
T_o	Initial uniform temperature of the package °F
T_∞	Temperature of the fluid °F
u	Displacement in the radial direction in
V_b	Volume of the base and lid in^3
V_{ch}	Volume of the chromel thermocouple wire in^3
V_{co}	Volume of the constantan thermocouple wire in^3
V_ℓ	Volume of the lead in^3
V_s	Volume of the solder in^3
y_i	Any temperature on the theoretical time-temperature curve °F
y_{ei}	Any temperature on the experimental time-temperature curve °F

α	Coefficient of thermal expansion in/in-°F
α_g	Coefficient of thermal expansion of glass in/in-°F
α_k	Coefficient of thermal expansion of Kovar in/in-°F
α_m	Coefficient of thermal expansion of any metal in/in-°F
α_{se}	Coefficient of thermal expansion of sealing material in/in-°F
α^*	Non-dimensional coefficient of thermal expansion ratio, α_m/α_{se}
ε_r	Strain in the radial direction in/in
ε_ϕ	Strain in the tangential direction in/in
ε_z	Strain in the axial direction in/in
θ	Difference between final and initial temperature during any temperature excursion °F
θ_o	Difference between final and initial temperature during a thermal shock test °F
θ_r	Difference between room temperature and the lower bath temperature of a thermal shock test °F
θ^*	Non-dimensional temperature difference, $\frac{\theta}{\theta_o}$
ν	Poisson's ratio
ν_g	Poisson's ratio of glass
ν_k	Poisson's ratio of Kovar
ν_m	Poisson's ratio of any metal
ν_{se}	Poisson's ratio of sealing material
ν^*	Non-dimensional ratio of Poisson's ratios, ν_m/ν_{se}
ρ_g	Density of glass lb/in^3

ρ_{ch}	Density of the chromel thermocouple wire	lb/in^3
ρ_{co}	Density of the constantan thermocouple wire	lb/in^3
ρ_k	Density of Kovar	lb/in^3
ρ_m	Density of any metal	lb/in^3
ρ_s	Density of solder	lb/in^3
ρ_{se}	Density of any sealing material	lb/in^3
σ_r	Thermal stress in the radial direction	psi
σ_ϕ	Thermal stress in the tangential direction	psi
σ_z	Thermal stress in the axial direction	psi
τ	Time	sec
τ_r	Reference time arbitrarily chosen to be the time necessary to bring to 90% of its equilibrium temperature 1 lb of Kovar when it is heated from 32°F to 212°F with $\bar{h}$ = 210 Btu/ft^2-hr-°F	
τ^*	Non-dimensional time, $\frac{\bar{h}A_o}{c_k \rho_k V_\ell} \tau$	

EVALUATION

The objective of this effort was to develop a mathematical model for predicting the transient thermal stresses that occur in a typical annular lead-through glass seal of a microelectronic package during a thermal shock test.

The study results show that the magnitude of the thermal stresses in the seal area depends upon the initial residual stresses that result from cooling the package to room conditions after the high temperature sealing process is completed. A computer program was developed to analyze the thermal stresses in any circular lead package while undergoing a thermal shock test. A method has been developed for predicting the stresses which are present in the lead-through seal area of a microelectronic package when subjected to a thermal shock.

Subsequent experiments will be conducted to verify the predicted strengths of the seal and how it is influenced by the manufacturing process, and establish the validity of the assumptions used in this work. These experiments will extend the present work to include microelectronic packages with flat leads and test fluids other than water.

The results of this program will be used by RADC to develop design guidelines, for use in conjunction with the screening procedures of MIL-STD-883, applicable to hybrid and integrated microcircuit packages and electrical feed throughs for microwave device packages.

PETER F. MANNO
Project Engineer

CHAPTER I

INTRODUCTION

In order to ensure the reliability of microelectronic packages which are used by the Armed Services, these packages are subjected to various tests which simulate the environments which the packages may experience in service. The test methods which are in use are described in Military Standard 883B, Test Methods and Procedures for Microelectronics. The present study concerns a detailed investigaton of the Thermal Shock Test (Method 1011.2).

As described in MIL-STD-883B, the purpose of the thermal shock test is to determine the resistance of the device to sudden exposure to extreme changes in temperature which may be encountered in equipment which is operated intermittently in low temperature areas. Physical damage may be experienced by the seals of a package during thermal shock as a result of thermal stresses which accompany the extreme temperature distribution which must exist during the transient heat transfer process associated with the sudden change in temperature.

The thermal shock test apparatus consists of temperature-controlled baths containing fluids appropriate for the temperature extremes which are desired. The least severe test level consists of baths of ice water and boiling water (Test Level A). The most severe test level uses baths of liquid nitrogen and silicon oil FC 70 or UCON 100 with temperatures of -195°C and 200°C (Test Level F). The thermal shock test

procedure involves bringing the device to equilibrium temperature in the low temperature liquid, then rapidly transferring it to the high temperature liquid and allowing it to come to equilibrium, and then continuing this back and forth transferring between the two baths for a prescribed number of cycles, usually 15.

Thomas [1] conducted an experimental study of packages subjected to thermal shock and found that leakage appeared to be directly correlated with the thermal shock. He suggested that thermal stresses in the vicinity of the lead-through seals may be large enough to permit leakage during the thermal shock which might go undetected during subsequent gross leak testing of the package. Other literature [2] indicates that stresses during thermal shock testing can lead to fracture of the glass seal.

In view of these findings, it appears desirable to have a procedure for predicting or estimating the magnitude of the thermal stresses which may be present in the lead-through glass seal of microelectronics packages which are subjected to thermal shock testing. The predicted stress conditions can be used by the individual performing the thermal shock test to select the test level which is consistent with the level of stress which is desired in the test package. An analysis of thermal stress for conditions of thermal shock could also be used by the package designer to ensure that the fabricated package will perform satisfactorily during the anticipated environmental thermal shock conditions that it would be subjected to.

The objective of the present study is to develop a mathematical model for predicting the transient thermal stresses that occur in a typical annular lead-through glass seal of a microelectronics package during a thermal shock test. Since microelectronics packages typically have many lead-through seals and since the package geometry varies considerably from one case to the next it is necessary to develop a simplified model for purposes of analysis. The approximate model which is adopted in the present work is very similar to the one used by Borom and Giddings [5] which focuses attention on the stresses in the vicinity of a typical lead-through seal. The considerations underlying the formulation of the model are as follows.

Consider a typical package such as the one shown in Fig. 1. In this case the leads all pass through the base of the package. When a package such as this is subjected to a thermal shock by immersing it in a hot or cold liquid bath, the lead changes temperature most rapidly due to its small mass and high thermal conductivity. The base responds somewhat less rapidly because of its larger mass. Both the lead and the base are generally made of Kovar and therefore have a high thermal diffusivity. Because of this and because of the nature of the heat transfer process from the liquid to the lead and the base, it is quite reasonable to assume that the temperature of the lead and the temperature of the base are uniform throughout.[1] On the other

[1] For justification we can consider an infinitely large Kovar plate of 0.04 in. thickness, initially at 32°F and exposed to a 212°F fluid on one side while the other side is insulated. Using the non-dimensional temperature vs. non-dimensional time charts provided by Schneider [7], one finds the temperature-time histories of the two surfaces of this plate to be essentially identical.

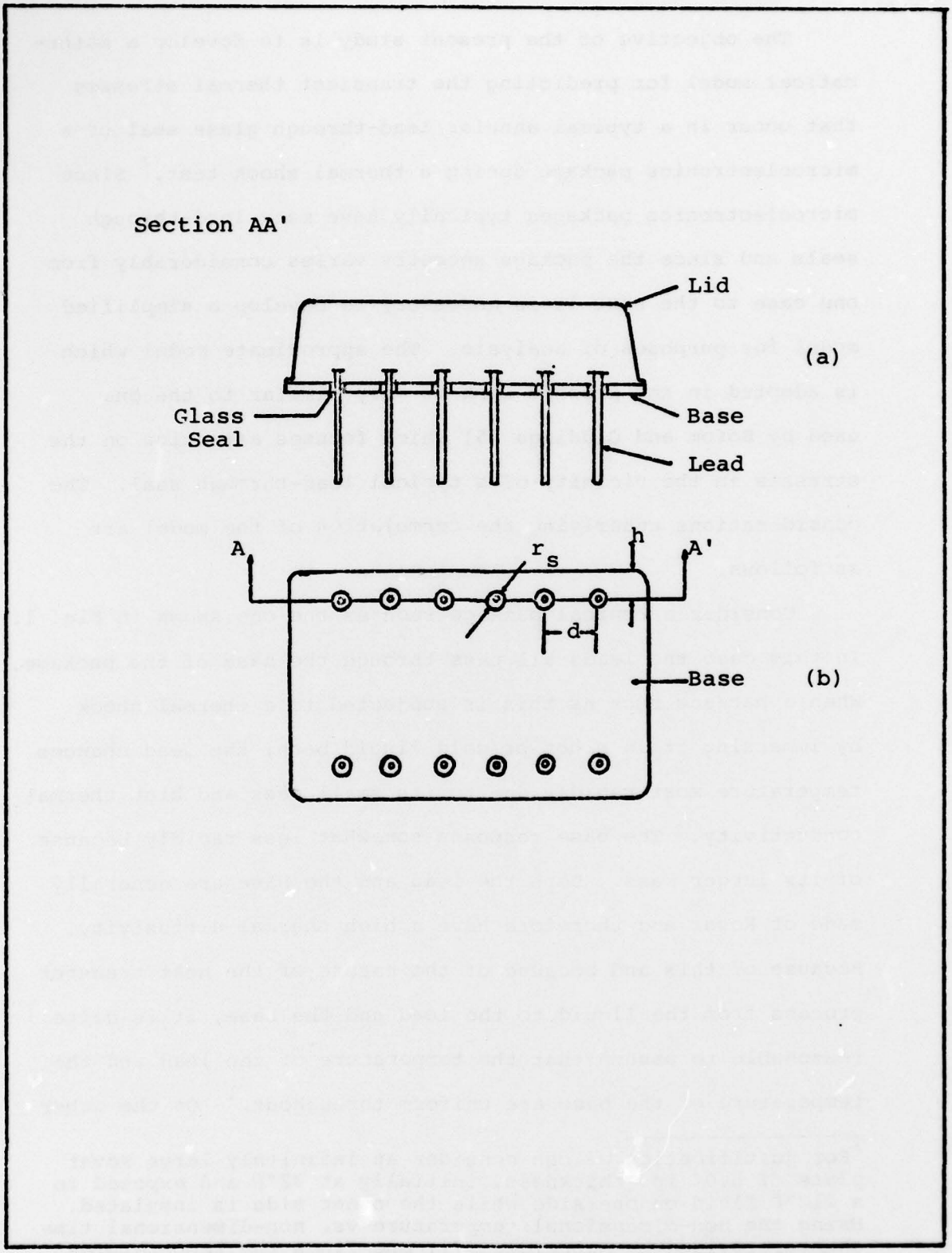

Fig. 1. Typical microelectronic package showing lead-throughs and glass seals.

hand, the annular glass seal has a much lower thermal diffusivity and has very little area exposed to the liquid bath environment. The temperature distribution in the glass seal can be approximately modelled as having a radial variation from the temperature of the lead on the inner annular surface to that of the base on the outer annular surface. The axial variation in temperature is neglected in view of the small surface area in contact with the fluid bath in comparison with the much larger areas of the glass seal in contact with the lead and the base.

It is anticipated that substantial mechanical stresses can be developed in the lead, and the base and the glass seal as a result of the time varying nonuniform temperature distribution existing in the package during thermal shock. Furthermore, it is suspected that the state of thermal stress can be reasonably approximated by using the simplified model of Borom and Giddings [5] which focuses attention on a typical glass seal. The model is illustrated by Fig. 2 which shows a typical glass seal consisting of a lead, the glass annulus, and an annular portion of the package base. The outside radius of the base annulus r_o is selected so that the radial stress on the outer annular surface could be assumed to be zero. As illustrated in Fig. 2, the radial stress at the free edge of the base of the package would be expected to be zero. The location of the edge of the package in relation to the lead and seal therefore defines a model radius r_o at which one can assume zero radial stress.

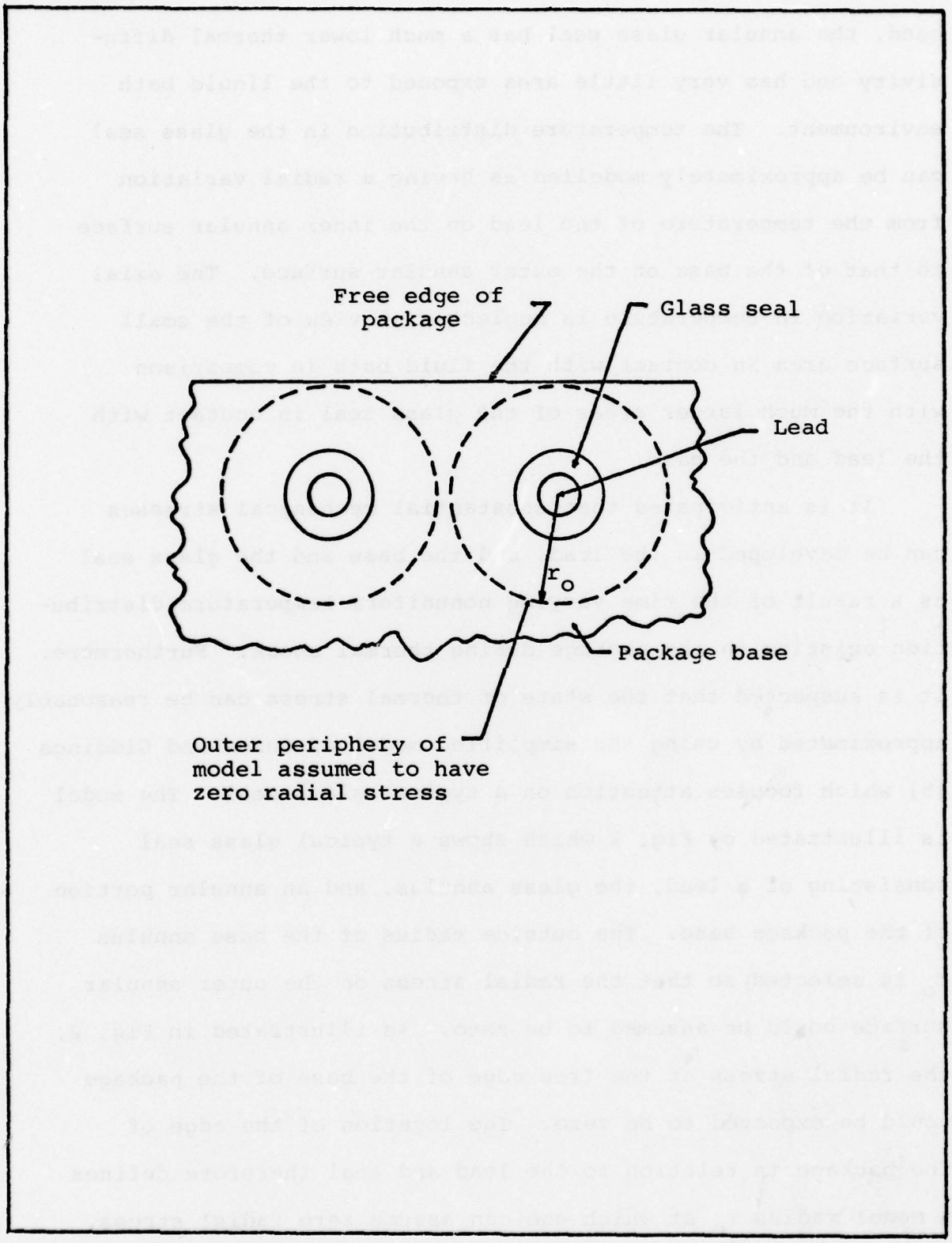

Fig. 2. Typical glass seal consisting of lead, annular glass seal and part of package base in the form of an annulus.

The model therefore consists of the lead, the annular glass seal and the annular segment of base material surrounding the seal as illustrated in Fig. 3. This model forms the basis of the thermal stress analysis which is presented in Chapter II.

In order to carry out the thermal stress analysis, a temperature analysis must be performed in order to determine: a) the uniform temperature of the lead, b) the uniform temperature of the base, and c) the radial temperature distribution of the glass seal, all as functions of time. The model which is used for the temperature analysis takes into account the entire amount of base material and lead material in the package and therefore is somewhat different than the model depicted in Fig. 3. The temperature analysis is presented in Chapter III.

A computer program was developed, incorporating the temperature distribution model and the thermal stress model. It can be used to obtain the transient thermal stresses occurring during a thermal shock test. This analysis was applied to a commercially used microelectronic package in which the leads and the base were made of Kovar and were sealed to each other with 7052 Corning glass. The transient thermal stresses developed in the seal during the thermal shock test level A of MIL-STD-883B were computed and presented in the form of graphs. The analysis was then applied to packages with different seal geometries but made of the same materials. These results were non-dimensionalized and presented in the form of graphs. These

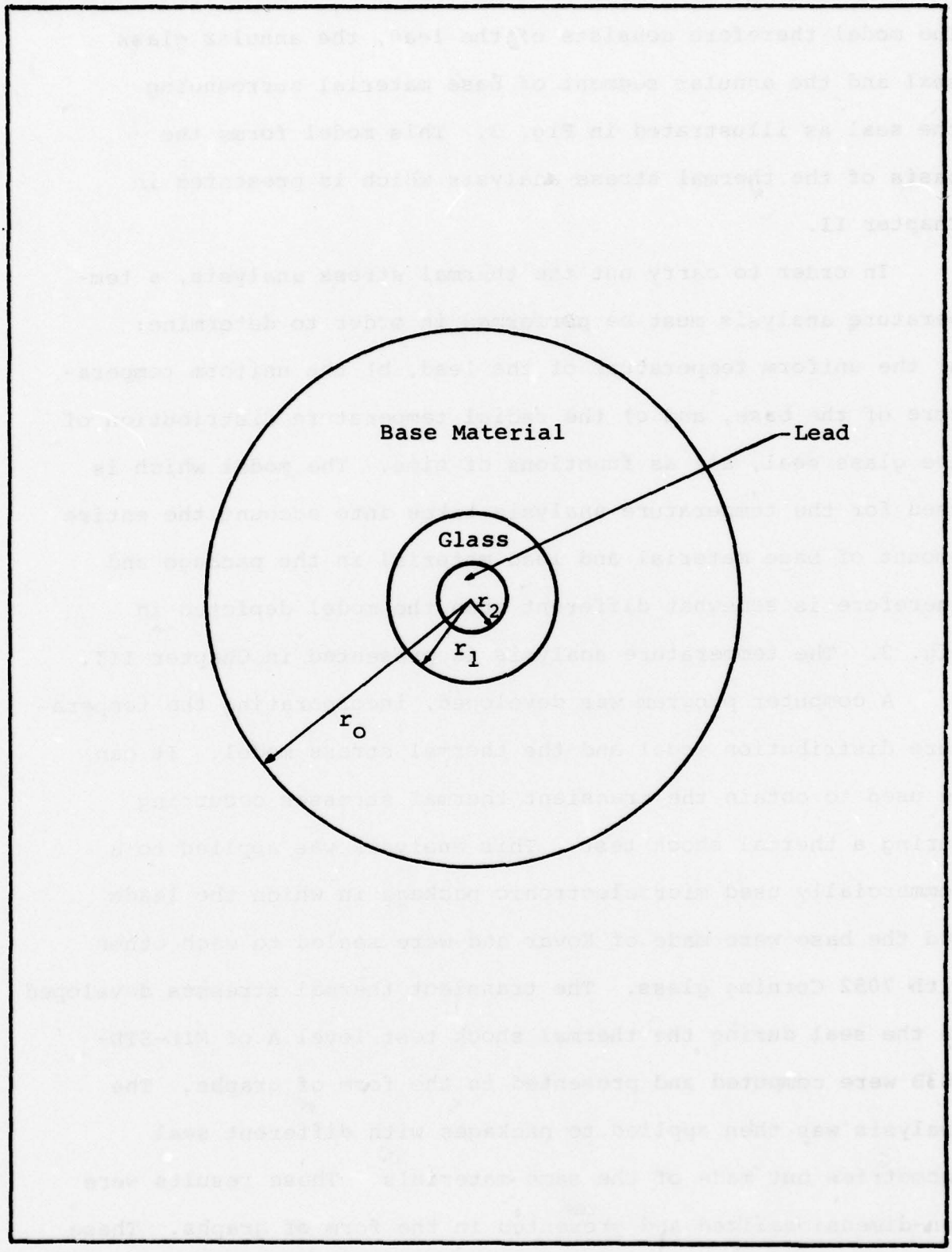

Fig. 3. Model of the lead-through consisting of lead, glass seal and a part of the base as three concentric cylinders.

graphs can be used directly to determine the thermal stresses in any package for which the ratio of the Young's modulus of the metal to that of the sealing material as well as the ratio of the coefficients of thermal expansion, the ratio of the values of the Poisson's ratio and the heat transfer property ratios are equal to the corresponding material property ratios $\left(\frac{\bar{h}L(A_b/N)}{k_{se}(L-L_o)^2} = 96.459,\ \frac{\rho_m c_m}{\rho_{se} c_{se}} = 1.681,\ E_m/E_{se} = 2.439,\right.$ $\left.\alpha_m/\alpha_{se} = 1.269,\ \nu_m/\nu_{se} = 1.364\right)$ of the experimental package used in this investigation. It should be noted that since the same combination of materials as above is used in most microelectronic packages, the present study can be of general use to designers and screeners of packages.

CHAPTER II

THERMAL STRESS ANALYSIS

The temperature analysis of the model lead-through seal is presented in Chapter III. The present chapter treats the analysis of stress in the three cylinder model which was introduced in Chapter I. The present analysis is carried out assuming that the time-temperature histories in the cylindrical lead, the cylindrical glass seal and the cylindrical base is known. The analysis which is presented below follows the same basic assumptions as those made by Poritsky [3] in his analysis of two concentric cylinders subjected to uniform temperature changes (hence stresses arising from the mismatch of thermal expansion coefficients of the glass seal and metal lead and base materials). It should be noted that Borom and Giddings [5] extended Poritsky's [3] analysis to include three concentric cylinders. The general problem of the thermal stresses in a system of many cylinders with nonuniform temperature distribution was studied by Gatewood [4]. The analysis presented below is essentially the same as that presented by Gatewood [4].

The thermal stress equations are obtained by writing the general equations of uncoupled thermo-elasticity for a typical element of material in each of the lead, glass seal and base cylinders. The solution of the elasticity equations with the appropriate boundary conditions at the surfaces of the cylinders provides the desired relations.

The equation of equilibrium for a typical element (cf. Fig. 4) is

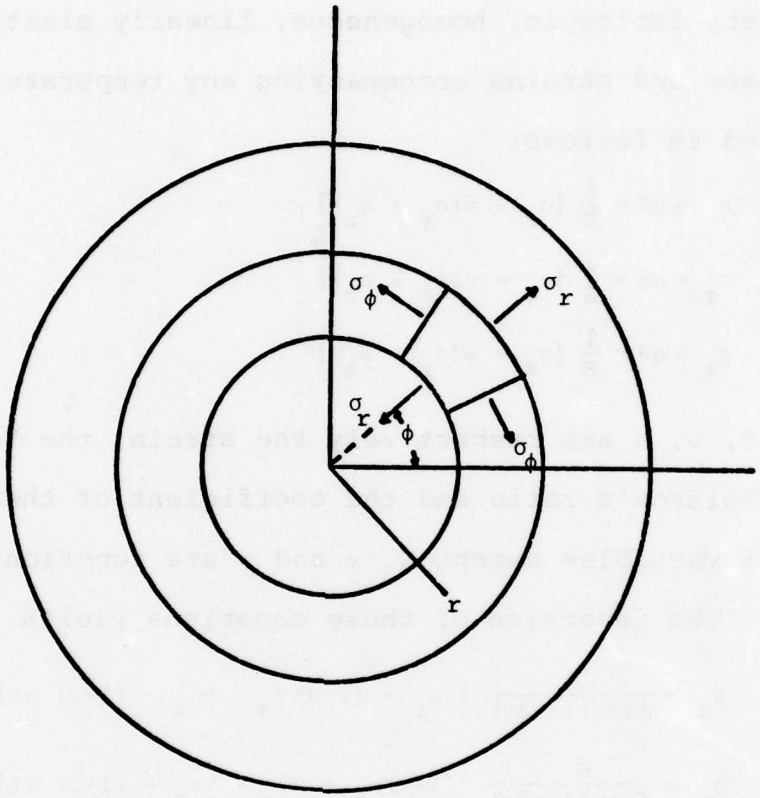

Fig. 4. Representation of a typical element with the stresses acting on it.

$$\frac{d\sigma_r}{dr} + \frac{\sigma_r - \sigma_\phi}{r} = 0 \tag{1}$$

Since the temperature distribution is assumed to depend only on the radius r, the problem is axisymmetric and only one equation of equilibrium is necessary.

In any isotropic, homogeneous, linearly elastic material, the stresses and strains accompanying any temperature rise θ are related as follows:

$$\begin{aligned}
\varepsilon_r - \alpha\theta &= \frac{1}{E}\left[\sigma_r - \nu(\sigma_\phi + \sigma_z)\right] \\
\varepsilon_\phi - \alpha\theta &= \frac{1}{E}\left[\sigma_\phi - \nu(\sigma_r + \sigma_z)\right] \\
\varepsilon_z - \alpha\theta &= \frac{1}{E}\left[\sigma_z - \nu(\sigma_r + \sigma_\phi)\right]
\end{aligned} \tag{2}$$

where ε, E, ν, α are respectively the strain, the Young's modulus, the Poisson's ratio and the coefficient of thermal expansion. All variables except E, ν and α are functions of radius and time. The inversion of these equations yields

$$\sigma_\phi = \frac{E}{(1+\nu)(1-2\nu)}\left[\nu\varepsilon_r + (1-\nu)\,\varepsilon_\phi + \nu\varepsilon_z - (1-\nu)\,\alpha\theta\right] \tag{3a}$$

$$\sigma_r = \frac{E}{(1+\nu)(1-2\nu)}\left[(1-\nu)\varepsilon_r + \nu\varepsilon_\phi + \nu\varepsilon_z - (1+\nu)\,\alpha\theta\right] \tag{3b}$$

The strain-displacement relations for an axisymmetric strain field are

$$\varepsilon_r = \frac{du}{dr} \qquad \varepsilon_\phi = \frac{u}{r} \tag{4}$$

where u represents the displacement in the radial direction. Substituting (4) in (3a) and (3b), then (3a) and (3b) into (1), one obtains

$$\frac{d^2u}{dr^2} + \frac{1}{r}\frac{du}{dr} - \frac{u}{r^2} = \frac{(1+\nu)}{(1-\nu)}\,\alpha\,\frac{d\theta}{dr} \tag{5}$$

The solution of (5) is of the form

$$u = \frac{(1+\nu)}{(1-\nu)} \alpha \frac{1}{r} \int_{r_i}^{r} \theta r dr + C_1 r + \frac{C_2}{r} \tag{6}$$

where C_1 and C_2 are constants of integration. r_i is the inner radius of the particular component. Substituting (6) in (4) and (3) yields

$$\begin{aligned} \varepsilon_r &= \frac{(1+\nu)}{(1-\nu)} \alpha \left[\theta - \frac{1}{r^2} \int_{r_i}^{r} \theta r dr\right] + C_1 - \frac{C_2}{r^2} \\ \varepsilon_\phi &= \frac{(1+\nu)}{(1-\nu)} \alpha \frac{1}{r^2} \int_{r_i}^{r} \theta r dr + C_1 + \frac{C_2}{r^2} \end{aligned} \tag{7}$$

and

$$\begin{aligned} \sigma_r &= -\frac{E\alpha}{(1-\nu)} \frac{1}{r^2} \int_{r_i}^{r} \theta r dr + \frac{E}{(1+\nu)} \left[\frac{C_1}{(1-2\nu)} - \frac{C_2}{r^2}\right] + \frac{\nu E \varepsilon_z}{(1+\nu)(1-2\nu)} \\ \sigma_\phi &= \frac{E\alpha}{(1-\nu)} \frac{1}{r^2} \int_{r_i}^{r} \theta r dr + \frac{E}{(1+\nu)} \left[\frac{C_1}{(1-2\nu)} + \frac{C_2}{r^2}\right] + \frac{\nu E \varepsilon_z}{(1+\nu)(1-2\nu)} - \frac{E\alpha\theta}{(1-\nu)} \\ \sigma_z &= E\varepsilon_z \left[\frac{(1-\nu)}{(1+\nu)(1-2\nu)}\right] - E\alpha\theta \left(\frac{1}{1-\nu}\right) + \frac{2\nu E C_1}{(1+\nu)(1-2\nu)} \end{aligned} \tag{8}$$

Representing the integral $\int_{r_i}^{r} \theta r dr$ by $I(r_i, r)$ and using a subscript j to denote each of the three concentric cylinders of the model, equations (6) and (8) can be written for each component.

$$u_j = \frac{(1+\nu_j)}{(1-\nu_j)} \frac{\alpha_j}{r} I(r_i, r) + C_{ij} r + \frac{C_{2j}}{r} \tag{9}$$

$$\sigma_{rj} = -\frac{E_j \alpha_j}{(1-\nu_j)} \frac{1}{r^2} I(r_i, r) + \frac{E_j}{(1+\nu_j)} \left[\frac{C_{1j}}{(1-2\nu_j)} - \frac{C_{2j}}{r^2}\right] + \frac{\nu_j E_j \varepsilon_z}{(1+\nu_j)(1-2\nu_j)} \tag{10}$$

$$\sigma_{zj} = E_j \varepsilon_z \left[\frac{(1-\nu_j)}{(1+\nu_j)(1-2\nu_j)}\right] + \frac{2\nu_j E_j C_{1j}}{(1+\nu_j)(1-2\nu_j)} - E_j \alpha_j \theta_j \left[\frac{1}{(1-\nu_j)}\right] \tag{11}$$

where j = 0,1,2 designate respectively the base made of Kovar, the glass seal and the lead made of Kovar. (See Fig. 3)

Equations (9), (10), (11) have two unknown constants for each cylinder. For the three cylinders, the total number of constants is six. Therefore, six equations are needed to determine the constants. An additional equation is required to evaluate ε_z, which is assumed to be constant. The equations derive from the following conditions:

1) The radial displacement at the center of the cylinders has to be finite.

2) The respective radial displacement u_2 and u_1 at the lead-glass interface, as well as u_1 and u_0 at the glass-base interface have to be equal to each other, i.e., $u_2 = u_1$ at $r = r_2$ and $u_1 = u_0$ at $r = r_1$.

3) The respective radial stresses at the same interfaces as above should be equal to each other, i.e., $\sigma_{r_2} = \sigma_{r_1}$ at $r = r_2$ and $\sigma_{r_1} = \sigma_{r_0}$ at $r = r_1$.

4) The outermost boundary should be free of radial stress, i.e., $\sigma_{r_o} = 0$ at $r = r_0$.

5) The total force in the axial direction should be zero, i.e., $\sum_{i=0}^{2} \int_A \sigma_{zi}\, dA = 0$.

These conditions yield 7 equations and 7 unknowns. The closed form solution of these equations would be too complex to evaluate. Therefore, the respective values of the known coefficients are placed in each equation and numerical results

are obtained for the unknowns. Hence the thermal stresses can be obtained at each increment of time. The results of this analysis are equivalent to B.E. Gatewood's analysis of thermal stresses in m + 1 concentric cylinders applied to the case of 3 cylinders [8].

The analysis presented in this chapter constitutes the main tool for the evaluation of the transient thermal stresses in and around the glass seals.

CHAPTER III

TEMPERATURE ANALYSIS

The evaluation of the thermal stresses requires the knowledge of the temperature distribution in the three cylinders at every instant of time. For this purpose a temperature distribution model is developed which takes into consideration the heat transfer and geometrical characteristics of the lead, the glass and the base assembly.

The physical characteristics of the temperature distribution model consist of a single lead surrounded by its annular glass seal which is in turn surrounded by a "base" which has 1/Nth the mass and 1/Nth the outside surface area of the total base. N is equal to the number of leads in the package. The lead and the base are considered to be lumped masses and as such conduct heat instantaneously. It is assumed that heat is transferred between fluid and lead and fluid and base but not between fluid and glass. In a heating situation (see Fig. 5) heat is conducted to the glass from the lead and (it will turn out) from the glass to the base. It is also assumed that the temperature distribution in the glass is axisymmetric at every instant of time and varies in the radial direction only. The temperature is assumed to be continuous across the glass-metal interfaces.

The assumption of a lumped mass for the lead and the base can be justified by the facts that the metal from which the lead and the base are constructed (usually Kovar) has a high thermal

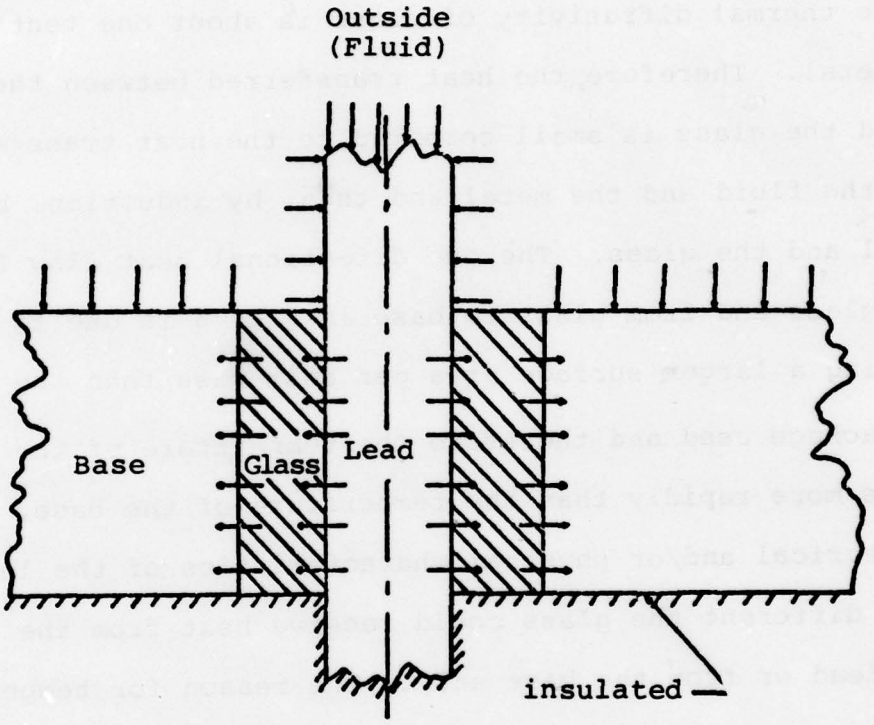

Fig. 5. Diagram representing the heat transfer to the seal when the seal is heating.

conductivity and the masses of the two components are small. (See also footnote on p. 3) The reason for assuming that no heat is transferred between the glass and the fluid is that the outside surface area of the glass is very small in relation to the outside surface areas of the lead and the base. In addition, the thermal diffusivity of glass is about one tenth that of the metal. Therefore, the heat transferred between the fluid and the glass is small compared to the heat transferred between the fluid and the metal and then, by induction, between the metal and the glass. The one directional heat flow from lead to glass and from glass to base in Fig. 5 is due to the lead having a larger surface area per unit mass than the base in the package used and therefore the temperature of the lead increases more rapidly than the temperature of the base. Were the geometrical and/or physical characteristics of the lead and the base different the glass could receive heat from the base and the lead or from the base only. The reason for temperature variation only in the radial direction is that no heat is transferred from the fluid to the glass. Also, since the lead and the base each are assumed to have a uniform temperature distribution the only temperature gradient exists in the radial direction.

The temperature distribution model is used to determine the transient temperature distribution in the glass. The transfer of heat is governed by the partial differential equation.

$$\frac{\partial T}{\partial \tau} = a\left(\frac{\partial^2 T}{\partial r^2} + \frac{1}{r}\frac{\partial T}{\partial r}\right) \qquad (12)$$

where $a = k_g/\rho_g c_g$ is the thermal diffusivity and k_g, ρ_g, c_g are respectively the thermal condictivity, the density and the specific heat of glass. τ and r indicate respectively the time and the radial coordinate. T is the temperature in the glass, which is a function of the radius and time.

The initial condition is:

$T(r,0) = T_o$, an initial uniform temperature for the lead-base-glass assembly corresponding to the beginning of the thermal shock.

The boundary conditions are:

$$-k_g \frac{\partial T}{\partial r}\Big|_{r=r_2} = \frac{\bar{h}A_o}{A_2}(T_\infty - T\Big|_{r=r_2}) - \rho_k c_k \frac{V_\ell}{A_2}\frac{\partial T}{\partial \tau}\Big|_{r=r_2} \qquad (14)$$

$$k_g \frac{\partial T}{\partial r}\Big|_{r=r_1} = \frac{\bar{h}A_b}{A_1 N}(T_\infty - T\Big|_{r=r_1}) - \rho_k c_k \frac{V_b}{A_1 N}\frac{\partial T}{\partial \tau}\Big|_{r=r_1} \qquad (15)$$

where T_∞ is the temperature of the fluid and $\bar{h}$ is an effective heat transfer coefficient governing the rate of heat transfer between the lead or the base and the fluid. $\bar{h}$ is determined through the experimentally measured temperature-time histories for the lead and the base as described below. The as yet undefined variables in equations (14) and (15) are defined as follows:

ρ_k = the density of the metal (usually Kovar)

c_k = the specific heat of the metal

A_o = the outside surface area of the lead in contact with the fluid

A_b = the outside surface area of the base and lid

A_1 = the surface area of the glass-base interface

A_2 = the surface area of the lead-glass interface

V_ℓ = the total volume of the lead

V_b = the total volume of the base and lid [1]

N = the total number of leads.

The differential equation (12) and boundary conditions (13,14,15) are solved using a finite element analysis. For this purpose the glass cylinder is divided into 5 radial elements of equal radial width. The physical properties of glass are assumed to be uniform. Details of the analysis are described in Appendix A.

The solution of equation (12) yields the transient temperature distribution in the glass as well as the temperature-time histories of the lead and the base.

---

[1] The microelectronic package used in this investigation consists of a base and a lid as shown in Fig. 8. Other packages have the base surrounded with vertical walls with a lid in the form of a plate. For these types of packages the walls should be included in the analysis. More generally, A_b and V_b refer to all the parts of the package except the glass seals and the leads.

CHAPTER IV

EXPERIMENTS

4.1 Procedure

The approximate radial temperature distribution throughout the 3 cylinder model can be determined analytically if the temperature of the lead and base cylinders is known as a function of time. These temperature histories can be determined if the effective heat transfer coefficient for the lead and base are known. In the present work, the temperature-time histories of the lead and the base of the package were measured experimentally. This data was then used to evaluate the effective heat transfer coefficient $\bar{h}$ which represents the rate of heat per unit area transferred to the package during given experimental conditions.

The standard procedure for performing thermal shock tests as given in MIL-STD-883B [6] requires that

(a) The package be immersed in the low temperature bath for a minimum of 5 minutes.

(b) The package be transferred from the low temperature to the high temperature bath and left there for 5 minutes.

(c) The package be transferred from the high temperature to the low temperature bath and left there for 5 minutes. The remaining stems are the repetition of b and c at least fourteen times.

The experiments which were performed consisted of recording the temperature of the lead and the base as a function of time during and subsequent to immersion of the package in the thermal shock fluid bath. Experiments were carried out for level A conditions of ice water and boiling water baths.

The packages used during the experiments were Tekform packages identified with part number 20133, style A in the manufacturer's catalog. A schematic representation of the packages is given in Fig. 6.

The temperature was measured using Chromel-Constantan thermocouples. The hot junction of the thermocouples was formed by twisting the two wires together. The thermocouple wires were of .005 in. diameter and about 2 ft long. They were soldered to the lead and the base with rosin fluxed 66 Sn - 34 Pb solder. (See Figures 7a and 7b.) The thermocouples were connected to a multichannel Honeywell Visicorder (Model 1108) instrumented with M40 350A type Honeywell galvanometers. The Visicorder was used to simultaneously record the output e.m.f. of each of the thermocouples. The experimental set up is shown in Fig. 8. No controlled reference cold junction was used during the experiments. Instead, the recorder was set to an initial position corresponding to the lower temperature bath. The calibration of the recorder and thermocouples was then used to determine the temperature corresponding to any voltage output. Also, the duration of the heating or cooling process was very short (7-8 sec). Therefore variation of temperature of the room had a negligible effect on the measurements.

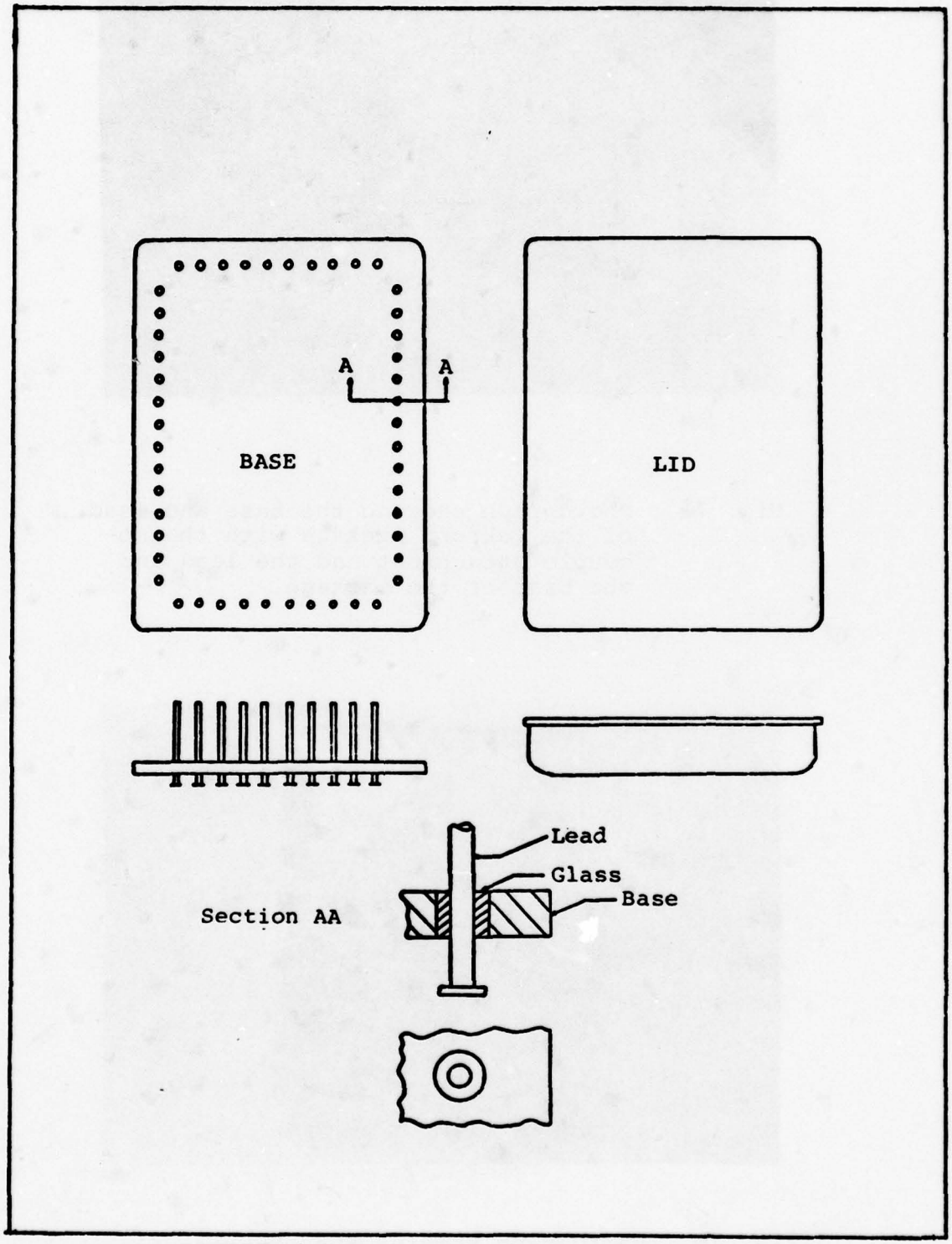

Fig. 6. Schematic representation of the Tekform package used during experiments.

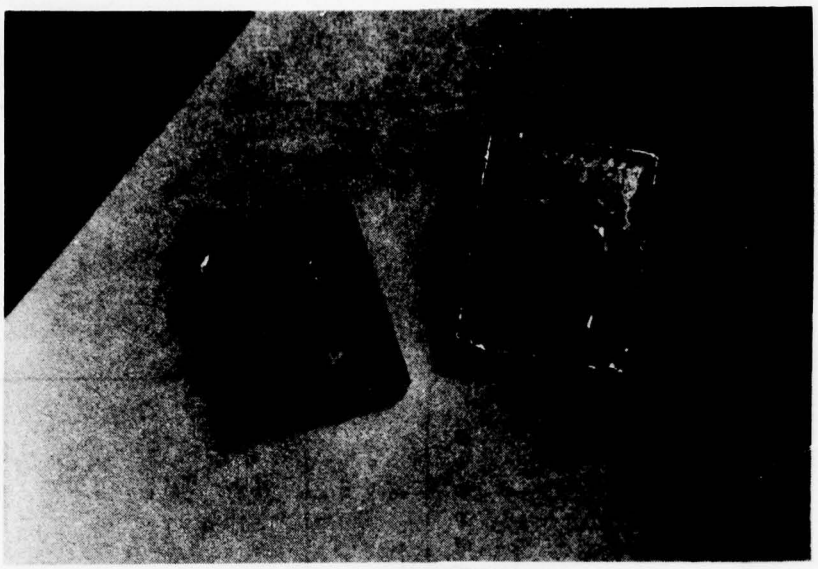

Fig. 7a. Photograph showing the base and lead of the Tekform package with thermocouple attachment and the lead and the base of the package.

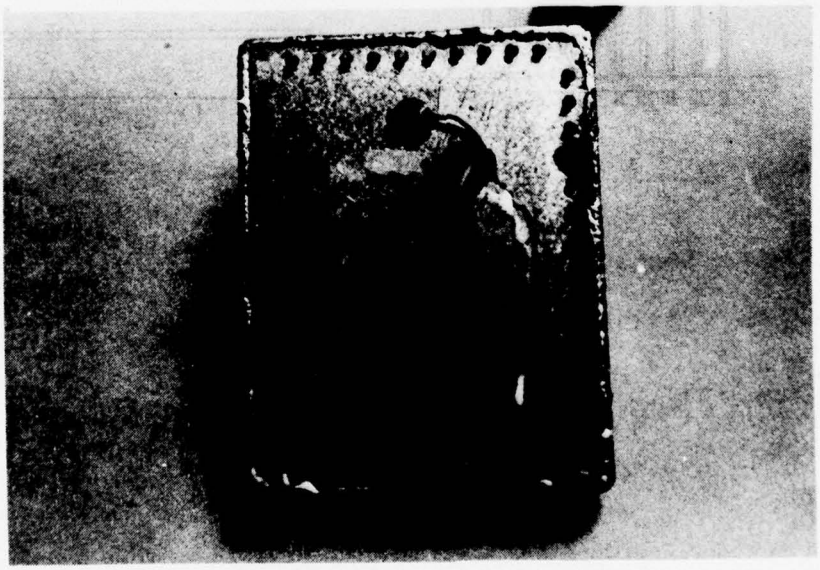

Fig. 7b. Photograph showing the thermocouple on the base and the thermocouple on lead. Note the solder on the four sides of the base.

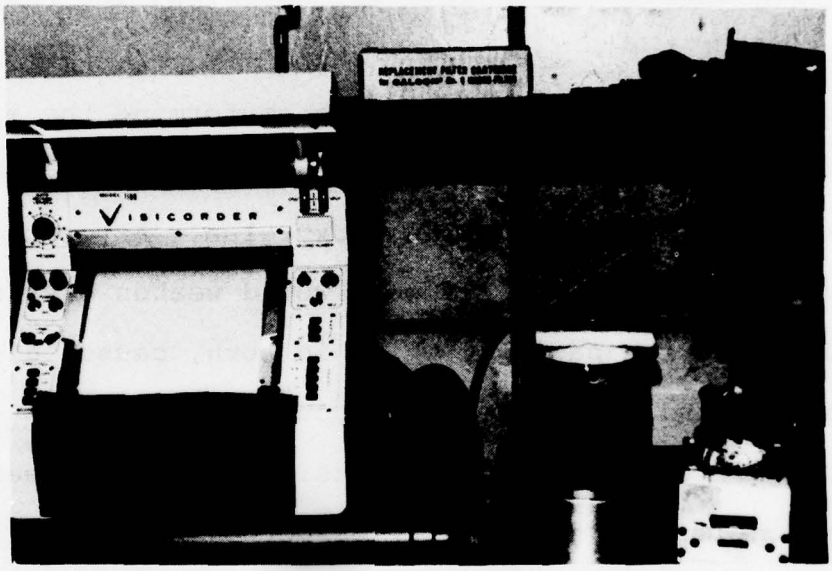

Fig. 8. Photograph showing the set-up for the experiment. From left to right: Visicorder, ice water container; boiling water on heater with the package in it.

Using this set up, the package was immersed in ice water (32°F) and left there for about 5 minutes. Then, the recorder was activated as the package was transferred to boiling water (212°F). After a few seconds the recorder was stopped. By this time the package had reached about 90 percent of its equilibrium temperature. After complete thermal equilibrium, the package was immersed back into ice water and the cooling process recorded.

The main problems encountered with performing the experiments were related to leakage of the package. The lid was sealed to the base initially using epoxy glue. After two repetitions of the cycle the lid seal would weaken causing water to leak into the package, which in turn, caused disturbances in the recording of the thermocouple e.m.f.

This difficulty was overcome by using solder instead of glue to seal the lid to the base. The method by which this was accomplished can be briefly described as follows:

The lid is placed on a hot plate and brought to a temperature of approximately 175°C. The base is then placed on the lid and brought to the same temperature. A heat sink consisting of copper blocks is placed on the base, preventing the solder attaching the thermocouple wires from melting. A fine bead of Indalloy solder (the melting temperature of which is lower than that of 66Sn - 34Pb solder) is put on the boundaries of the base and lid. Finally a soldering iron is run gently along the sides, causing the Indalloy solder to melt. The whole assembly is then left to cool.

The package thus sealed was tested for hermeticity using the following procedure. The package was subjected to a pressure of 10 psi for 30 minutes in a pressure bomb. (The applied pressure of 10 psi was calculated not to result in any bond failure [9]). The pressurized package was then immersed in warm water and checked for air bubbles.

4.2 Evaluation of the Effective Heat Transfer Coefficient

The experimental temperature-time histories of the lead and the base, recorded using the Visicorder are shown in Fig. 9a, b, c, d, e, f, g and h[1]. These curves were used to evaluate the effective heat transfer coefficient $\bar{h}$.

In the thermal model, presented in the preceding chapter, $\bar{h}$ determines the rate of heat transfer to the lead and the base. $\bar{h}$ appears in the boundary conditions of the partial differential equation governing the heat transfer to the glass. When this differential equation is solved, the temperature-time histories corresponding to the lead and the base are obtained. The experimental value of $\bar{h}$ is found in such a way as to ensure that the mathematically determined temperature-time histories provided best fit of the experimental temperature-time histories. The best fit is realized by solving the differential equation for different values of $\bar{h}$, until the $\bar{h}$ value yielding the smallest least square error between the values corresponding to the first 2.5 seconds of the mathematical and experimental temperature-time curves is obtained. The least square error is defined by $E_r = \sum_{i=1}^{n} (y_i - y_{ei})^2$, where y_i and y_{ei} are, respectively corresponding points on the theoretical and experimental time-temperature histories. A typical example illustrating

1 The code on these figures is explained on page 41.

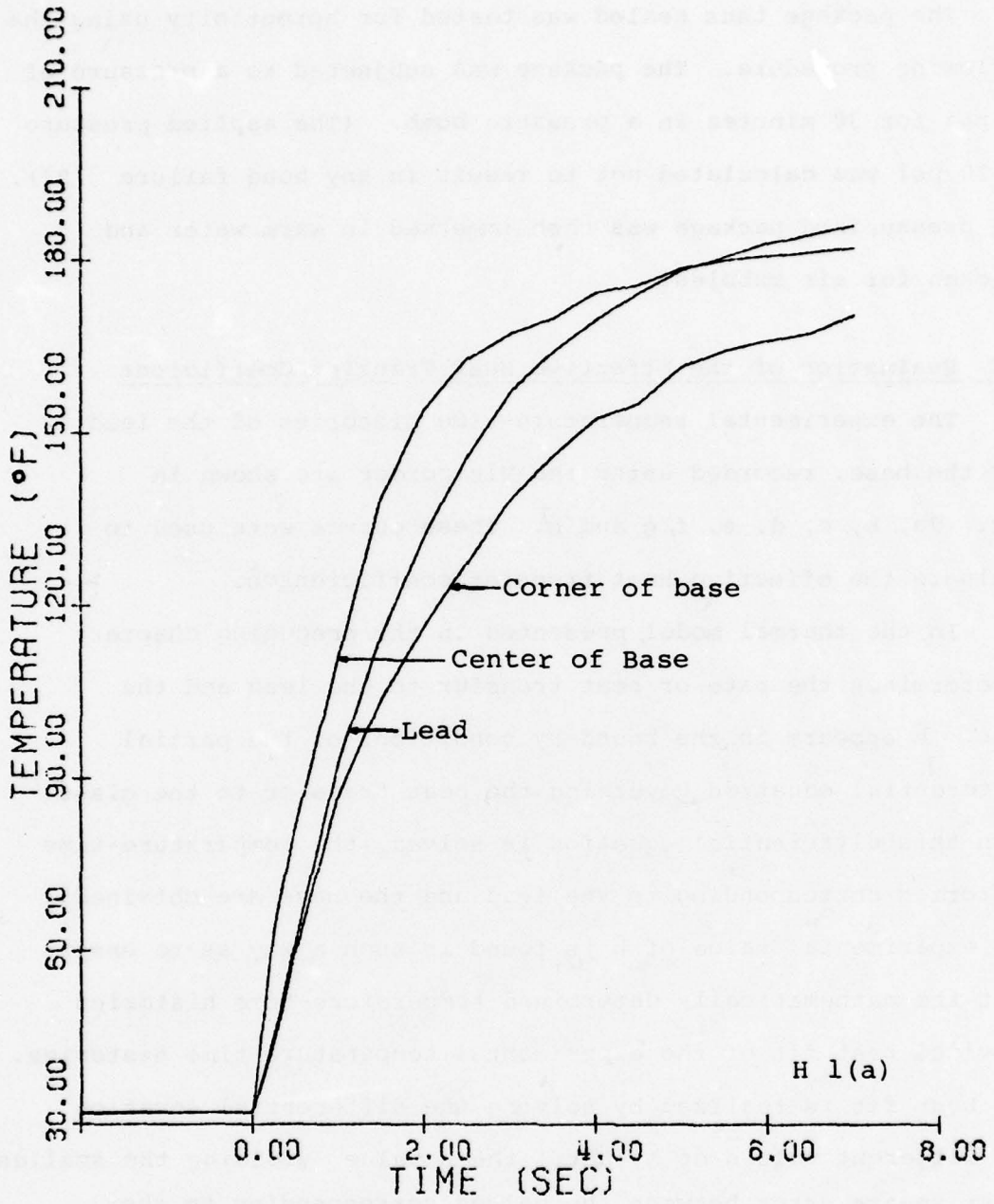

Fig. 9(a) Experimental temperature-time histories for the lead, the base and the corner of the base obtained from Experiment 1 when the package at 32°F is immersed into a 212°F bath.

C 1(a)

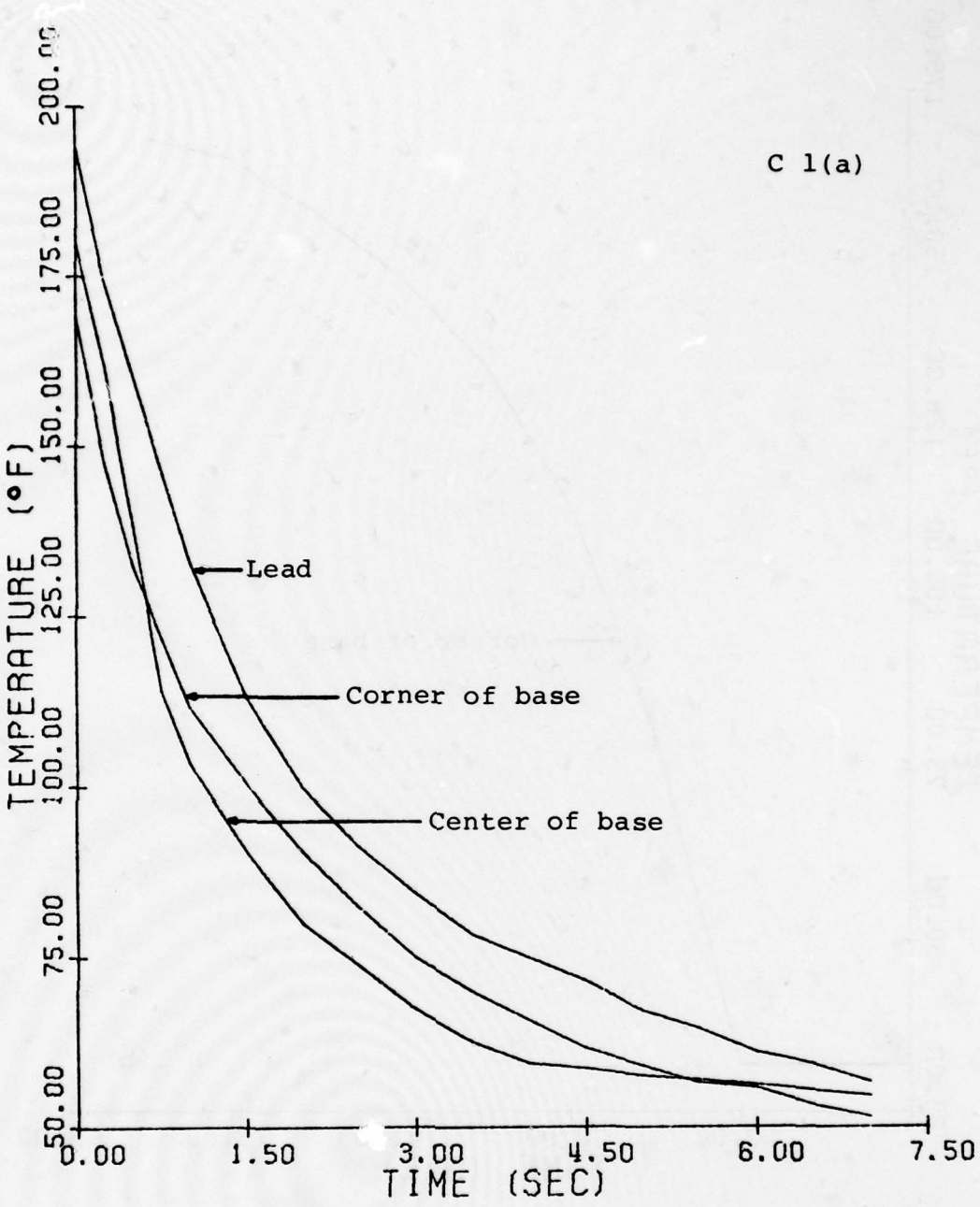

Fig. 9(b) Experimental temperature-time histories for the lead, the base and the corner of the base obtained from Experiment 1 when the package at 212°F is immersed into a 32°F bath.

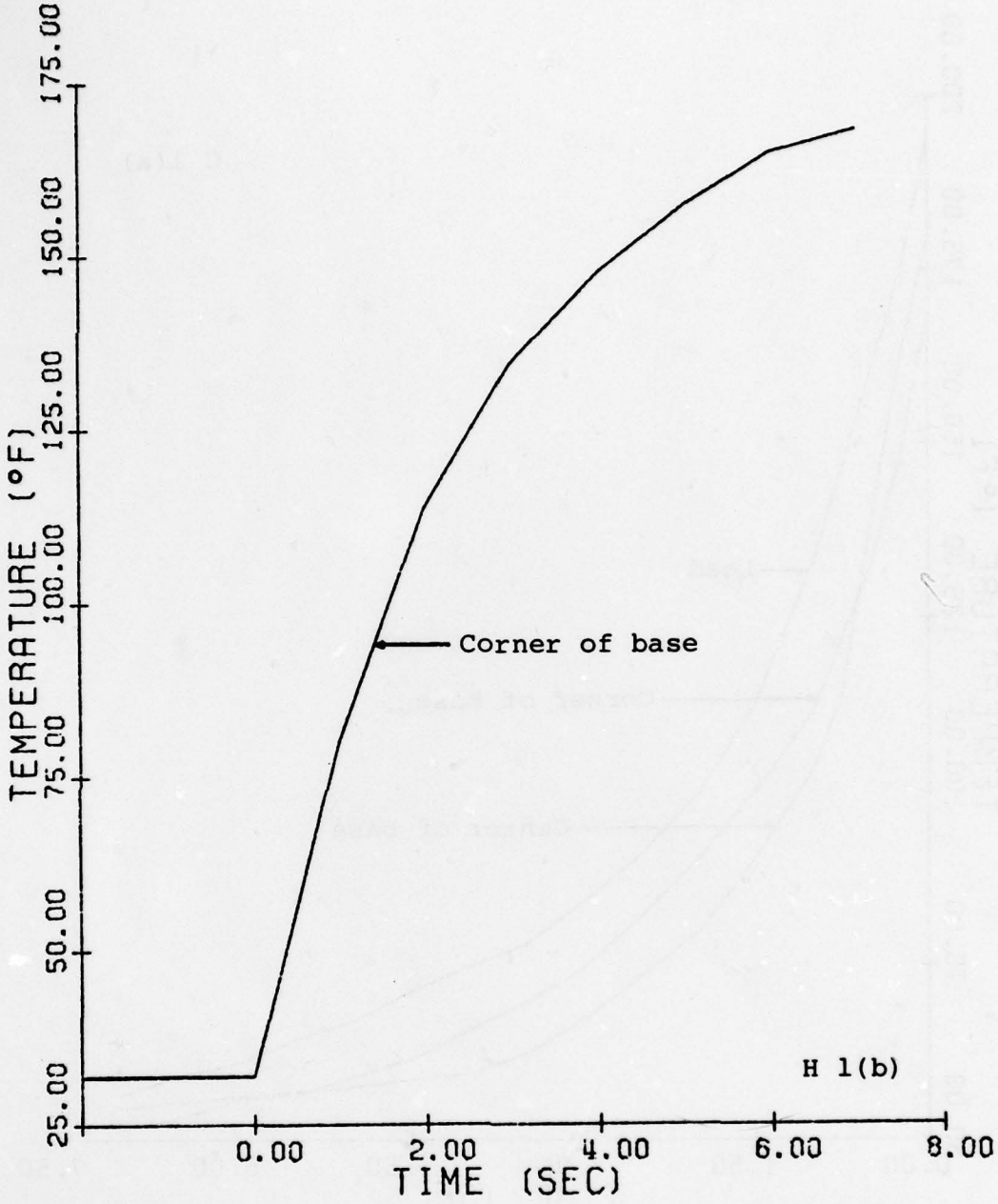

Fig. 9(c) Experimental temperature-time history for the corner of the base obtained from Experiment 1(b) when the package at 32°F is immersed into a 212°F bath.

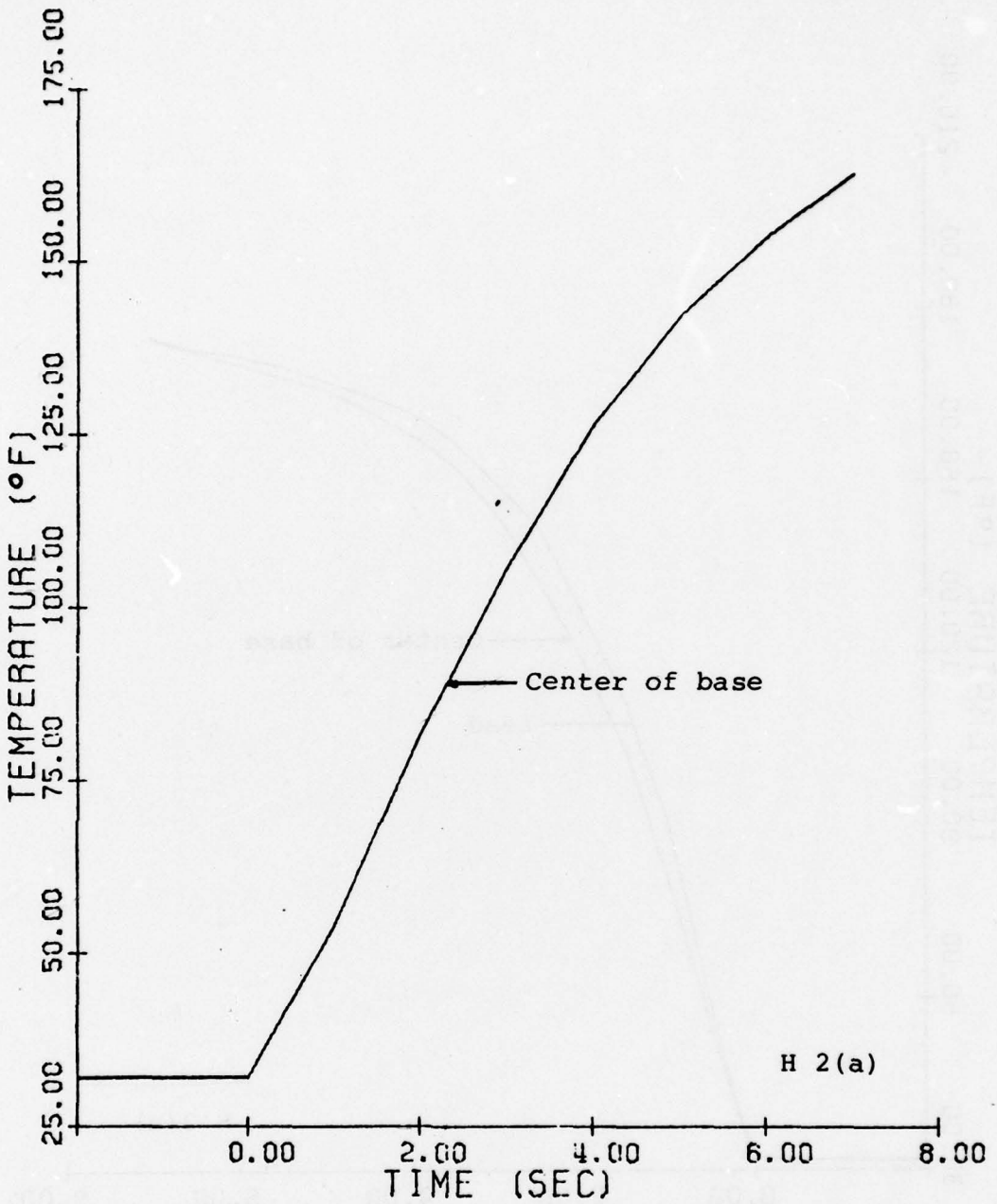

Fig. 9(d) Experimental temperature-time history for the base obtained from Experiment 2 when the package at 32°F is immersed into a 212°F bath.

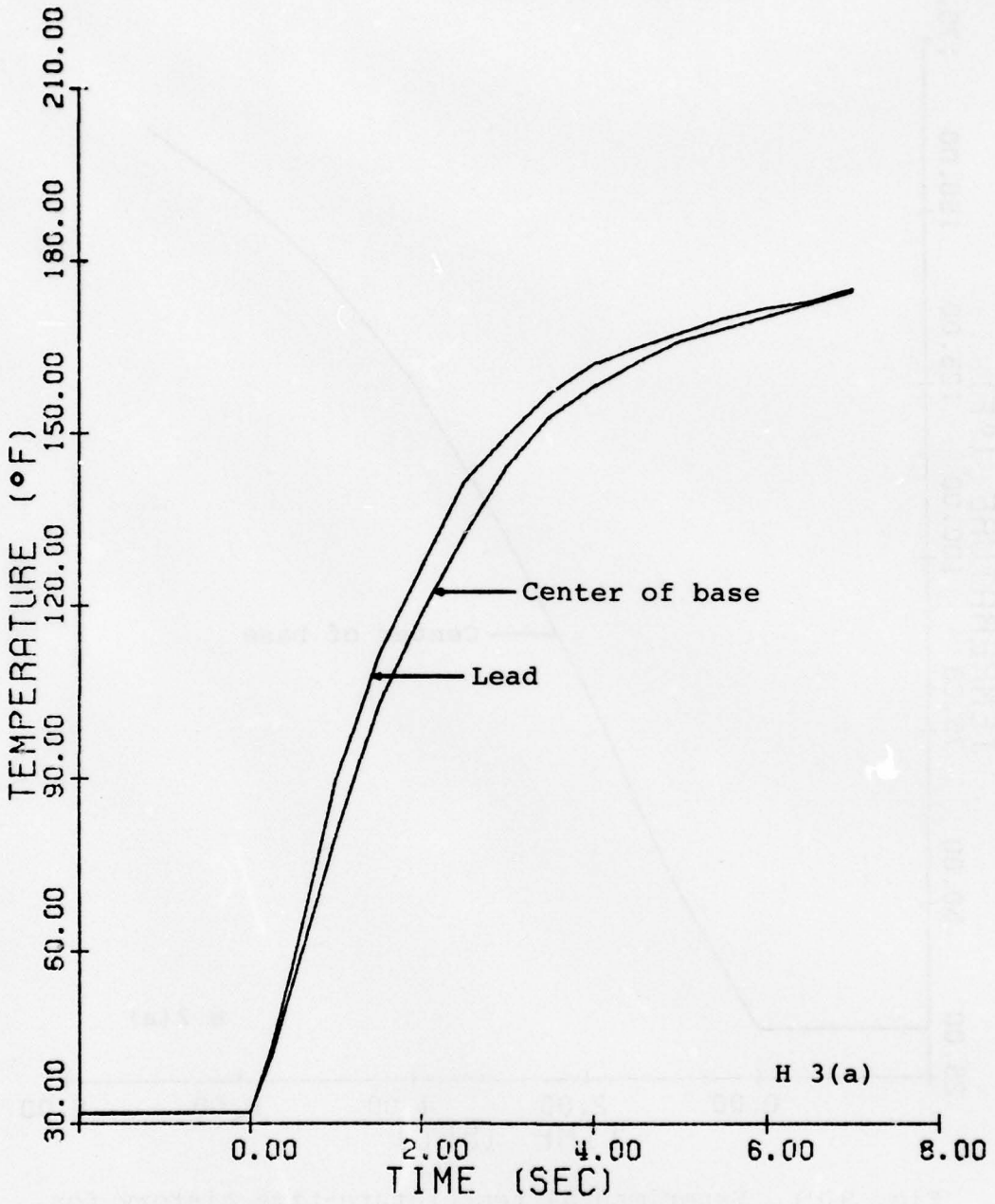

Fig. 9e Experimental temperature-time histories for the lead and the base obtained from Experiment 3 when the package at 32°F is immersed into a 212°F bath.

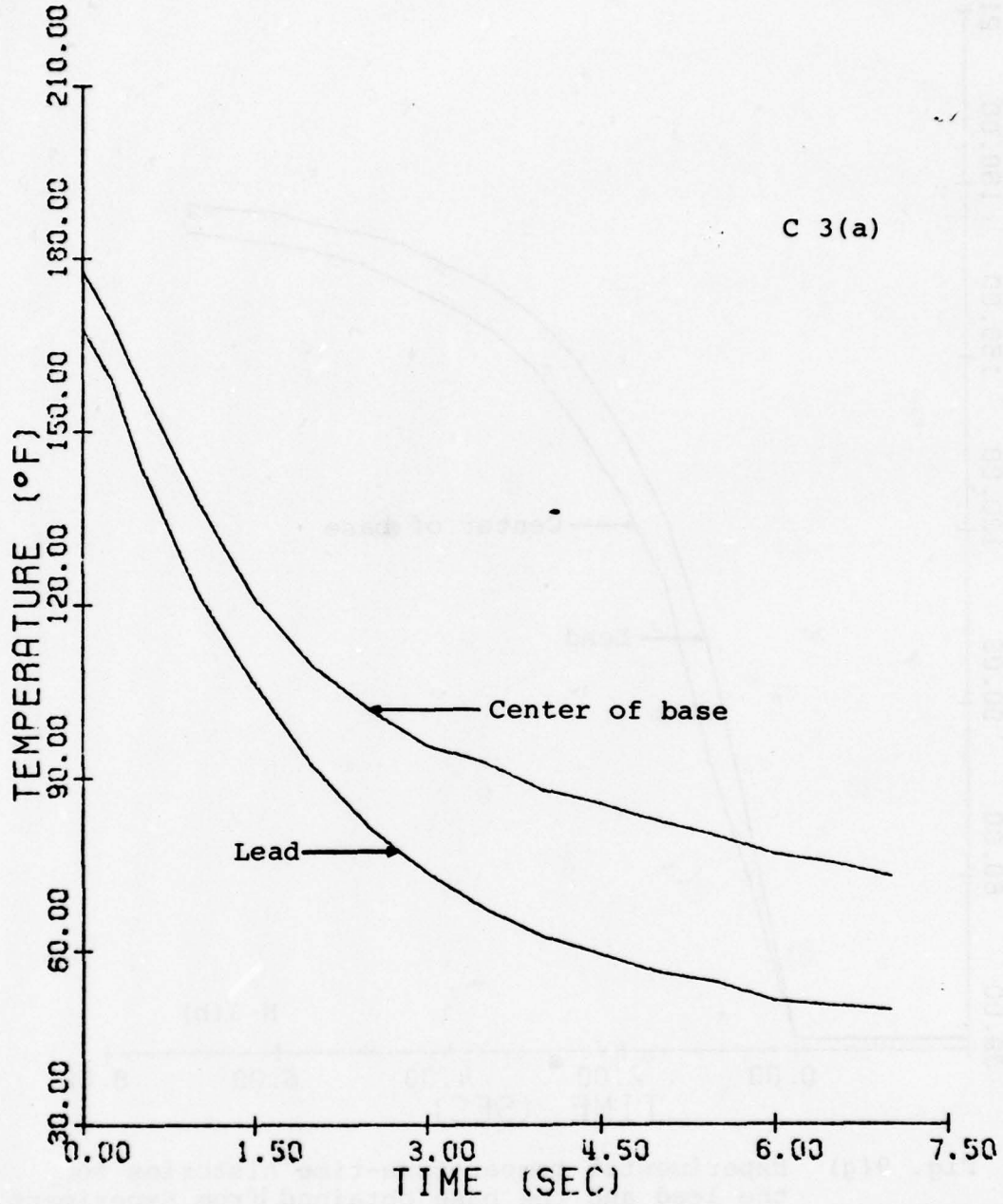

Fig. 9(f) Experimental temperature-time histories for the lead and the base obtained from Experiment 3 when the package at 212°F is immersed into a 32°F bath.

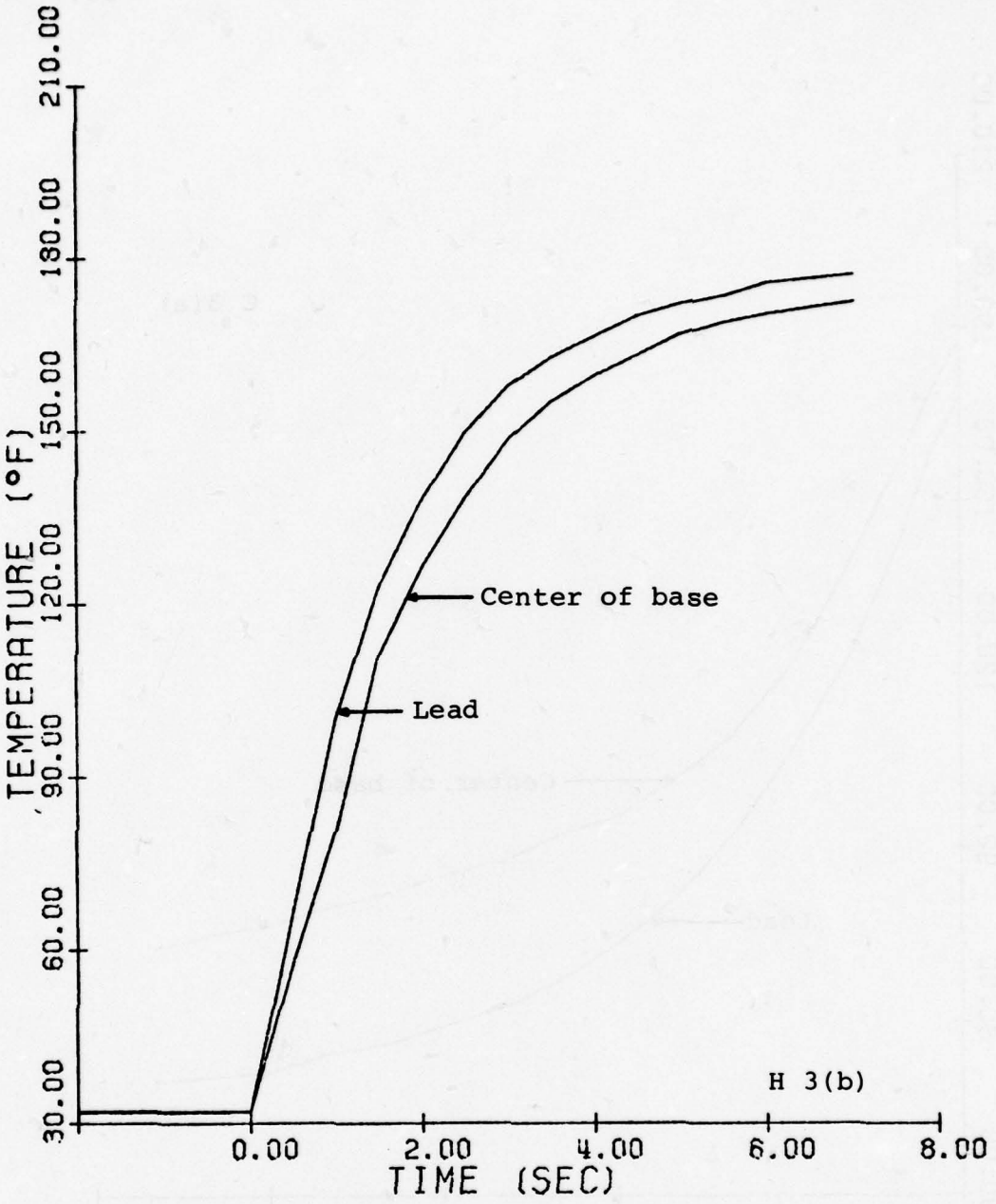

Fig. 9(g) Experimental temperature-time histories for the lead and the base obtained from Experiment 3(b) when the package at 32°F is immersed into a 212°F bath.

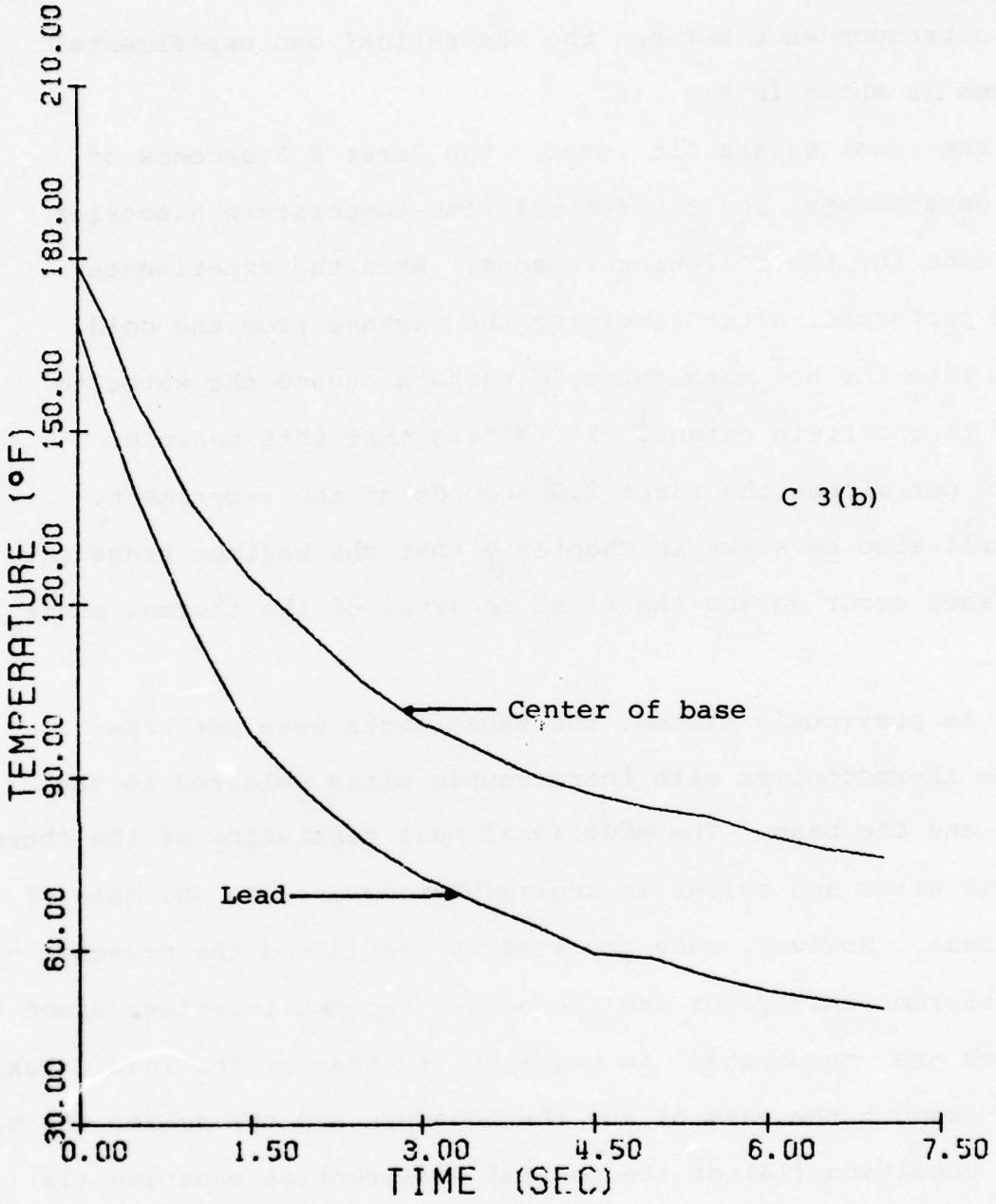

Fig. 9(h) Experimental temperature-time histories for the lead and the base obtained from Experiment 3(b) when the package at 212°F is immersed into a 32°F bath.

the correspondence between the theoretical and experimental curves is shown in Fig. 10.

The least square fit over the first 2.5 seconds of the experimental and theoretical time-temperature histories was done for the following reasons. When the experiments were performed, after immersing the package from the cold bath into the hot bath, the cold package caused the water to cool to a certain extent.[1] It is felt that this behavior would not affect the first 2.5 seconds of the experiment. It will also be shown in Chapter V that the maximum transient stresses occur during the first interval of the thermal shock test.

As previously stated, the experiments were performed using thermocouples with thermocouple wires soldered to the lead and the base. The additional mass consisting of the thermocouple wires and solder is negligible compared to the mass of the base. However, when the lead is considered the presence of the thermocouple wires and the solder becomes important since these masses are comparable in magnitude to that of the lead. Taking into account the mass of the thermocouple and the solder the boundary condition (14) of the partial differential equation (12) becomes

$$-k_g \left.\frac{\partial T}{\partial r}\right|_{r=r_2} = \bar{h} A_o \left(T_\infty - \left. T \right|_{r=r_2}\right)$$

$$- \left(\rho_k c_k V_\ell + \rho_s c_s V_s + \rho_{ch} c_{ch} V_{ch} + \rho_{co} c_{co} V_{co}\right) \left.\frac{\partial T}{\partial \tau}\right|_{r=r_2} \qquad (14b)$$

1 The theoretical and experimental curves in Fig. 10 diverge because the theoretical curve reaches 212°F while the experimental curve remains at a lower value due to the cooling of the bath.

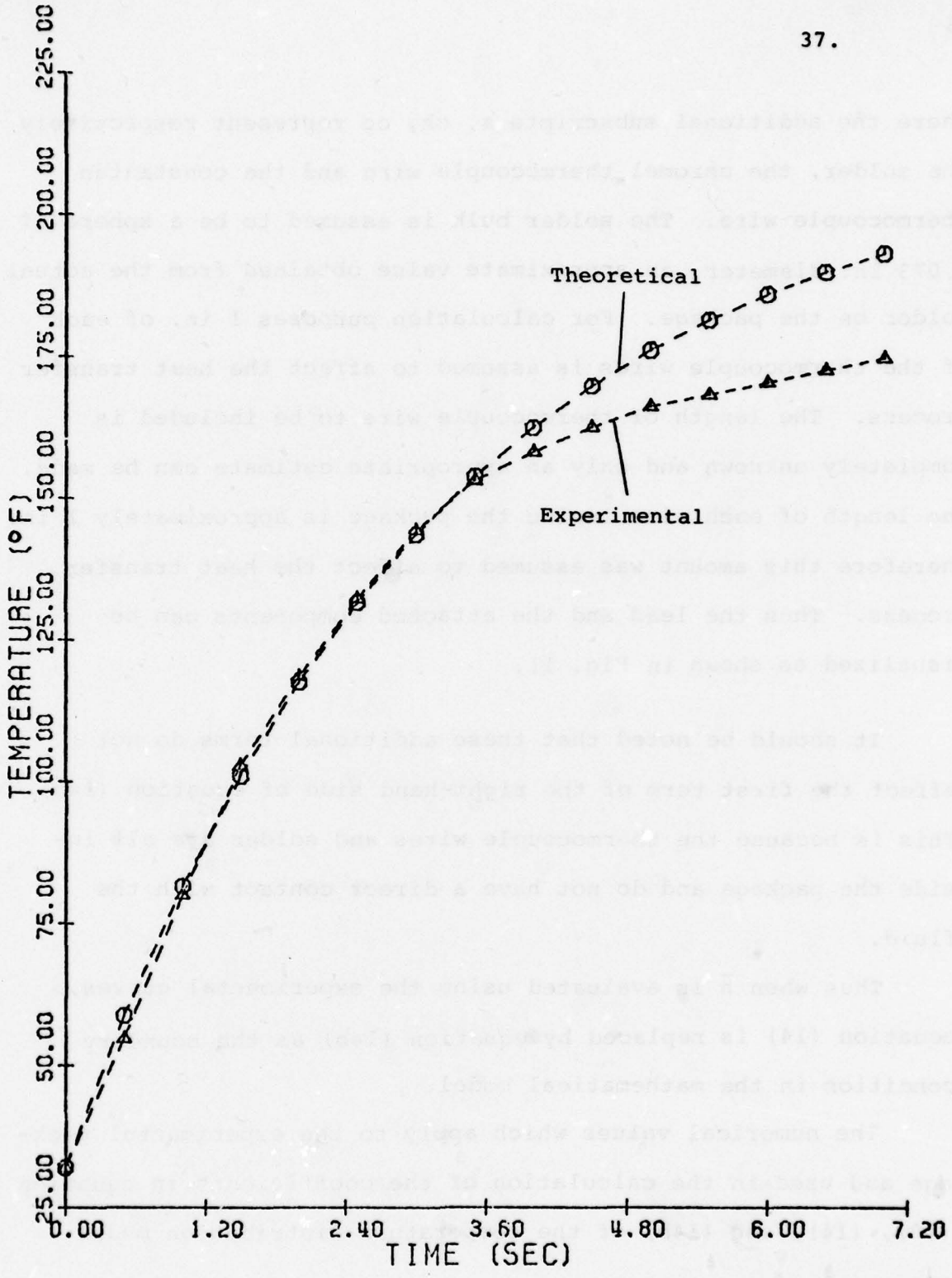

Fig. 10. Graph showing the correspondence between the experimental and theoretical time-temperature history for the base.

where the additional subscripts s, ch, co represent respectively the solder, the chromel thermocouple wire and the constantan thermocouple wire. The solder bulk is assumed to be a sphere of 0.073 in. diameter, an approximate value obtained from the actual solder on the package. For calculation purposes 1 in. of each of the thermocouple wires is assumed to affect the heat transfer process. The length of thermocouple wire to be included is completely unknown and only an appropriate estimate can be made. The length of each wire inside the package is approximately 1 in. Therefore this amount was assumed to affect the heat transfer process. Thus the lead and the attached components can be visualized as shown in Fig. 11.

It should be noted that these additional terms do not affect the first term of the right-hand side of equation (14b). This is because the thermocouple wires and solder are all inside the package and do not have a direct contact with the fluid.

Thus when $\bar{h}$ is evaluated using the experimental curves, equation (14) is replaced by equation (14b) as the boundary condition in the mathematical model.

The numerical values which apply to the experimental package and used in the calculation of the coefficients in equation (12), (14), and (14b) of the temperature distribution model are:

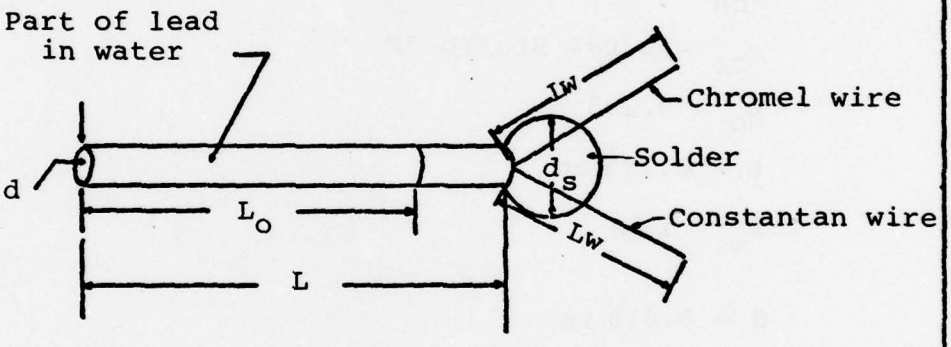

Fig. 11. Schematic representation of the lead and the attached components.

$k_g = 1.366 \times 10^{-5}$ Btu/sec-in-°F

$\rho_g = 8.2 \times 10^{-2}$ lb/in^3

$\rho_k = 0.302$ lb/in^3

$\rho_s = 0.304$ lb/in^3

$\rho_{ch} = 0.315$ lb/in^3

$\rho_{co} = 0.322$ lb/in^3

$c_g = 0.23$ Btu/lb-°F

$c_k = 0.105$ Btu/lb-°F

$c_s = 0.051$ Btu/lb-°F

$c_{ch} = 0.107$ Btu/lb-°F

$c_{co} = 0.094$ Btu/lb-°F

$L_o = 0.205$ in

$L = 0.295$ in

$L_w = 1$ in

$d = 0.018$ in

$d_s = 0.073$ in

$d_{ch} = d_{co} = 0.005$ in

$V_b = 0.15434605$ in^3

$A_b = 4.2874$ in^2

$V_\ell = 0.000075068$ in^3

$A_o = 0.0115925$ in^2

$N = 48$

4.3 Experimental Results

The effective heat transfer coefficient was determined from results of experiments carried out with three Tekform packages which were submitted to thermal shock tests. The packages were prepared and tested using the experimental technique described in the preceding section. The first two packages were sealed with glue and the third with solder. The effective heat transfer coefficients which were evaluated using the experimentally determined temperature-time histories are tabulated in Table 1.

Each row in Table 1 corresponds to a single experiment (i.e., Experiment 1 indicates that the first package was submitted to one thermal shock). The experiment numbering code is as follows: H denotes a heating experiment (package at $32^{o}F$ transferred to a $212^{o}F$ bath); C denotes a cooling experiment (package at $212^{o}F$ transferred to a $32^{o}F$ bath). 1, 2, and 3 denote the package numbers. (a) and (b) signify the first and 2nd experiment of the designated type if these were more than one. E.g, Experiment C3(b) is the second cooling experiment performed with package 3.

The columns in Table 1 refer to the location of the thermocouple on the package. The first column represents the effective heat transfer coefficient $\bar{h}$ calculated from a temperature-time history obtained from a thermocouple attached to the lead. Columns (2) and (3) are the effective heat transfer coefficients $\bar{h}$ for the package as determined by temperature measurement at the center of the base and at the corner of the base respectively. Values for both columns (2) and (3) represent the $\bar{h}$ for the base since in the temperature distribution model, the base was assumed to be one lumped mass having a uniform temperature at each instant of time.

		(1) Lead	(2) Base	(3) Corner
HEATING	Experiment H 1(a)	150	325	190
	Experiment H 1(b)	-	-	115
	Experiment H 2(a)	-	70	-
	Experiment H 3(a)	145	190	-
	Experiment H 3(b)	175	210	--
COOLING	Experiment C 1(a)	165	375	275
	Experiment C 3(a)	175	175	-
	Experiment C 3(b)	160	190	-

TABLE 1

Effective Heat Transfer Coefficient $\bar{h}$
Evaluated Using the Experimental Curves
(Btu/hr - ft^2 - °F)

It should be noted that in Table 1, certain values of $\bar{h}$ (e.g., Experiment 2, "cooling") are not given. This is because water leakage through the lid seal of the package during these experiments rendered the thermocouple voltage of the recorder unreadable. Thus, the value of $\bar{h}$ for these cases could not be determined.

The effective heat transfer coefficient of an object depends on the convection process and therefore also depends on its geometry, its position in the surrounding environment and the process by which heat is transferred to or from it. It is conceivable therefore that the true value of $\bar{h}$ for the lead differs from that of the base since the conditions mentioned above are different for the lead and the base. This difference can be explained by use of Fig. 12(a) and 12(b). Fig. 12(a) represents a cold lead situated in a hot fluid. The entire surface of the cold lead is continually in contact with new particles of hot fluid. Fig. 12(b) shows the cold base standing in the hot fluid. A point A on the bottom part of the base is in contact with the hot fluid which transfers heat to this part and moving towards B becomes colder. So B is in contact with cooler particles of fluid. This heating process would cause the lead to heat faster than the base which would result in a higher effective heat transfer coefficient for the lead than for that for the base.

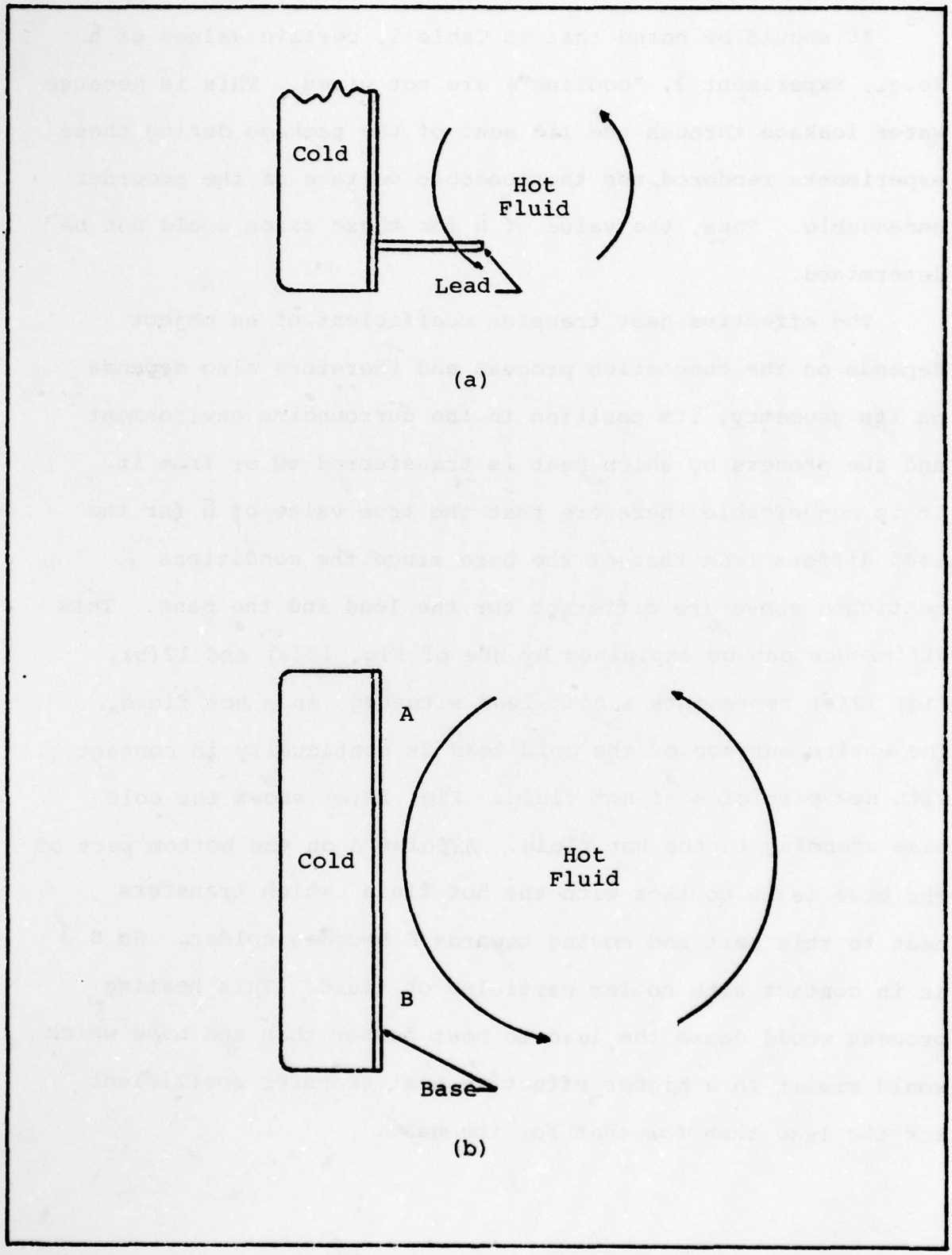

Fig. 12. Schematic representation of heat transfer process to the lead and the base.

However, as explained before, the assumption of a certain mass of solder and an estimated length for the thermocouple wires results in considerable uncertainty in the calculation for the effective heat transfer coefficient for the lead. Furthermore, the experimentally measured values of $\bar{h}$ shown in Table 1 vary from 70 to 375 Btu/ft^2-hr-°F, a rather large range. Due to this large range in experimentally determined values coupled with the uncertainty in the calculation for the lead it is difficult to justify the assumption that the heat transfer coefficient for the lead is different from that of the base. The evaluation of $\bar{h}$ for the base is considered to be more accurate , therefore the average value of $\bar{h}$ determined for the base is taken to be the most reliable estimate of the overall effective heat transfer coefficient for both the lead and the base.

The transient temperature distribution in the glass seal which consists of the solution of Eq. (12) and boundary conditions (14) and (15) can be obtained when $\bar{h}$ is known. The transient temperature distribution in the glass seal of the experimental package, thus obtained, is shown in Fig. 13 and 14. (It should be noted that these temperature distributions correspond to the package without any attachment (thermocouple wires and solder) in it).

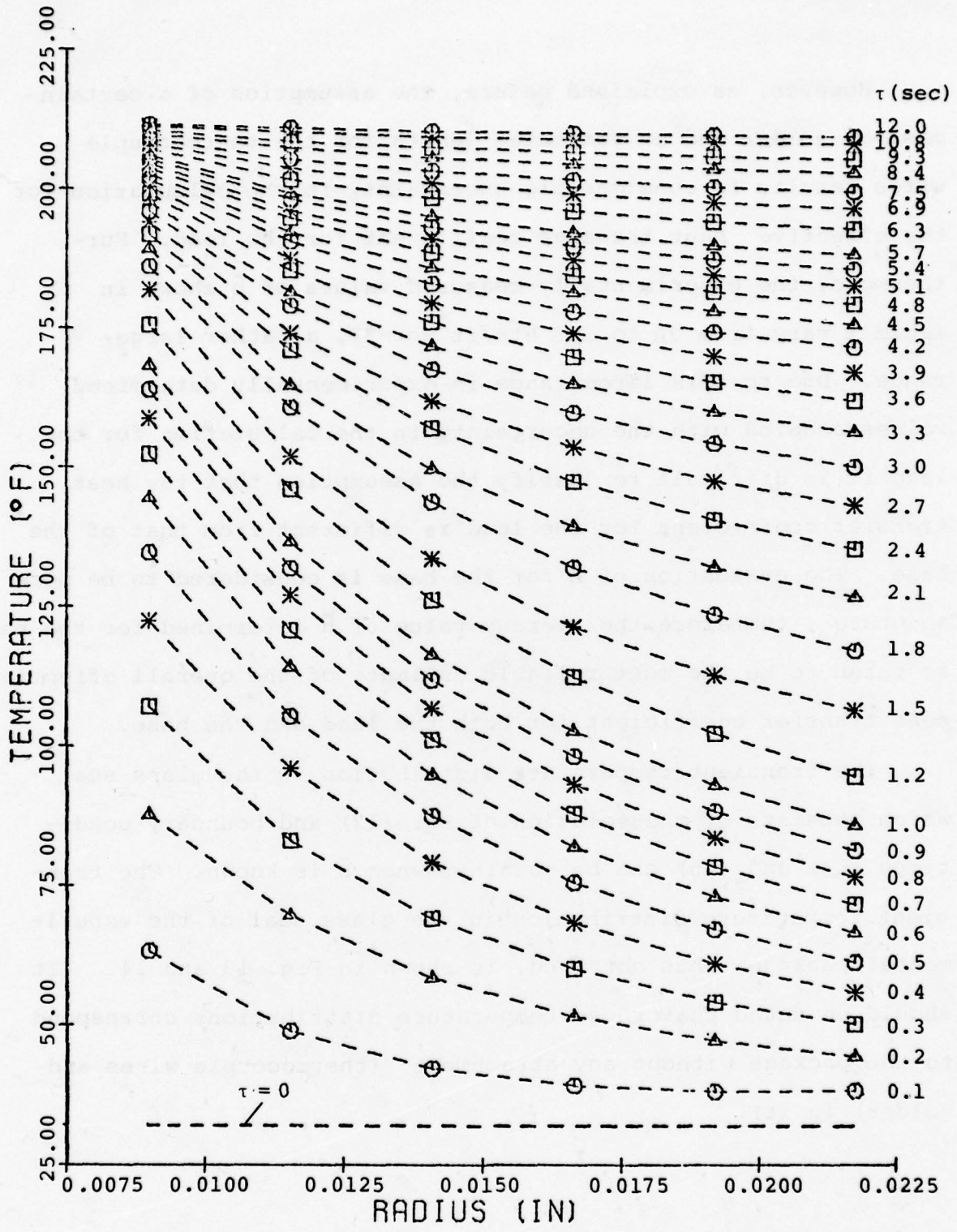

Fig. 13. Radial temperature distribution in the glass annulus at different increments of time when the seal is heated from 32°F to 212°F.

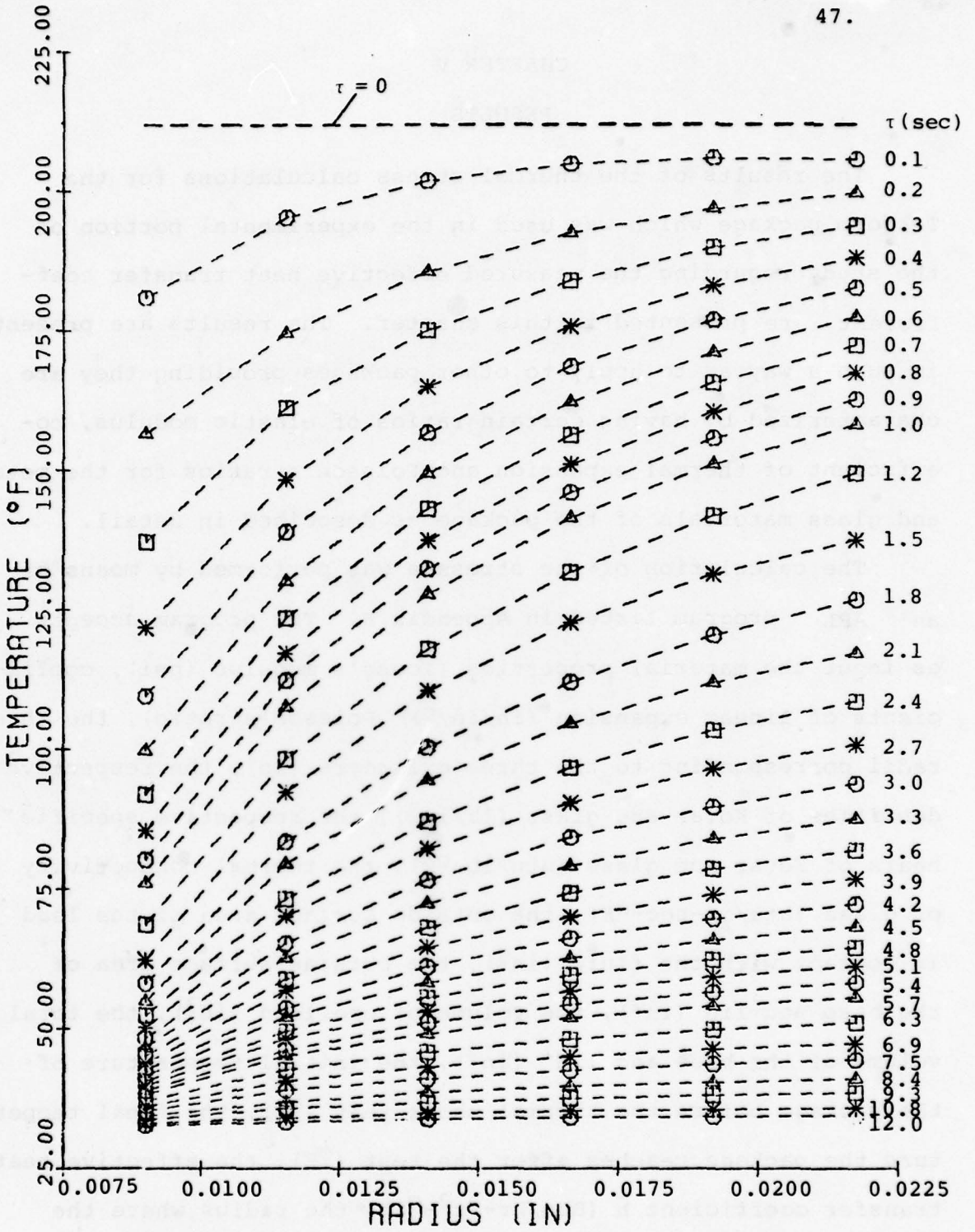

Fig. 14. Radial temperature distribution in the glass annulus at different increments of time when the seal is cooled from 212°F to 32°F.

CHAPTER V

RESULTS

The results of the thermal stress calculations for the Tekform package which was used in the experimental portion of the study regarding the measured effective heat transfer coefficient are presented in this chapter. The results are presented in such a way as to apply to other packages providing they are characterized by having certain ratios of elastic modulus, coefficient of thermal expansion and Poisson's ratios for the metal and glass materials of the package as described in detail.

The calculation of the stresses was performed by means of an APL program listed in Appendix B. The program accepts as input the material properties (Young's modulus (psi), coefficients of linear expansion (in/in/^{o}F), Poisson's ratio), the three radii corresponding to the three cylinders (in), the respective densities of Kovar and glass (lb/in^3), the respective specific heats of Kovar and glass (Btu/lb-^{o}F), the thermal conductivity of glass (Btu/in-sec-^{o}F), the outside surface area of the lead in contact with the fluid (in^2), the outside surface area of the base and lid (in^2), the volume of one lead (in^3), the total volume of the base and lid[1] (in^3), the initial temperature of the package before the thermal shock test (^{o}F), the final temperature the package reaches after the test (^{o}F), the effective heat transfer coefficient $\bar{h}$ (Btu/hr-ft^2-^{o}F), the radius where the stresses are to be evaluated (in), the total number of leads,

---

[1] See footnote on page 20.

the time increment (sec), and the total number of time increments. The output consists of the transient absolute and nondimensional radial and tangential stresses developed at the given radius. A typical example illustrating the use of the program and the output is given in Appendix C.

The results are presented in terms of the following nondimensional parameters:

$$r^* = \frac{\bar{h}A_o}{k_g A_2} r \tag{16}$$

$$\theta^* = \frac{\theta}{\theta_o} \tag{17}$$

$$\tau^* = \frac{\bar{h}A_o}{c_k \rho_k V_\ell} \tau \tag{18}$$

$$\bar{h}^* = \frac{\bar{h}A_o}{c_k \rho_k V_\ell} \tau_r \tag{19}$$

$$E^* = \frac{E_k}{E_g} \tag{20}$$

$$\alpha^* = \frac{\alpha_k}{\alpha_g} \tag{21}$$

$$\sigma^* = \frac{\sigma}{E_g \alpha_g \theta_o} \tag{22}$$

where

r^* = non-dimensional radial parameter

θ^* = non-dimensional temperature ratio

τ^* = non-dimensional time parameter

$\bar{h}^*$ = non-dimensional effective heat transfer coefficient

E^* = non-dimensional Young's modulus ratio

α^* = non-dimensional thermal expansion coefficient ratio

σ^* = non-dimensional stress

θ_o = difference between the high and low extreme temperatures of a thermal shock test

k = subscript representing Kovar

g = subscript representing glass

τ_r = 2.05 sec. which is the time necessary to bring to 90% of its equilibrium temperature a cube of Kovar with a mass of 1 lb when $\bar{h}$ = 210/Btu/hr-ft^2-^{o}F while heating from 32^{o}F to 212^{o}F.

When the thermal stress analysis is applied to the experimental package the results obtained are presented in non-dimensional form. It should be noted that Fig. 15a through Fig. 18 are the illustration of the results for the specific package used in this investigation. Graphs shown in Fig. 19 through 25 apply to packages with circular leads and with the lead and the base made of the same material. Also to be able to use these graphs, the ratio of the Young's modulus of the metal to that of the sealing material for the package under consideration, as well as the ratio of the coefficients of thermal expansion and the ratio of the values of the Poisson's ratio must be equal to the corresponding material property ratio of the experimental package (viz., $E_k/E_g = 2.439$; $\alpha_k/\alpha_g = 1.269$; $\nu_k/\nu_g = 1.364$. For Fig. 19 and 20 which represent the maximum transient stresses, the conditions that $\bar{h}L(A_b/N)/k_g(L-L_o)^2 = 96.459$ and $\rho_k c_k/\rho_g c_g = 1.681$ must be satisfied.

When the Tekform package was taken from $32^{o}F$ to $212^{o}F$ the resulting transient non-dimensional radial and tangential stresses were computed and plotted in Figs. 15a, 15b, 16a, 16b. The dimensional values of the stresses can be obtained for the stresses in these graphs by using Eq. 22 which can be written as $\sigma = \sigma^{*}E_{g}\alpha_{g}\theta_{o}$. The dashed lines in each of these figures represents the stress distribution in the 3-cylinder model. The 3 regions are identified on the graphs as the lead, the glass and the base. Each line shows the stress distribution at a different time. The direction of the change in the stress distribution as time increases is shown on each of these figures.

It is assumed in these graphs that at $\tau = 0$ the entire package is stress-free. Fig. 15a shows that as time increases the radial stresses become compressive for all values of radius and the magnitude of the compressive stress at each radius increases until $\tau = 0.9$ sec. (At this time the maximum non-dimensional compressive radial stress at the lead-glass interface is -0.617 which corresponds to -2333 psi) Fig. 15b represents the continuation of the process. The graph shows that the magnitude of the compressive radial stress at each radial position decreases as time increases. When finally thermal equilibrium is reached at $\tau \triangleq 12$ sec, the radial stress achieves a relatively small tensile value at the lead-glass interface and at the glass-base interface. Inspection of Figs. 15a, and 15b shows that the largest radial stress magnitude occurs at the lead-glass interface soon after immersion in the hot fluid bath. Investigation of several examples

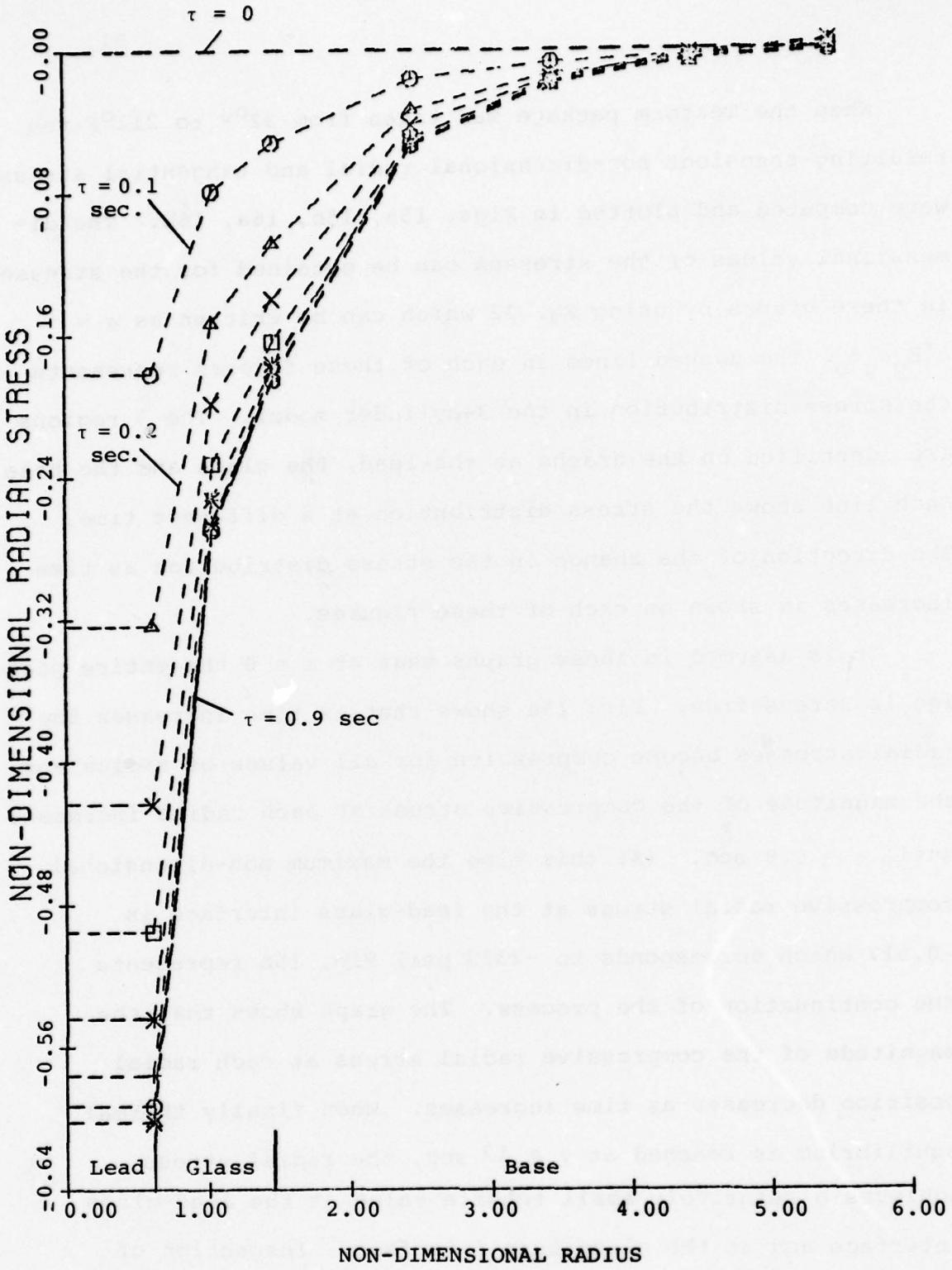

Fig. 15a Non-dimensional radial stress at each radius as a function of time.

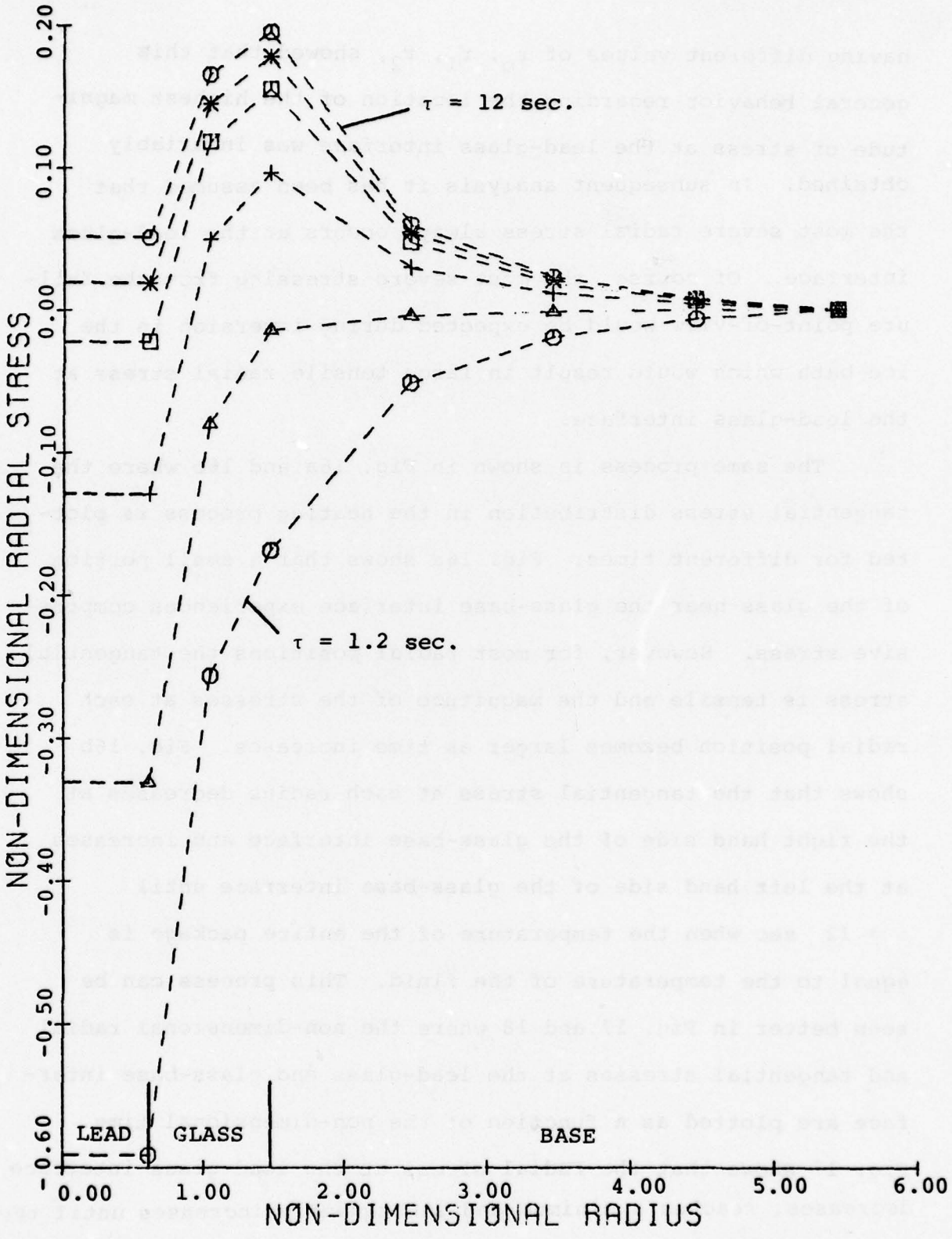

Fig. 15b Non-dimensional radial stress at each radius as a function of time.

having different values of r_o, r_1, r_2, showed that this general behavior regarding the location of the highest magnitude of stress at the lead-glass interface was invariably obtained. In subsequent analysis it has been assumed that the most severe radial stress always occurs at the lead-glass interface. Of course, the most severe stressing from the failure point-of-view would be expected during immersion in the ice bath which would result in large tensile radial stress at the lead-glass interface.

The same process is shown in Fig. 16a and 16b where the tangential stress distribution in the heating process is plotted for different times. Fig. 16a shows that a small portion of the glass near the glass-base interface experiences compressive stress. However, for most radial positions the tangential stress is tensile and the magnitude of the stresses at each radial position becomes larger as time increases. Fig. 16b shows that the tangential stress at each radius decreases at the right hand side of the glass-base interface and increases at the left hand side of the glass-base interface until $\tau \doteq 12$ sec when the temperature of the entire package is equal to the temperature of the fluid. This process can be seen better in Fig. 17 and 18 where the non-dimensional radial and tangential stresses at the lead-glass and glass-base interface are plotted as a function of the non-dimensional time. Fig. 17 shows that the radial stress at the lead-glass interface decreases, reaches a minimum and subsequently increases until the equilibrium value is obtained. The radial stress at the glass base interface also decreases initially until a minimum is

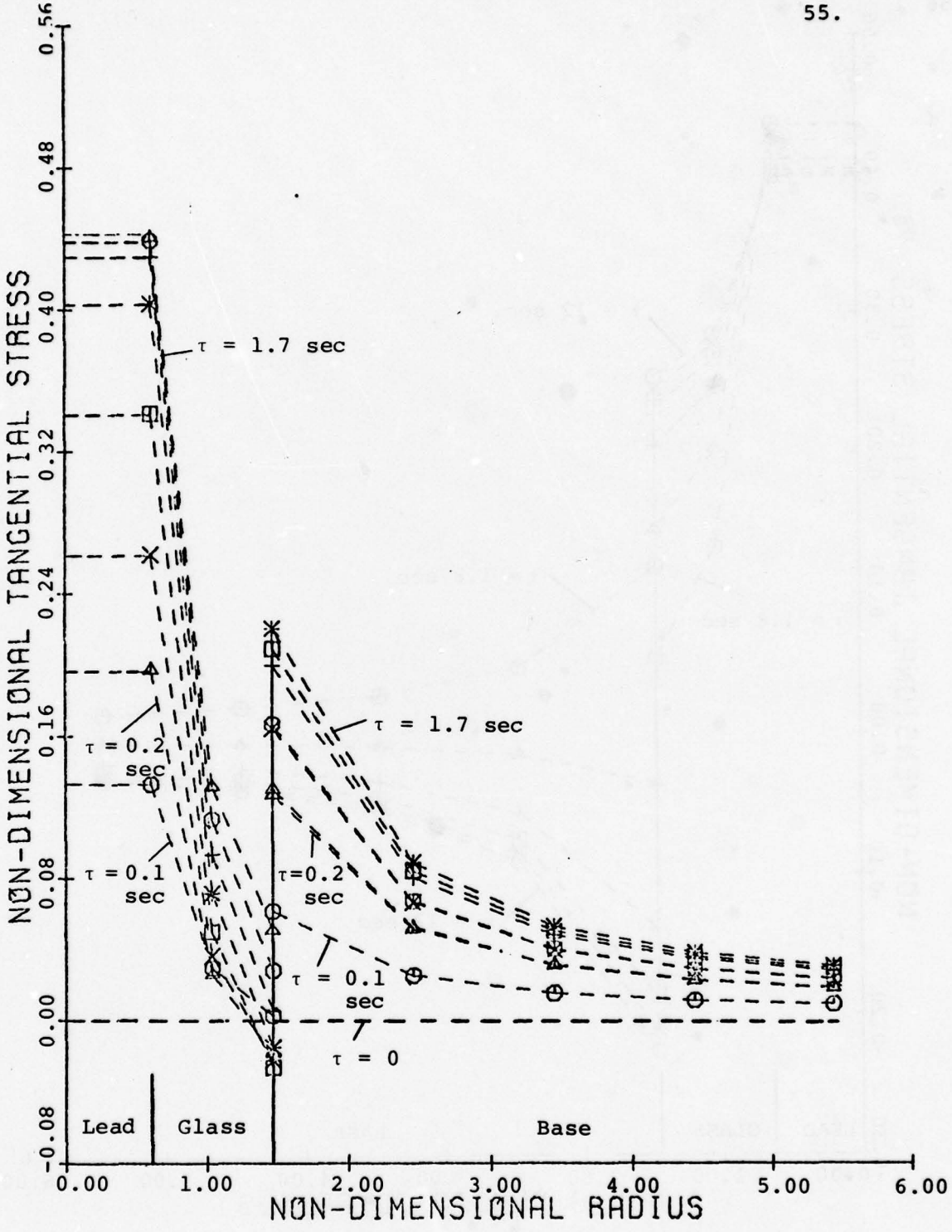

Fig. 16a Non-dimensional tangential stress at each radius as a function of time.

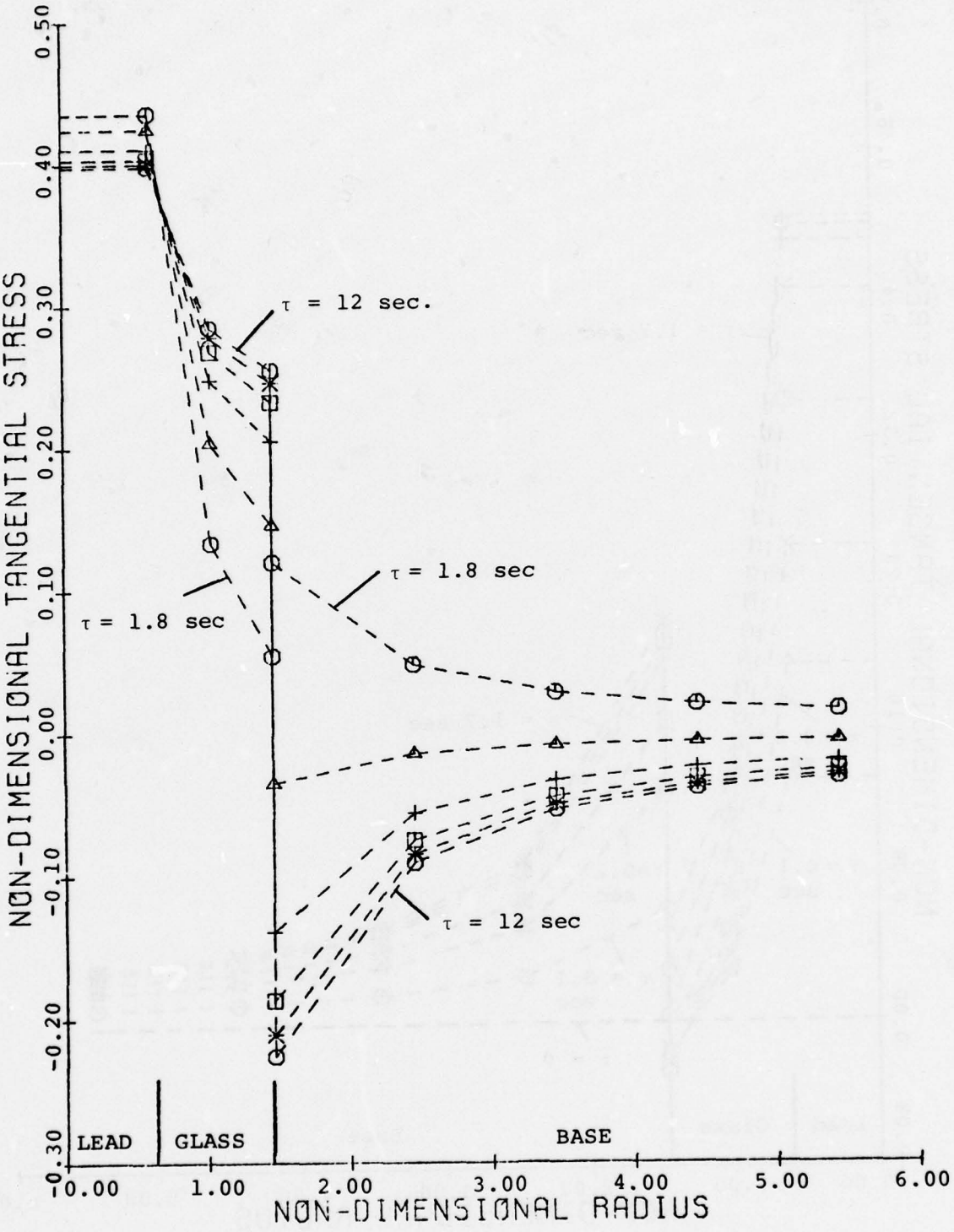

Fig. 16b Non-dimensional tangential stress at each radius as a function of time.

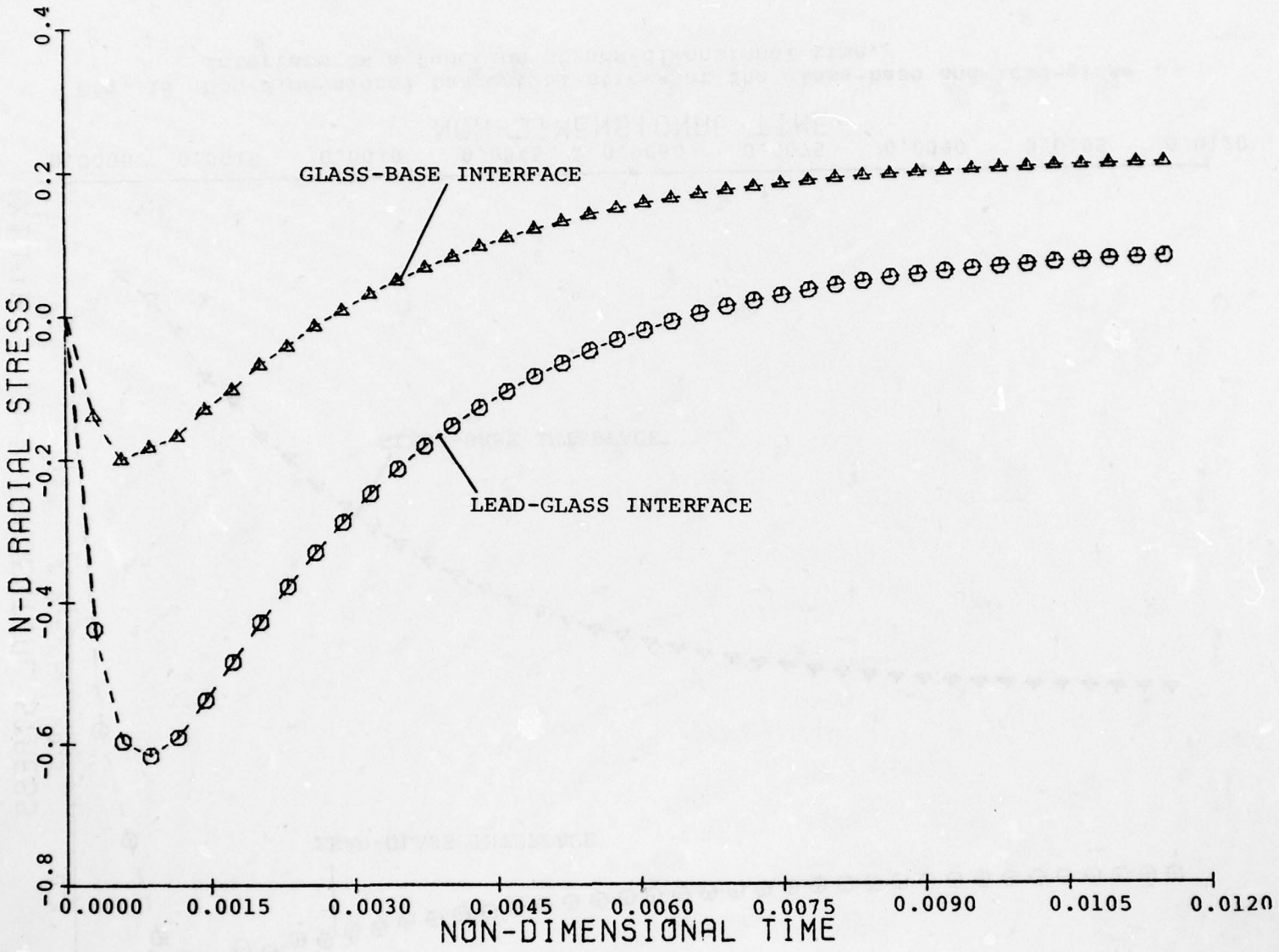

Fig. 17 Non-dimensional radial stress at the glass-base and lead-glass interface as a function of non-dimensional time.

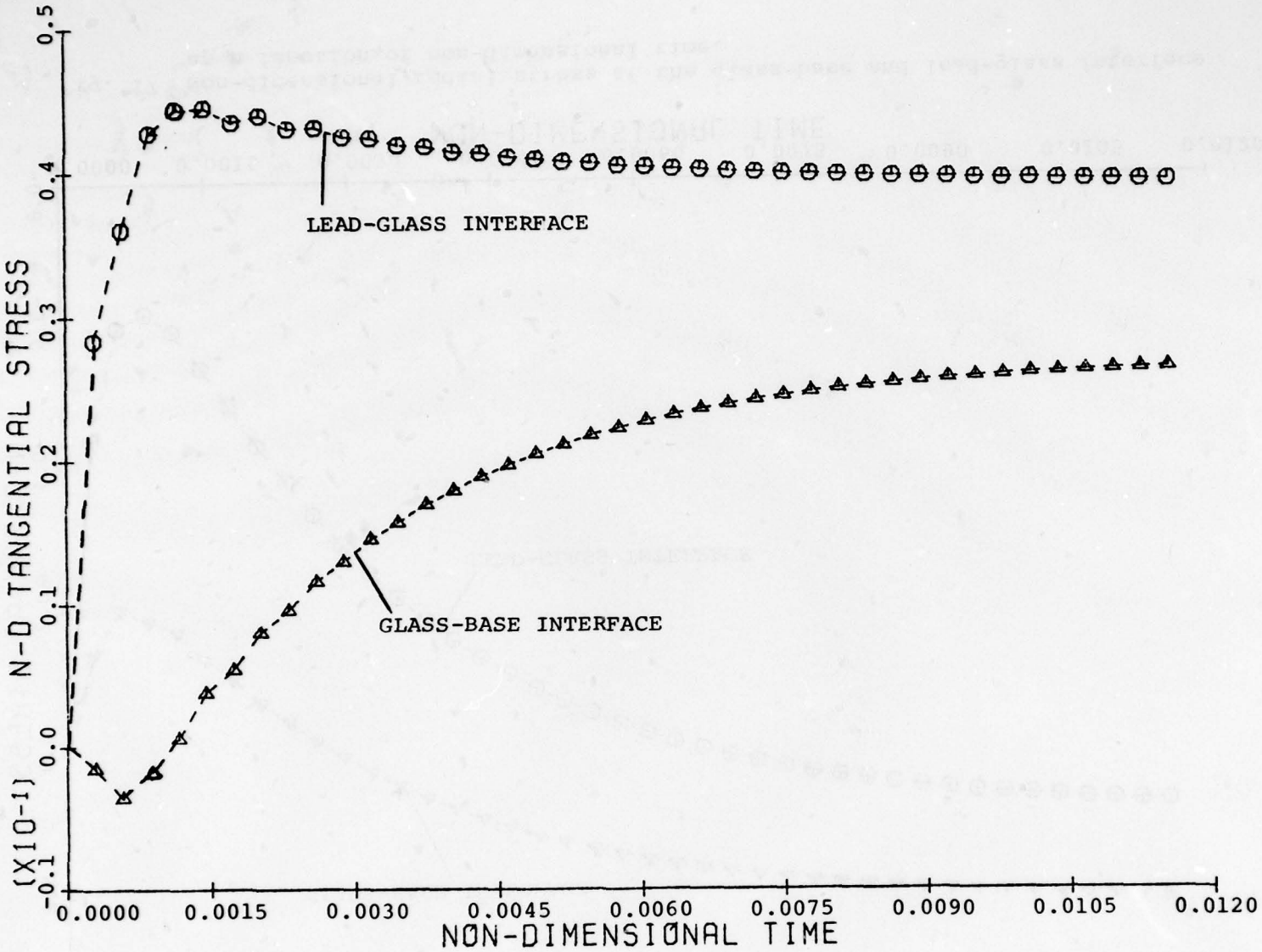

Fig. 18 Non-dimensional tangential stress at the glass-base and lead-glass interface as a function of non-dimensional time.

reached. Thenceforth, the radial stress increases until its equilibrium value is achieved. These maximum and minimum stresses occur when the temperature difference across the 3 cylinders becomes the largest. As the heating process continues this gradient decreases causing the radial stresses to diminish. When the steady-state temperature is reached the radial stresses come to a steady-state value. This residual stress is caused by the mis-match in thermal expansion coefficients of Kovar and glass for this temperature range ($\alpha_k = 3.25 \times 10^{-6}$ in/in-°F, $\alpha_g = 2.56 \times 10^{-6}$ in/in-°F for $32°F < T < 572°F$). Recall that it was assumed that the stresses are zero at the beginning of the heating period.

The transient tangential stress at the lead-glass interface is shown in Fig. 18. This stress passes also through a maximum, then decreases to come to steady-state. The absolute value of the maximum tangential stress in this case is 1685 psi. On the other hand, the tangential stress at the glass-base interface decreases slightly to reach minimum value and then increases until it reaches the steady-state value. These results illustrate the stress behavior of the seal when it is submitted to the heating cycle of the thermal shock test. In the case of a cooling cycle, the numerical results for all of the stresses would be the same as those illustrated for a heating cycle, however, the stresses would be of opposite sign.

In order to assess the importance of knowing the true value of the overall effective heat transfer coefficient $\bar{h}$ for the package insofar as the calculated maximum stress is concerned,

calculations were made for a range of values of $\bar{h}$ consistent with the probable range of uncertainty as determined by experiment. As described in section 4.3, the average value of $\bar{h}$ was found to be 210 Btu/ft^2-hr-^{o}F, however, the experimental values ranged from a low of 70 Btu/ft^2-hr-^{o}F to a high of 375 Btu/ft^2-hr-^{o}F. The influence of changing the value of $\bar{h}$ in the calculation for the stresses is illustrated in Table 2 which records the maximum value of non-dimensional radial stress (at the lead-glass interface) for varying values of $\bar{h}$ ranging from 130-290 Btu/ft^2-hr-^{o}F. As shown in the table, the maximum difference from the stress calculated from 210 Btu/ft^2-hr-^{o}F was about 10 percent. This is not judged to be a large difference, and it is felt that some uncertainty in the true value of $\bar{h}$ does not result in a very large uncertainty in the maximum value of the calculated radial stress at the lead-glass interface. On the other hand, calculations have shown that if $\bar{h}$ is assumed to be ten times larger than its average value (210 Btu/ft^2-hr-^{o}F) the maximum radial stress becomes about 37 percent larger and if $\bar{h}$ is ten times smaller than its average value the maximum radial stress is about 48 percent smaller than the maximum radial stress corresponding to the average value of $\bar{h}$. This represents an important variation. However an effective heat transfer coefficient which is that much different than the average value would correspond to a different heat transfer environment. In fact, the heating and cooling procedure used in thermal cycling tests (as opposed to thermal shock tests) is characterized by a very slow heat transfer process for which $\bar{h}$ would be expected to be very small compared to the $\bar{h}$

$\bar{h}$ (Btu/ft^2 - hr-^{o}F) / σ_{max}^*	130	150	170	190	210	230	250	270	290
Radial	-0.554	-0.574	-0.587	-0.605	-0.617	-0.625	-0.638	-0.653	-0.665
$\%\Delta$ ($\Delta=\lvert\sigma^*_{max}-\sigma^*\rvert_{\bar{h}=210}\rvert$)	10.2	7.6	4.9	1.9	0	1.3	3.4	5.8	7.8
Tangential	0.406	0.418	0.428	0.437	0.447	0.453	0.458	0.464	0.473
$\%\Delta$	8.8	6.1	3.8	1.8	0	1.8	2.9	4.3	6.3

TABLE 2

Maximum non-dimensional transient stresses at the lead-glass interface for different values of $\bar{h}$ compared to the maximum value of the stresses obtained when $\bar{h}$ = 210 Btu/ft -hr-^{o}F

obtained in the thermal shock experiments. Therefore, it would be reasonable to conclude that the small stresses evaluated using an effective heat transfer coefficient 10 times smaller than the average experimentally obtained $\bar{h}$ could be indicative of the stresses occurring during a temperature cycling test.

The analysis concerning the uncertainty of $\bar{h}$ was based on the assumption that the lead and the base have an equal effective heat transfer coefficient. In Chapter IV, however, it was shown that there is some justification for believing that the lead and the base could have different values of $\bar{h}$. The effect of such variation was investigated by assuming values of $\bar{h}$ for the lead and the base differing by 20, 40 and 60 Btu/ft^2-hr-^{o}F and calculating the thermal stresses in each case. The values of $\bar{h}$ given to the base and the lead were always centered around the average value of $\bar{h}$ obtained experimentally. The results are tabulated in Table 3. The percent change between the stresses evaluated using different $\bar{h}$'s (for the lead and the base)[1], and the stresses obtained using the average $\bar{h}$ for both of them is shown to have a maximum value of 15.5 percent. This is not judged to be a large difference. This result justifies the assumption of a unique effective heat transfer coefficient for both the base and the lead.

The results which have been presented to this point were obtained by applying the mathematical model developed for the Tekform package used in the experimental work. However, other microelectronic packages which are commercially available exhibit different characteristics. The present study applies to

---

[1] When $\bar{h}$ for the lead and the base are different, $\bar{h}_{lead}$ instead of $\bar{h}$ is used in Eq. (14) and $\bar{h}_{base}$ instead of $\bar{h}$ is used in Eq. (15).

$\Delta\bar{h}$ Btu/ft^2-hr-^{o}F / Average σ^*_{max}	0	20	40	60
Radial Stress	-0.617	-0.650	-0.681	-0.713
%Δ Percent change	0	5.3	10.3	15.5
Tangential Stress	0.445	0.454	0.460	0.467
%Δ Percent change	0	2.0	3.3	4.9

TABLE 3

Maximum non-dimensional transient stresses at the lead-glass interface when $\bar{h}$ is different for the lead and the base compared to the maximum value of the stresses when $\bar{h}$ = 210 Btu/ft^2-hr-^{o}F. ($\Delta\bar{h} = \bar{h}_{lead} - \bar{h}_{base}$)
Average σ^*_{max} is calculated by averaging the values of the maximum stresses obtained with various values of $\bar{h}_{lead}$ and $\bar{h}_{base}$ for a given $\Delta\bar{h}$. (e.g., for $\Delta\bar{h}$ = 40, the maximum stresses obtained using $\bar{h}_{lead}$ = 250 and $\bar{h}_{base}$ = 210, $\bar{h}_{lead}$ = 230 and $\bar{h}_{base}$ = 190, $\bar{h}_{lead}$ = 210 and $\bar{h}_{base}$ = 170 Btu/ft^2-hr-^{o}F were averaged to obtain the average σ^*_{max}).

all packages which are characterized by certain material property ratios (Young's modulus, thermal expansion coefficients, Poisson's ratio, heat transfer properties) similar to the ratios of the Tekform package which was studied. When this similarity condition is fulfilled the only other factor that affects the stress level is the geometrical characteristic of the package. Since the lead, the glass and the base were modeled as 3 concentric cylinders, the ratios of the cylinder radii (r_o/r_1 and r_1/r_2) influence the stresses. The non-dimensional radial and tangential stresses at the lead-glass interface were computed for different radius ratios and plotted in Fig. 19 and 20. It is believed that these graphs provide the means for evaluating the effect of package geometry on the maximum stresses for most of the microelectronic packages which are commercially available.

Fig. 19 and 20 illustrate the influence of the choice made for the radius of the third cylinder which represents the base of the package. The Tekform package which was used in this study was characterized by a ratio r_1/r_2 equal to 2.417. From Fig. 19 it can be determined that the percent change in the value of the maximum radial stress for $r_1/r_2 = 2.5$ when r_o/r_1 is varied from 1.5 to 4 is 12.6 percent. Fig. 20 shows that the percent change in the tangential stress corresponding to the same value of r_1/r_2 and for the same variation in r_o/r_1 is 4.4 percent. Thus, it appears that for the specific package used for experimental purposes, the choice of the outside radius of the third cylinder is relatively unimportant insofar as the determination of the maximum stress is concerned. It should be

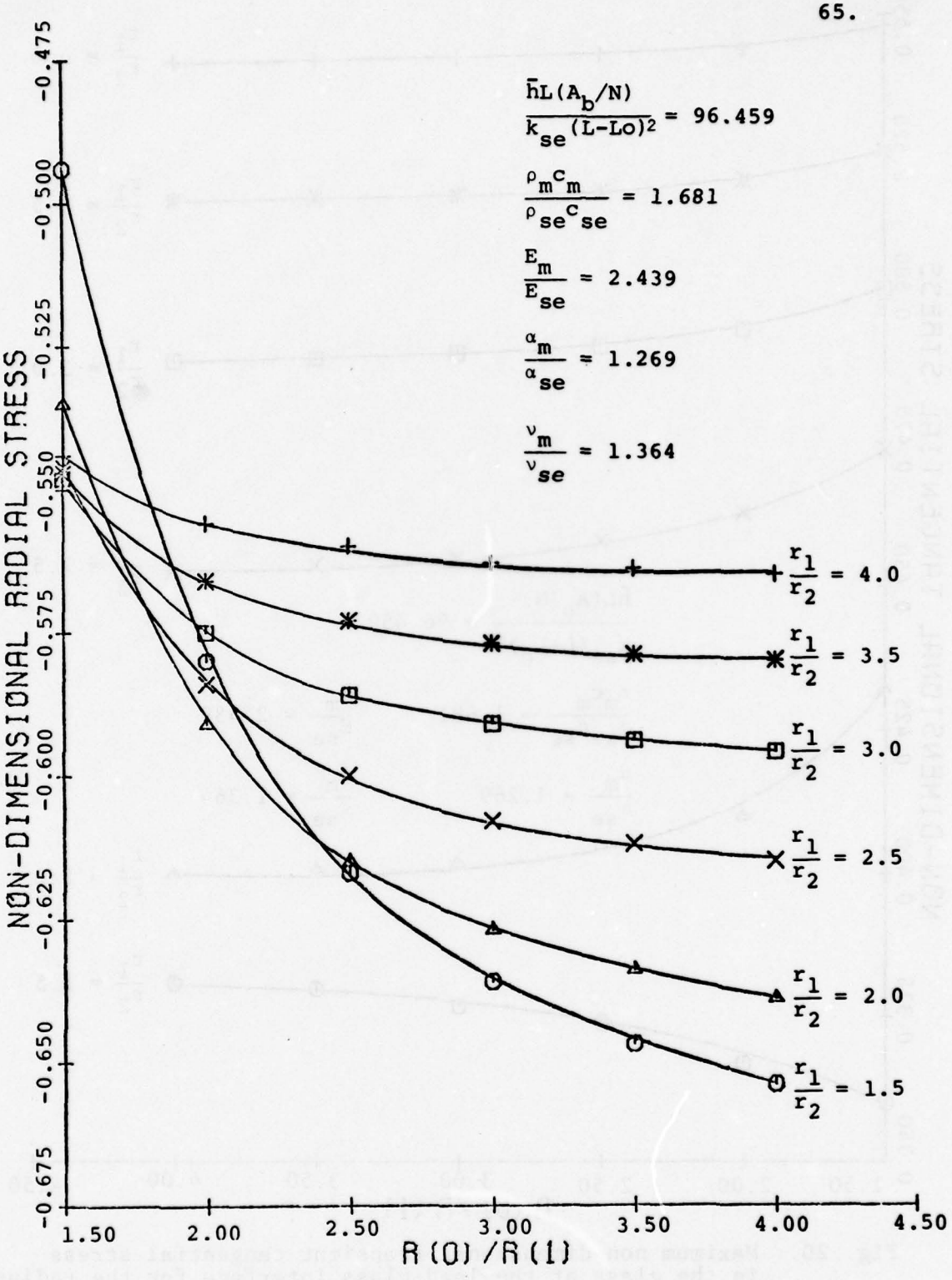

Fig. 19 Maximum non-dimensional transient radial stress in the glass at the lead-glass interface for the radius and material property ratios shown on the figure.

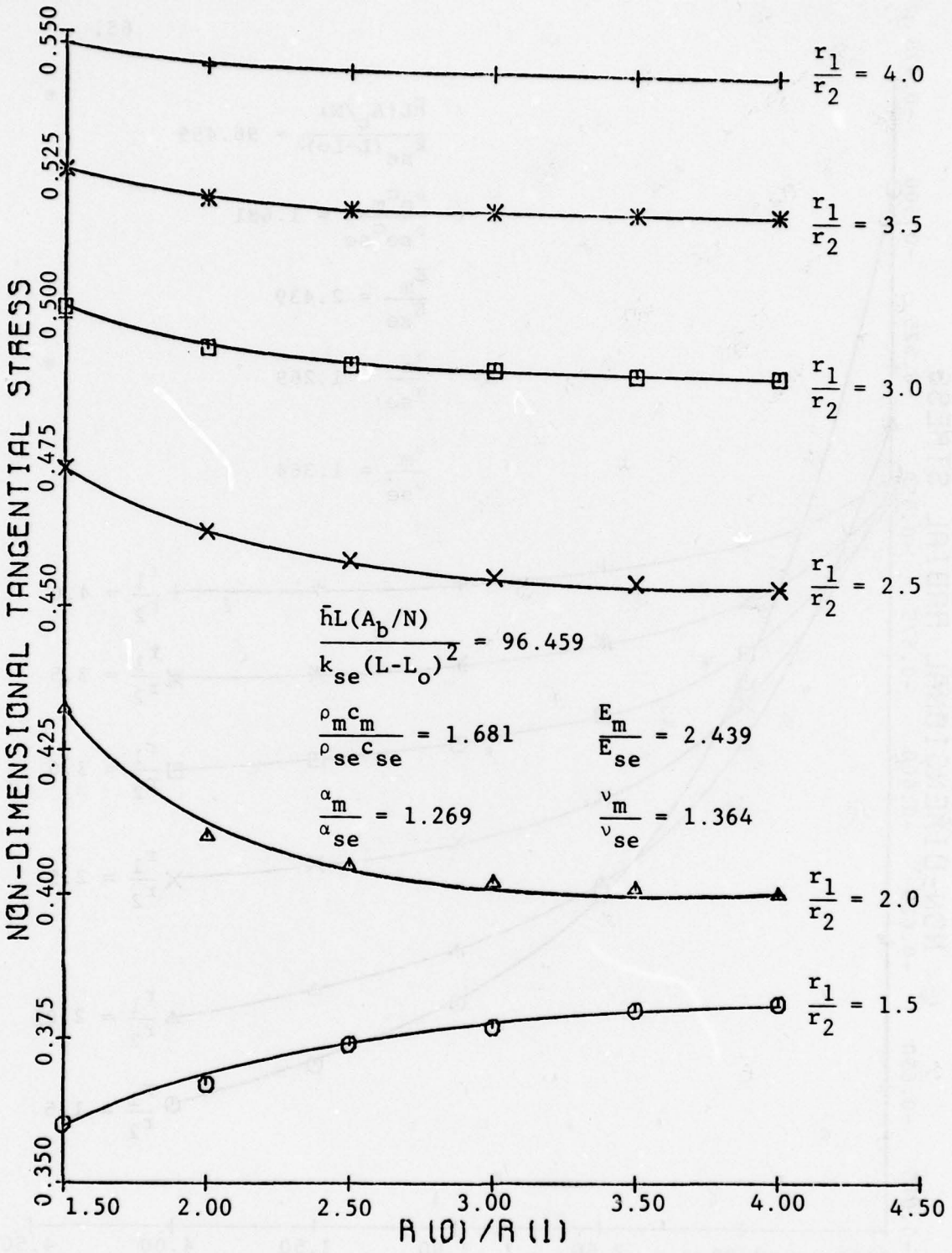

Fig. 20. Maximum non-dimensional transient tangential stress in the glass at the lead-glass interface for the radius and material property ratios shown on the figure.

noted, however, that for other values of the corresponding ratio r_1/r_2 it is possible that the choice of r_o/r_1 could significantly influence the calculated maximum stress.

The thermal shock test condition A (32°F to 212°F) of the MIL-STD-883B was applied to the Tekform package used during the experiments. The maximum radial and tangential stresses occurring during this thermal shock test were presented in non-dimensional form. The thermal shock test procedure includes test levels which are more severe because they require larger temperature extremes. The maximum stress values depend linearly on the temperature of the cold and hot baths. Therefore, the results presented for test A can be easily calculated for any other test level provided that the effective heat transfer coefficient is the same as that determined for test level A. The maximum stress values corresponding to the various test levels for the Tekform experimental package, based on this proviso are presented in Table 4. It should be noted that 5000 psi is a reasonable estimate of the radial tensile strength of the glass-lead interface. Thus, Table 4 indicates that the higher test levels could be damaging to this interface.

	A	B	C	D	E	F
T_i (^oF)	32	-67	-85	-85	-319	-319
T_f (^oF)	212	257	302	392	302	392
σ_{max} (Radial) (psi)	-2333	-4199	-5015	-6181	-8047	-9215
σ_{max} (Tang.) (psi)	1685	3033	3623	4465	5813	6656

TABLE 4

Maximum transient stresses at lead-glass interface for the different levels of thermal shock test conditions as described in MIL-STD-883B.

CHAPTER VI

PRACTICAL APPLICATIONS OF THE RESULTS

The results obtained from this investigation can be used by the designer or the screener of a microelectronic package to predict the maximum stresses in the glass seal when the package is subjected to a thermal shock test.

The package considered must have circular leads and, the leads and the base must be made of the same material. In order to be able to use the graphs provided in the preceding Chapter 5 the package under study must have the same material property ratios as those used in preparing the graphs (19,20,21,22,23,24)

$(E_m/E_{se} = 2.04;\quad \alpha_m/\alpha_{se} = 1.27;\quad \nu_m/\nu_{se} = 1.2;$

$\bar{h}L(A_b/N)/k_{se}(L-L_o)^2 = 96.459;\quad \rho_m c_m/\rho_{se}c_{se} = 1.681)$

The general procedure which is to be followed in order to evaluate the maximum thermal stresses during the thermal shock test is as follows:

1) The maximum values of the stresses at the lead-glass interface are plotted as a function of the radius ratios r_o/r_1 and r_1/r_2. First evaluate r_1/r_2, the ratio of the outside radius of the glass annulus to the radius of the lead. Theoretically, the outside radius of the third cylinder is that radius for which the radial stress is zero. Determine the two possible choices for r_o as shown on Fig. 21. Assume $[r_o]_1$, to be the outside radius of the annulus representing the base and evaluate r_o/r_1.

2) When a microelectronic package is manufactured, residual stresses are present in the glass seal due to the cooling of the seal from the setting point of the glass to room temperature, and the fact that the thermal expansion coefficients of the metal and the glass are usually not equal. Evaluate the non-

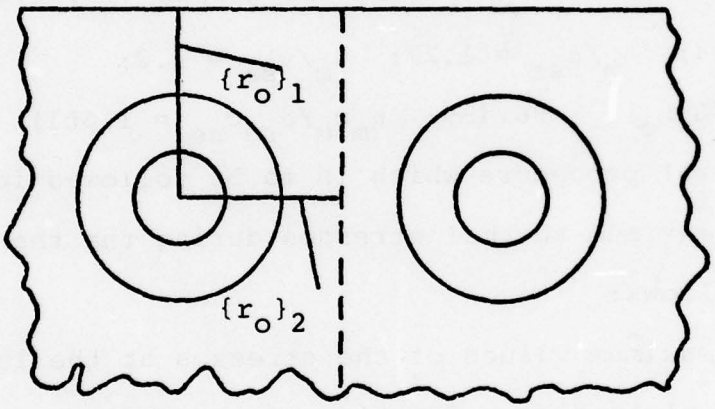

Fig. 21 Representation of the two possible choices of an outside radius in the 3-cylinder model.

dimensional radial and tangential residual stresses in the seal using Fig. 22 and 23. Note that α_m/α_{se} for this case is very close to 1 since for this temperature interval the coefficients of thermal expansion for the metal and glass are matched. Determine the absolute value of the stresses using

$$\sigma^* = \frac{\sigma}{E_g \sigma_g \theta_o} \tag{22}$$

or

$$\sigma = \sigma^* E_g \sigma_g \theta_o \tag{23}$$

where θ_o represents the temperature difference $T_{\text{HIGHER TEMP. BATH}} - T_{\text{LOWER TEMP. BATH}}$.

3) At the end of each thermal shock cycle, after thermal equilibrium has been reached, the thermal stresses reach their steady-state values. Determine the steady-state non-dimensional radial and tangential stress when the package is taken from the lower temperature bath to the higher temperature bath by means of Fig. 24 and 25. Compute the absolute value of the stresses using Eq. 23.

4) The first step in the thermal shock test procedure is to immerse the package in the lower temperature bath. Evaluate the residual stresses when temperature equilibrium is reached at the lower temperature bath by multiplying the absolute values of the stresses obtained in step 3 by θ_r/θ_o where $\theta_r = T_{\text{LOW TEMP. BATH}} - T_{\text{ROOM}}$.

5) When the package is transferred from the lower temperature bath to the higher temperature bath a transient maximum stress occurs. Evaluate the transient maximum non-dimensional

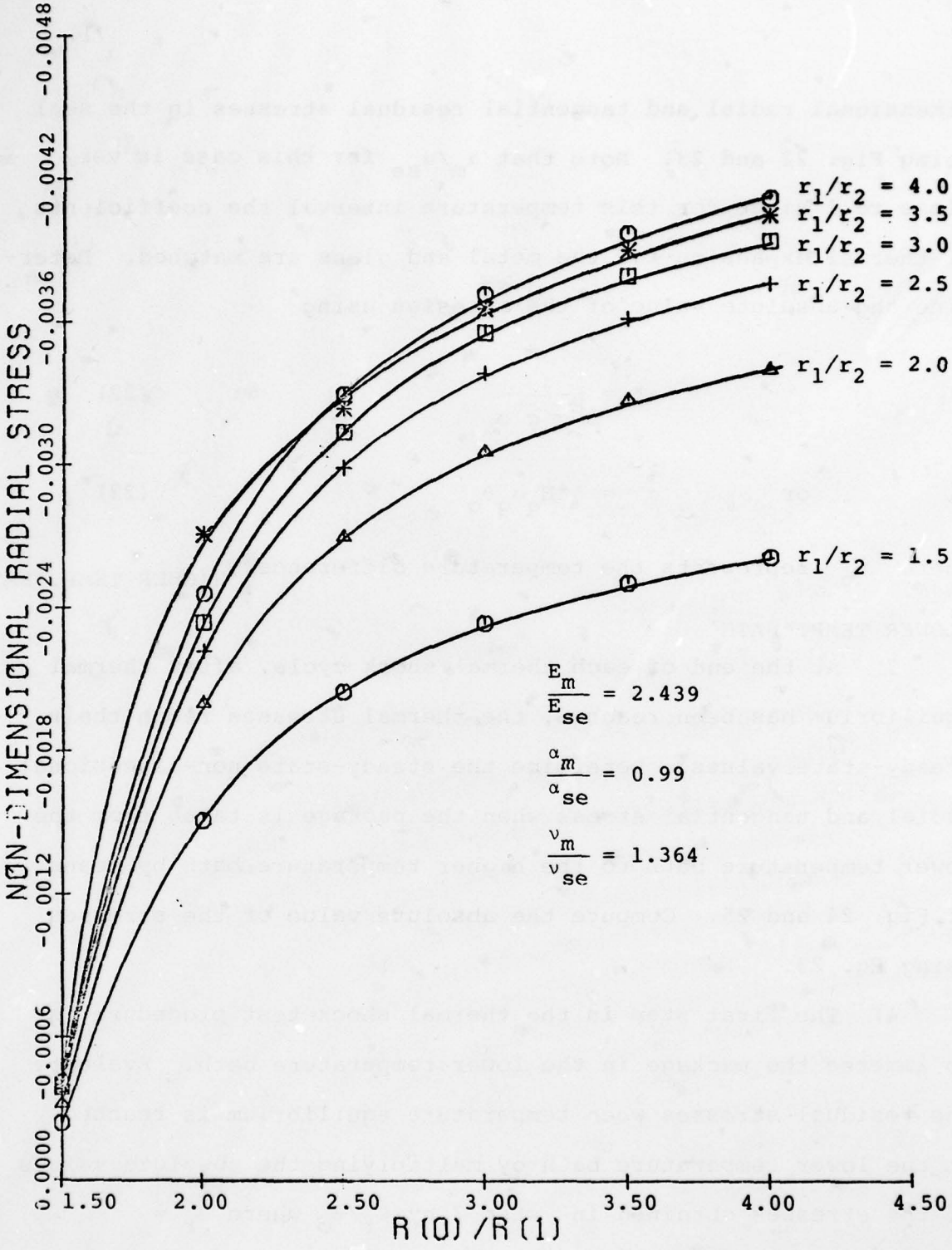

Fig. 22 Non-dimensional residual radial stress in the glass at the lead-glass interface for the radius and material ratios shown on the figure.

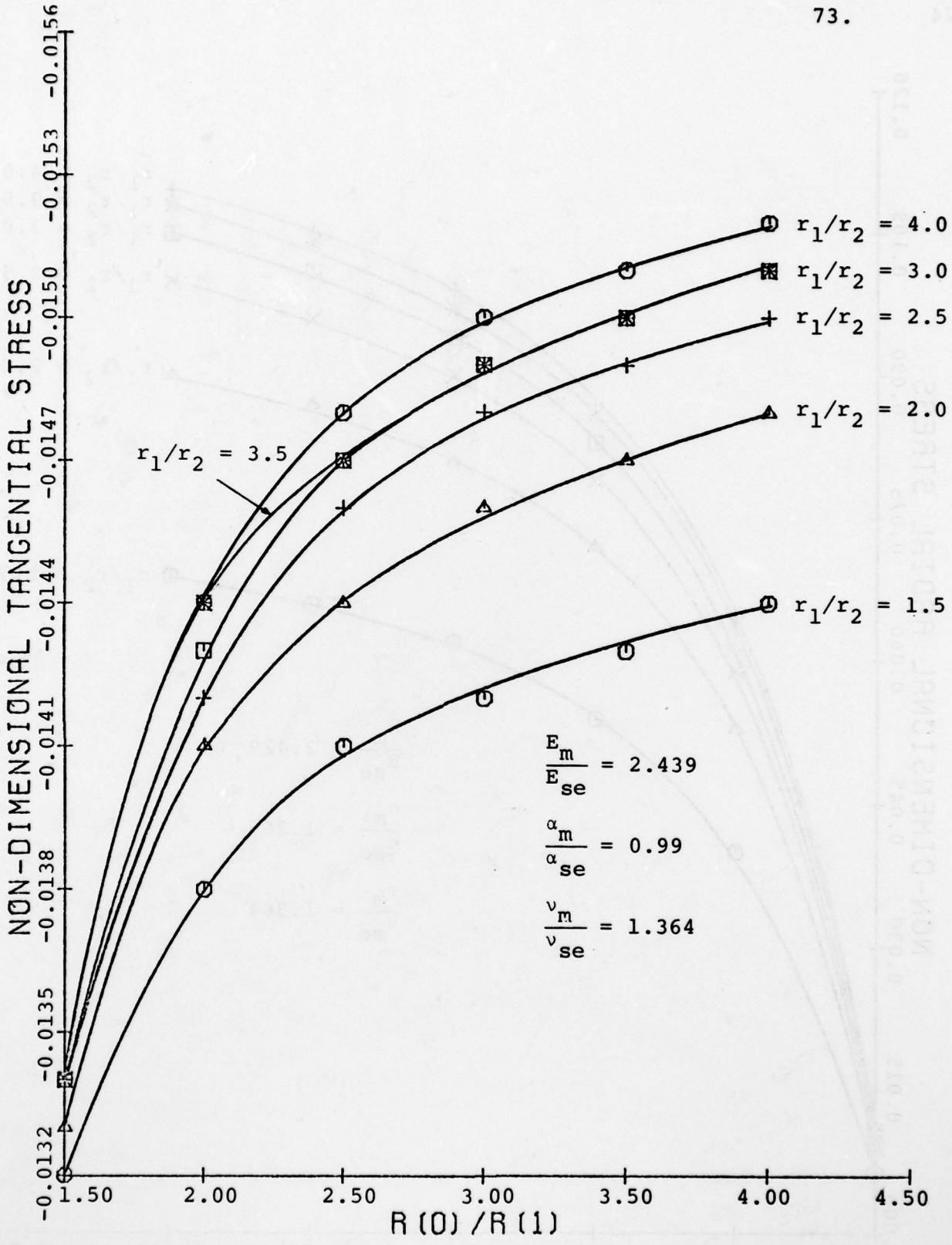

Fig. 23 Non-dimensional residual tangential stress in the glass at the lead-glass interface for the radius and material property ratios shown on the figure.

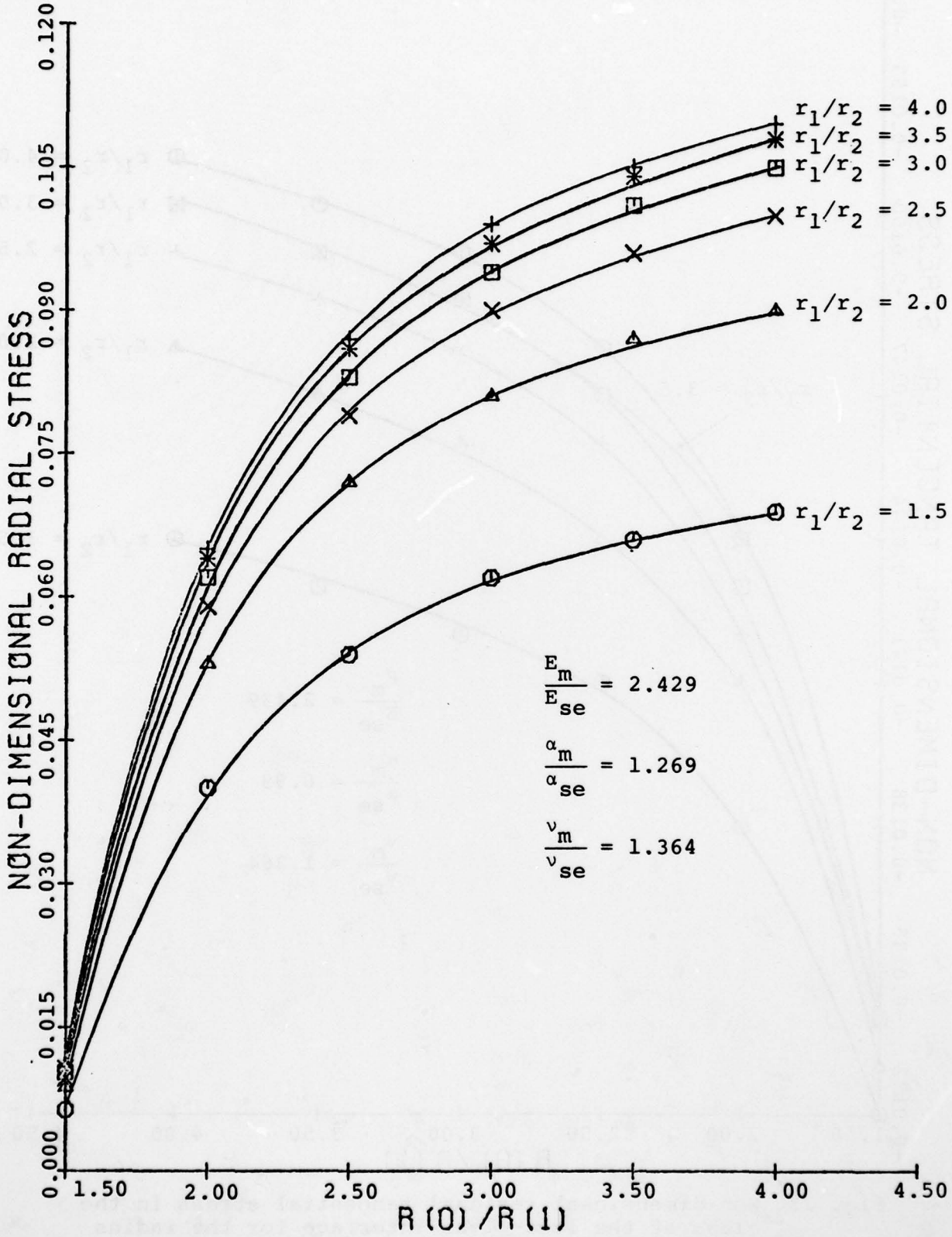

Fig. 24 Non-dimensional steady-state stress in the glass at the lead-glass interface for the radius and material property ratios shown on the figure.

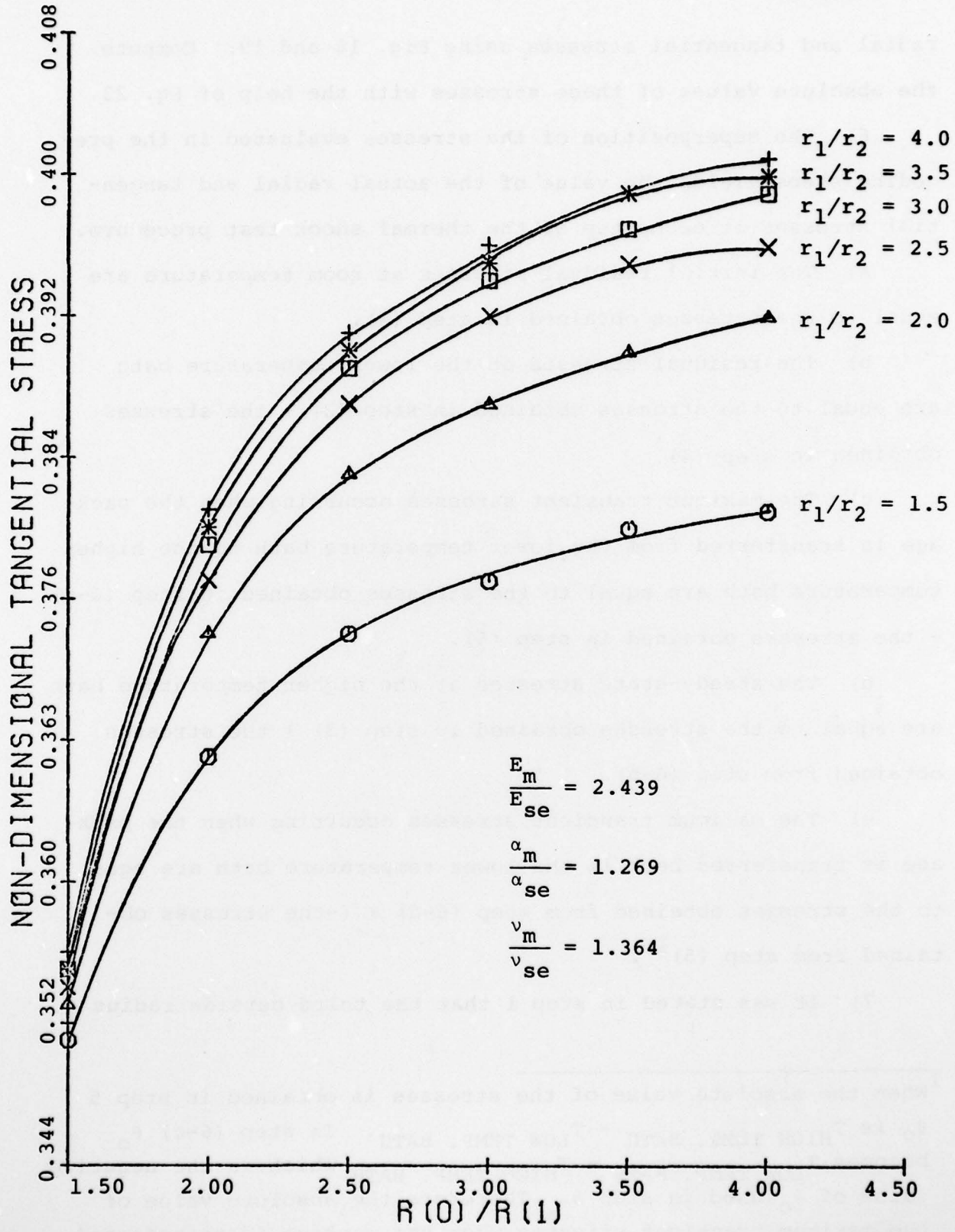

Fig. 25 Non-dimensional steady-state tangential stress in the glass at the lead-glass interface for the radius and material property ratios shown on the figure.

radial and tangential stresses using Fig. 18 and 19. Compute the absolute values of these stresses with the help of Eq. 23.

6) The superposition of the stresses evaluated in the preceding steps yields the value of the actual radial and tangential stresses at each step of the thermal shock test procedure.

a) The initial residual stresses at room temperature are equal to the stresses obtained in step (2).

b) The residual stresses at the lower temperature bath are equal to the stresses obtained in step (2) + the stresses obtained in step (4).

c) The maximum transient stresses occurring when the package is transferred from the lower temperature bath to the higher temperature bath are equal to the stresses obtained in step (6-b) + the stresses obtained in step (5).

d) The steady-state stresses at the higher temperature bath are equal to the stresses obtained in step (3) + the stresses obtained from step (6-b).

e) The maximum transient stresses occurring when the package is transferred back in the lower temperature bath are equal to the stresses obtained from step (6-d) + (-the stresses obtained from step (5)[1]).

7) It was stated in step 1 that the third outside radius

---

[1] When the absolute value of the stresses is obtained in step 5 θ_o is $T_{\text{HIGH TEMP. BATH}} - T_{\text{LOW TEMP. BATH}}$. In step (6-c) θ_o becomes $T_{\text{LOW TEMP. BATH}} - T_{\text{HIGH TEMP. BATH}}$ which is the negative value of θ_o used in step 5. Therefore the absolute value of the maximum transient stresses when the package is transferred from the higher to the lower temperature bath is the negative of the ones obtained in step 5.

representing the base can have two values. To compare the effects of the two possible radii on the thermal stress history of the seal, replace $[r_o]_1$ by $[r_o]_2$ and repeat the entire procedure until the end of step 6.

Repeating the transfer of the package from the lower temperature bath to the higher temperature bath and back again as required by the thermal shock test procedure yields the maximum transient stresses determined in steps (6-c) and (6-e).

The following example illustrates the procedure explained above.

EXAMPLE: An Isotronics flatpack type package with the lead-glass-base configuration as shown in Fig. 26 is subjected to the test condition B of the thermal shock test. The temperature extremes for this test are given as $-67^{o}F$ and $257^{o}F$. The leads and the base are made of Kovar and it is assumed that 7052 Corning glass is used for sealing the leads to the base. Using the procedure described above, the history of the maximum thermal stresses is calculated.

Step 1 - The radius of the lead is 0.01" and the radius of the glass is 0.035". Therefore the ratio is

$$r_1/r_2 \approx 3.5$$

The reasonable candidates for the assumed outside radii are $[r_o]_1 = .06"$ and $[r_o]_2 = .05"$. $[r_o]_1$ is chosen first and the other radius ratio becomes

$$[r_o]_1/r_1 = 1.71$$

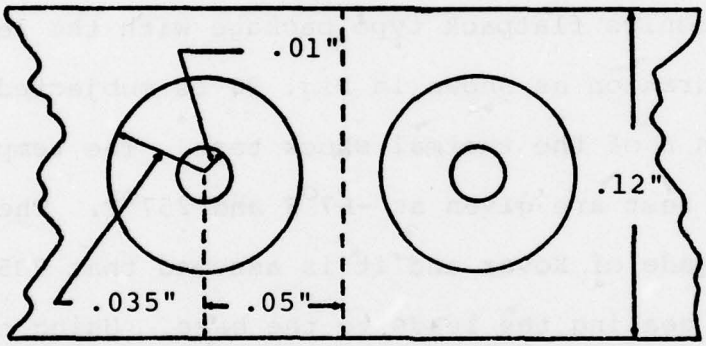

Fig. 26 Schematic Representation of the lead-through and the base of an Isotronics Package.

Step 2 - The non-dimensional residual stresses after cooling to room temperature are

(Using Fig. 22) Radial stress = -.00146

(Using Fig. 23) Tangential stress = -0.0139

The materials (Kovar and glass) being the same as the ones used in this study, the ratios of material properties are equal to those on Fig. 22 and 23. The absolute value of the stresses is evaluated using Eq. (23) where $E_g = 8.2 \times 10^6$ psi, $\alpha_g = 2.95 \times 10^{-6}/^{o}F$, $\theta_o = 77 - 817 = -740^{o}F$ for this step. The absolute values for the stresses are

Radial stress = $-.00146 \times 8.2 \times 10^6 \times 2.95 \times 10^{-6} \times -740 = 26.13$ psi

Tangential stress = $-0.0139 \times 8.2 \times 10^6 \times 2.95 \times 10^{-6} \times -740 = 248.82$ psi.

Step 3 - The non-dimensional steady-state stresses at the higher temperature bath are

(Using Fig. 24) Radial stress = 3.87×10^{-2}

(Using Fib. 25) Tangential stress = 36.3×10^{-2}

The absolute values of these stresses using $E_g = 8.2 \times 10^6$ psi, $\alpha_g = 2.56 \times 10^{-6}/^{o}F$ and $\theta_o = 257 - (-67) = 324^{o}F$ is

Radial stress = $3.87 \times 10^{-2} \times 8.2 \times 10^6 \times 2.56 \times 10^{-6} \times 324 = 263.21$ psi

Tangential stress = $36.3 \times 10^{-2} \times 8.2 \times 10^6 \times 2.56 \times 10^{-6} \times 324 = 2468.91$ psi.

Step 4 - The steady-state stresses after immersing the package from room temperature in the low temperature bath are evaluated using

$$\theta_r = -67 - 77 = 144^{o}F$$

Thus using the absolute values of the stresses obtained in Step 3 these stresses are

$$\text{Radial stress} = 263.21 \times \frac{-144}{324} = -116.98 \text{ psi}$$

$$\text{Tangential stress} = 2468.91 \times \frac{-144}{324} = -1097.29 \text{ psi.}$$

Step 5 - The non-dimensional maximum transient thermal stresses are

(Using Fig. 19) Radial stress = -55.7×10^{-2}

(Using Fig. 20) Tangential stress = 52.4×10^{-2}

with absolute values

$$\text{Radial stress} = -55.7 \times 10^{-2} \times 8.2 \times 10^{6} \times 2.56 \times 10^{-6} \times 324 = -3788.38 \text{ psi}$$

$$\text{Tangential stress} = 52.4 \times 10^{-2} \times 8.2 \times 10^{6} \times 2.56 \times 10^{-6} \times 324 = 3563.94 \text{ psi.}$$

Step 6 - The sequence of the thermal stress is:

a) Initial residual stresses:

$\sigma_r = 26.13$ psi

$\sigma_\phi = 248.82$ psi

b) Steady-state stresses at low temperature bath:

$\sigma_r = 26.13 - 116.98 = -90.85$ psi

$\sigma_\phi = 248.82 - 1097.29 = -848.47$ psi

c) Maximum transient stresses going from low to high temperature bath

$\sigma_r = -90.85 - 3788.38 = -3879.23$ psi

$\sigma_\phi = -848.47 + 3563.94 = 2715.47$ psi

d) Steady-state stresses at higher temperature bath:

$\sigma_r = 263.21 - 90.85 = 172.36$ psi

$\sigma_\phi = 2468.91 - 848.47 = 1620.44$ psi

e) Maximum transient stresses going from high to low temperature bath:

$$\sigma_r = 172.36 - (-3788.38) = 3960.74 \text{ psi}$$

$$\sigma_\phi = 1620.44 - 3563.94 = -1943.50 \text{ psi}$$

This cycle is shown in Fig. 26.

Step 7 - The same procedure is repeated using $[r_o]_2$. In this case $[r_o]_2/r_1 = 1.43$. Since this ratio is not given in the graphs it will be assumed that $r_o/r_1 = 1.5$. r_1/r_2 is the same as before, i.e., 3.5.

Step 2 - The non-dimensional residual stresses at room temperature are:

(Using Fig. 22) Radial stress = -.00040
(Using Fig. 23) Tangential stress = $-.134 \times 10^{-1}$

The absolute values are

$$\text{Radial stress} = -.00040 \times 8.2 \times 10^6 \times 2.95 \times 10^{-6} \times -740 = 7.16 \text{ psi}$$

$$\text{Tangential stress} = -.134 \times 10^{-1} \times 8.2 \times 10^6 \times 2.95 \times 10^{-6} \times -740 = 239.87 \text{ psi}$$

Step 3 - The non-dimensional steady-state stresses at the higher temperature bath are:

(Using Fig. 24) Radial stress = .0107
(Using Fig. 25) Tangential stress = .355

The absolute values of these stresses are

$$\text{Radial stress} = .0107 \times 8.2 \times 10^6 \times 2.56 \times 10^{-6} \times 324 = 72.78 \text{ psi}$$

$$\text{Tangential stresses} = .355 \times 8.2 \times 10^6 \times 2.56 \times 10^{-6} \times 324 = 2414.50 \text{ psi}$$

Step 4 - The steady-state stresses after immersing the package from room temperature in the low temperature bath are evaluated using

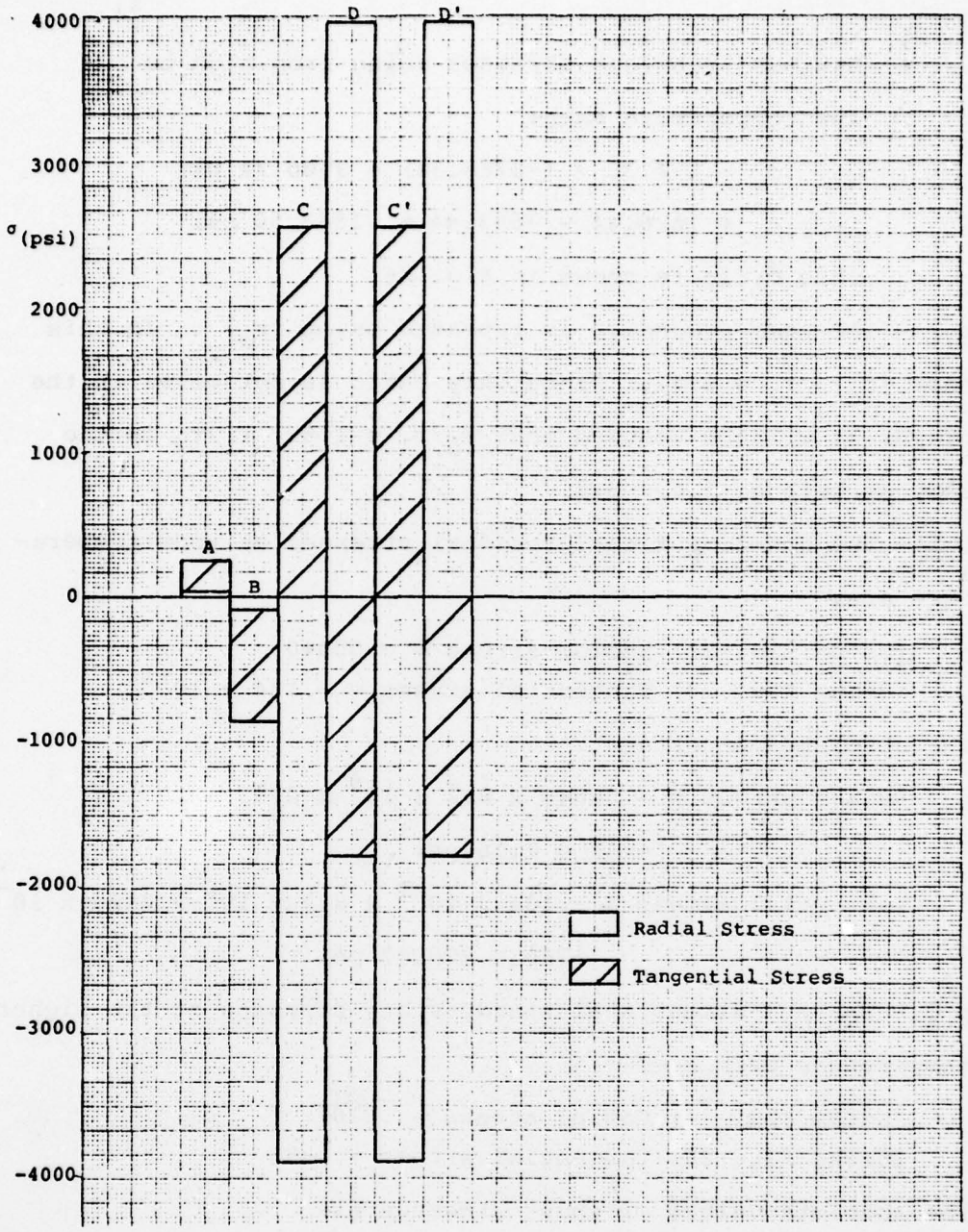

Fig. 26. Thermal stresses for test condition B (-67°F - 257°F) when $r_o = [r_o]_1 = 0.06"$.

A = stress at room temperature; B = stress at lower temperature bath; C = maximum transient stress when the package is immersed in the higher temperature bath; D = maximum transient stress when the package is immersed back in the lower temperature bath; C' = repetition of low-to-high cycle; D' = repetition of high-to-low cycle.

$\theta_r = -67 - 77 = -144^{\circ}F$

Thus using the absolute values of the stresses obtained in Step 3 these stresses are

Radial stress = $72.78 \times \frac{-144}{324} = -32.35$ psi

Tangential stress = $2414.50 \times \frac{-144}{324} = -1073.11$ psi

Step 5 - The non-dimensional maximum transient thermal stresses are:

(Using Fig. 19) Radial stress = -.547

(Using Fig. 20) Tangential stress = .526

The absolute values of these stresses are

Radial stress = $-.547 \times 8.2 \times 10^6 \times 2.56 \times 10^{-6} \times 324 = -3720.37$ psi

Tangential stress = $.526 \times 8.2 \times 10^6 \times 2.56 \times 10^{-6} \times 324 = 3577.54$ psi

Step 6 - The sequence of the thermal stresses is:

a) Initial residual stresses

$\sigma_r = 7.16$ psi

$\sigma_\phi = 239.87$ psi

b) Steady-state stresses at low temperature bath:

$\sigma_r = 7.16 - 32.35 = -25.19$ psi

$\sigma_\phi = 239.87 - 1073.11 = -833.24$ psi

c) Maximum transient stresses going from low to high temperature bath:

$\sigma_r = -25.19 - 3720.37 = -3745.56$ psi

$\sigma_\phi = -833.24 + 3577.54 = 2744.30$ psi

d) Steady-state stresses at higher temperature bath:

$\sigma_r = 72.78 - 25.19 = 47.59$ psi

$\sigma_\phi = 2414.50 - 833.24 = 1581.26$ psi

e) Maximum transient stresses going from high to low temperature bath:

$\phi_r = 47.59 - (-3720.37) = 3767.96$ psi

$\sigma_\phi = 1581.26 - 3577.54 = -1996.28$ psi

This cycle is shown in Fig. 27.

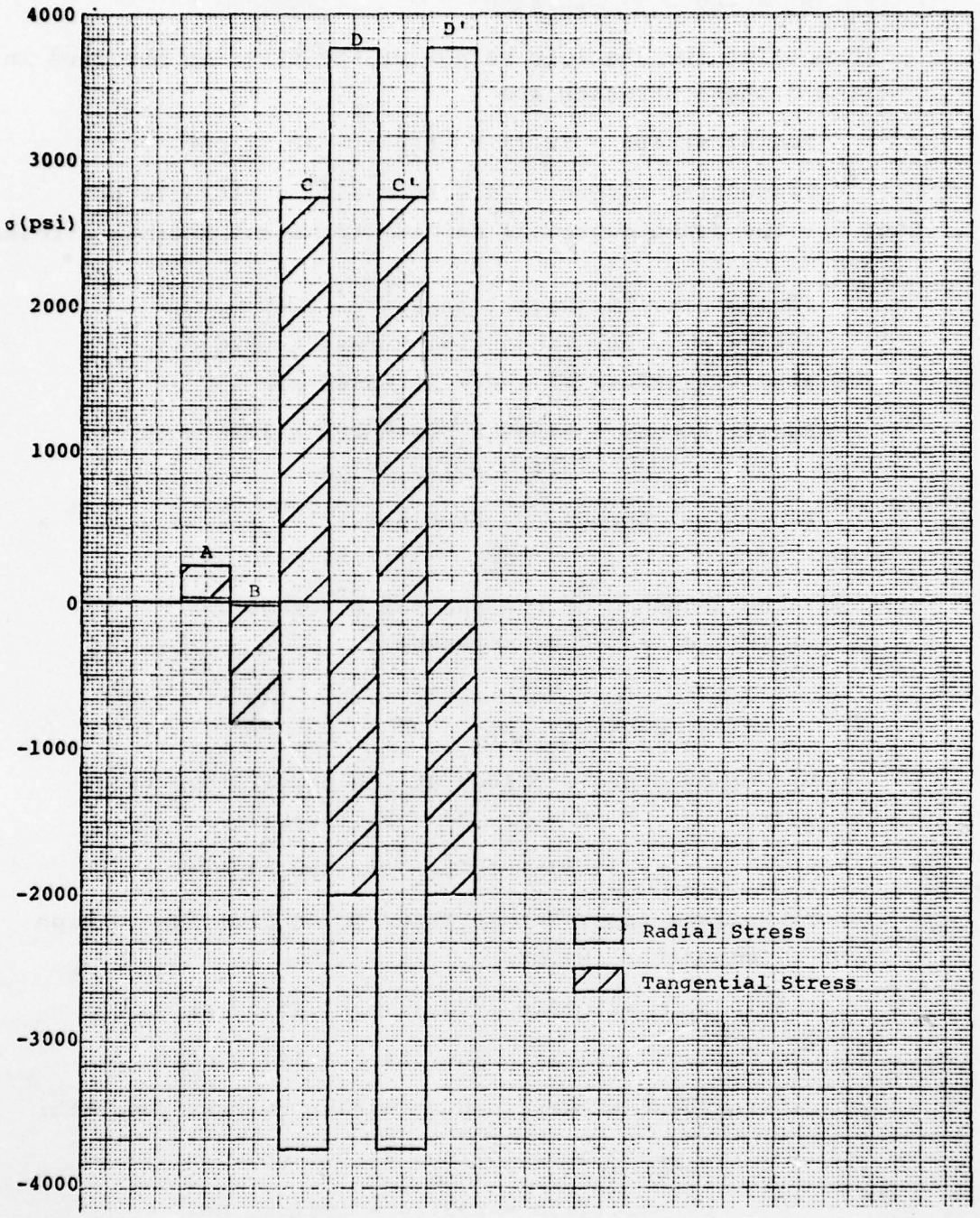

Fig. 27. Thermal stresses for test condition B (-67°F - 257°F) when $r_o = [r_o]_2 = 0.05"$.

A = stress at room temperature; B = stress at lower temperature bath; C = maximum transient stress when the package is immersed in the higher temperature bath; D = maximum transient stress when the package is immersed back in the lower temperature bath; C' = repetition of low-to-high cycle; D' = repetition of high-to-low cycle.

CHAPTER VII
CONCLUSIONS AND RECOMMENDATIONS

The mathematical model developed in this study enables one to evaluate the transient thermal stresses that are experienced in the annular glass seal of a microelectronic package with circular leads when it is subjected to a thermal shock test.

The results show that the transient radial stresses occurring during the thermal shock test which are caused by large temperature gradients can become significantly higher than the stresses associated with a uniform temperature distribution which are due to a mis-match in the thermal expansion coefficients of the metal and the glass. When the transient tangential stress is compared with the stresses that would occur due to only a mis-match in thermal expansion coefficients α_m and α_{se}, the difference is shown to be very small. The comparison made above can be illustrated using the results of the example given in the preceding chapter. The transient maximum radial stress when the package is heating was calculated to be -3788.38 psi whereas the steady-state stress value at thermal equilibrium was 263.21 psi. For the tangential stresses, the maximum transient stress was 3393.90 psi while the steady-state value was 2468.91 psi.

Information concerning the expected values of the maximum transient thermal stresses as influenced by the geometry of the seal, the effective heat transfer coefficient and the different thermal shock test conditions as presented in this study is important in two ways. From a design point of view, the factors affecting the stress level can be adjusted in order to reduce the maximum stresses so that the possibility of failure of the

AD-A073 654 SYRACUSE UNIV NY DEPT OF MECHANICAL AND AEROSPACE E--ETC F/G 20/13
THERMAL STRESS ANALYSIS OF GLASS SEALS IN MICROELECTRONIC PACKA--ETC(U)
JUL 79 K KOKINI, R W PERKINS, C LIBOVE F30602-78-C-0083

UNCLASSIFIED MAE-1233-T2 RADC-TR-79-201 NL

2 OF 2
AD A073654

END
DATE FILMED
10-79
DDC

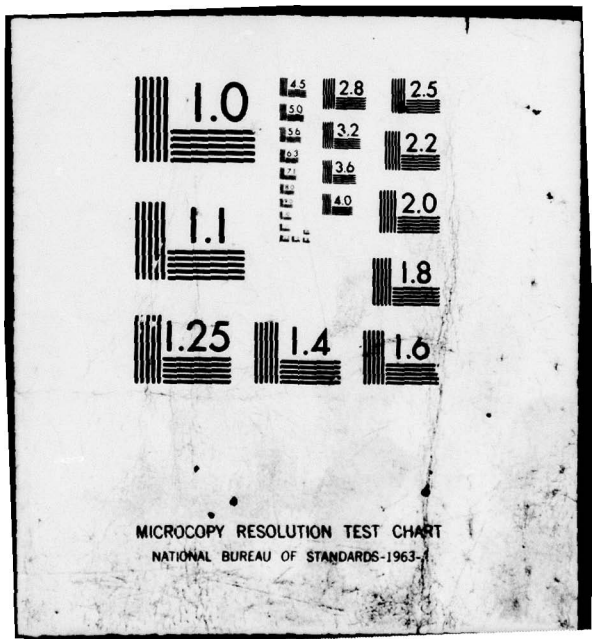
1.0
1.1
1.25
1.4
1.6
1.8
2.0
2.2
2.5
2.8
3.2
3.6
4.0
4.5
5.0
5.6
6.3
7.1
MICROCOPY RESOLUTION TEST CHART
NATIONAL BUREAU OF STANDARDS-1963-A

seal could be diminished. From the screener's point of view, the results can be used to predict what regions of the seal will be stressed significantly and how severe the test will be when a given thermal shock procedure is applied to the package. Conversely, when a certain stress level is desired in the seal, the proper test level can be selected by the use of the results of the present study.

The APL programs which have been developed to compute the transient thermal stresses have been described in Chapter V. The inputs for these programs (consisting of the Young's moduli for the 3 materials, the coefficients of thermal expansion for the 3 materials, the Poisson's ratios for the 3 materials, the 3 radii corresponding to the 3 cylinders, the densities for the 3 materials, the specific heats for the 3 materials, the thermal conductivity of the sealing material, the outside surface area of the lead in contact with the fluid, the outside surface area of the base and lid, the volume of one lead, the total volume of the base and lid, the initial temperature of the package, the final temperature of the package, the effective heat transfer coefficient, the radius where the stresses are to be evaluated, the total number of leads, the time increment and the total number of time increments) are not restricted to materials with property ratios equal to those specified on the graphs presented in the preceding chapters. The computer programs may be used to determine the thermal stress history of any package during a thermal shock test provided that the leads are circular. An example illustrating the use of the program is given in Appendix C.

The work herein reported provides a method for estimating

the stresses which are present in the vicinity of a lead-through seal of a microelectronic package when subjected to a thermal shock. The following recommendations are made for further work with the objectives of verifying the validity of certain simplifying assumptions which were made in the development of the mathematical model and extending the work to include other important aspects of the general problem of estimating the conditions which would cause failure of the lead-through seal during thermal shock.

It is suspected that failure of the glass-metal seal will occur when the tensile radial stress at the glass-metal interface reaches a critical value. At the present time little is known about the magnitude of this critical value and how it is influenced by the manufacturing process. It is recommended that experimental studies be carried out to determine the strength of the seal. Subsequently, experiments should be performed to verify the predictions of the present model with regard to seal failure. This could be accomplished by testing a variety of different microelectronic packages at different thermal shock levels.

In order to investigate the validity of the assumptions inherent in the present model it is suggested that a more refined finite element analysis be performed for a typical situation covered by the present theory. It would be especially interesting to know whether the assumptions which have been made with regard to neglecting the axial temperature distribution in the glass lead to serious error. A further important assumption made in the mathematical model was the modeling of the base as a third

outside cylinder, having a certain assumed outer radius. A more realistic evaluation of the stresses could be obtained if a finite element analysis were made to evaluate the thermal stresses in the seal taking into account the real shape of the package including the influence of any neighboring seals. This would provide an evaluation of the accuracy of the 3-cylinder model used in the present study.

On the experimental side, the uncertainties involved in the determination of the effective heat transfer coefficient for the package have been discussed in Chapter IV. A more refined experimental technique incorporating the effects of other package variables such as the package contents should be undertaken in order to provide a more accurate determination of the true effective heat transfer coefficient for test condition A of the MIL-STD-883B. Improved results may be achieved by assuming that the effective heat transfer coefficient is a function of the temperature difference between the fluid and the package.

Investigation should be carried out for other test levels described in MIL-STD-883B to determine the effective heat transfer coefficient for the other fluids during the specified test conditions.

In view of the fact that many microelectronic packages have leads which are not circular, further analysis should be performed to provide means for estimating thermal stresses for the case of rectangular leads or other lead-through geometries.

It was shown in the practical applications of the results that the magnitude of the thermal stresses in the seal depended on the initial residual stresses in the seal caused by the cooling of the package to room temperature after the sealing process is performed at high temperatures. In view of the fact that these residual stresses affect directly the maximum thermal stresses, further investigation is needed to evaluate accurately the initial residual stresses in the glass-to-metal seal.

APPENDIX A

FINITE ELEMENT ANALYSIS FOR EVALUATING THE TRANSIENT TEMPERATURE DISTRIBUTION IN THE GLASS AND RELATED APL PROGRAMS

A.1 Evaluation of the Transient Temperature Distribution in the Glass Using the Finite Element Analysis

A finite element analysis is used to solve the partial differential equation (12) in Chapter III together with the boundary conditions (14) and (15). The mathematical development of the analysis can be found in reference (11).

The finite element model used consisted of five circular elements dividing the glass seal. (See Fig. 28). This model requires that 6 nodal temperatures be evaluated using the finite element method. T_1 and T_6 correspond respectively to the temperatures of the lead and the base. The intermediate temperatures determine the radial temperature distribution through the glass seal. This set of temperatures can be represented by a matrix.

$$\{T\} = \begin{Bmatrix} T_1 \\ T_2 \\ T_3 \\ T_4 \\ T_5 \\ T_6 \end{Bmatrix}$$

The mathematical development of the analysis applied to the partial differential equation (12) leads then to the following system of equations

$$[C]\frac{\partial\{T\}}{\partial\tau} + [K]\{T\} + [F] = 0 \qquad \text{(A1)}$$

where $[C]$ is the total "capacitance" matrix expressed for each element as

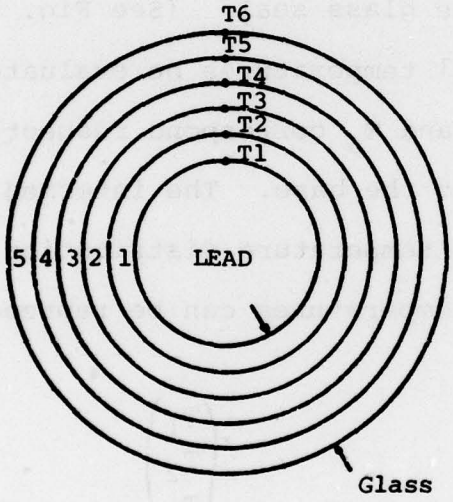

Fig. 28. Model Used for Finite Element Analysis

$$[c] = \frac{2\pi\rho c}{60(r_2-r_1)^2}\begin{bmatrix}(2r_2^5-20r_2^2r_1^3+30r_2r_1^4-12r_1^5) & (3r_2^5-5r_2^4r_1+5r_2r_1^4-3r_1^5)\\ \text{symmetrical} & (12r_2^5-30r_2^4r_1+20r_2^3r_1^2-2r_1^5)\end{bmatrix}$$

r_1 and r_2 being respectively the inner and outer radius of each element. For the inner boundary element, $[c] = \rho_k c_k V_\ell \begin{bmatrix}1 & 0\\ 0 & 0\end{bmatrix}$ is added to [c] above. For the outer boundary element, $[c] = \frac{\rho_k c_k V_b}{N}\begin{bmatrix}0 & 0\\ 0 & 1\end{bmatrix}$ is added to [c] above. [K] is the total "conductivity" matrix and for each element

$$[k] = \frac{2\pi k(r_2^3-r_1^3)}{3(r_2-r_1)^2}\begin{bmatrix}1 & -1\\ -1 & 1\end{bmatrix}$$

For the inner boundary element, $[k] = \bar{h}A_o\begin{bmatrix}1 & 0\\ 0 & 0\end{bmatrix}$ is added to [k] above. For the outer boundary element, $[k] = \frac{\bar{h}A_b}{N}\begin{bmatrix}0 & 0\\ 0 & 1\end{bmatrix}$ is added to [k] above. [F] is the "forcing" matrix and applies to the boundary elements. For the inner boundary

$$[f] = -\bar{h}A_o T_\infty \begin{bmatrix}1\\ o\end{bmatrix}$$

For the outer boundary $[f] = -\frac{\bar{h}A_b}{N} T_\infty \begin{bmatrix}0\\ 1\end{bmatrix}$

Equation (A1) is solved in the time domain using a finite difference method.

The time derivative is represented by:

$$\frac{\partial\{T\}}{\partial\tau} = \frac{1}{\Delta\tau}(\{T\}_1 - \{T\}_o) \qquad (A2)$$

where $\Delta\tau$ is a finite time increment and $\{T\}_1$ and $\{T\}_o$ are the model temperature matrices corresponding to the beginning and end of the time interval $\Delta\tau$. At the mid point of the time interval the temperature matrix can be written as

$$\{T\}^* = \frac{1}{2}(\{T\}_1 + \{T\}_o) \qquad \text{(A3)}$$

Replacing (A2) and (A3) in (A1) and rearranging terms, one obtains,

$$([K] + \frac{2}{\Delta\tau}[C])\{T\}_1 = (\frac{2}{\Delta\tau}[C]-[K])\{T\}_o - 2[F] \qquad \text{(A4)}$$

Equation (A4) is solved to yield the nodal temperature values at time $\tau + \Delta\tau$ (represented by $\{T\}_1$) given the nodal values at time τ (represented by $\{T\}_o$). The initial temperature distribution is used here to start the evaluation process.

The calculations based on this analysis were carried out using the APL programs listed in Sections A.2 and A.3.

A.2 Programs "TEMPDIS" and "FEM" to evaluate the [K],[C] and [F] matrices.

```
      ∇TEMPDIS[□]∇
    ∇ W TEMPDIS DT;N;NE;CM;LOC;ROW;COL;K;C;FE;TIN;MB;M;A;A1;A2;A3;A4;P;P1;P2;TB;TA
[1]   N←6
[2]   NE←5
[3]   RR←R[3],R[3]+((R[2]-R[3])÷NE)×(⍳NE)
[4]   NOD←(NE,2)⍴0
[5]   I←1
[6]  L1:J←I+1
[7]   NOD[I;]←I,J
[8]   →L1×⍳(I←I+1)≤NE
[9]   F←(N,1)⍴0
[10]  CT←KT←(N,N)⍴0
[11]  EL←1
[12]  EC←1,5
[13] L2:FEM DT
[14] L5:LOC←2⍴0
[15]  LOC[⍳2]←NOD[EL;]
[16]  I←0
[17] L3:I←I+1
[18]  ROW←LOC[I]
[19]  J←0
[20] L4:J←J+1
[21]  COL←LOC[J]
[22]  KT[ROW;COL]←KT[ROW;COL]+K[I;J]
[23]  CT[ROW;COL]←CT[ROW;COL]+C[I;J]
[24]  →L4×⍳(J<2)
[25]  →L7×⍳EL∈EC
[26]  →L8
[27] L7:F[ROW;1]←F[ROW;1]+FS[I;1]
[28] L8:→L3×⍳(I<2)
[29]  EL←EL+1
[30]  →L2×⍳EL≤NE
[31]  K←KT
[32]  C←CT
    ∇
```

```
      ∇FEM[□]∇
    ∇ FEM DT;R;KV;KS;CV;CS
[1]   R←RR[NOD[EL;]]
[2]   KV←((○2)×KR×((R[2]*3)-(R[1]*3))÷3×(R[2]-R[1])*2)×(2 2 ⍴ 1 ¯1 ¯1 1)
[3]   KS← 2 2 ⍴0
[4]   K←KV+KS
[5]   C←(2×R[2]*5)+(30×R[2]×R[1]*4)-(((20×R[2]*2)×R[1]*3)+12×R[1]*5)
[6]   C←C,C1,C1←(3×R[2]*5)+(5×R[2]×R[1]*4)-(5×R[1]×R[2]*4)+3×R[1]*5
[7]   C←C,(12×R[2]*5)+(20×(R[2]*3)×R[1]*2)-(30×R[1]×R[2]*4)+2×R[1]*5
[8]   CV←((○2)×DK[2]×SK[2]÷60×(R[2]-R[1])*2)×(2 2 ⍴C)
[9]   C←CV+CS← 2 2 ⍴0
[10]  →KL×⍳(EL∈EC)∧(EL=EC[1])
[11]  →KM×⍳(EL∈EC)∧(EL=EC[2])
[12]  →KN
[13] KL:KS←(K1←(HE÷3600×144)×AO)×(2 2 ⍴1,(3⍴0))
[14]  K←KV+KS
[15]  CS←(CS1←DK[3]×SK[3]×VL)×(2 2 ⍴1,(3⍴0))
[16]  C←CV+CS
[17]  FS←(F1←K1×TFINAL)×(2 1 ⍴1,0)
[18]  →KN
[19] KM:KS←(K1×AB÷AO×N)×(2 2 ⍴(3⍴0),1)
[20]  K←KV+KS
[21]  CS←(DK[1]×SK[1]×VB÷N)×(2 2 ⍴(3⍴0),1)
[22]  C←CV+CS
[23]  FS←(F1×AB÷AO×N)×(2 1 ⍴0,1)
[24] KN:' '
    ∇
```

A.3 Program "GTS" to compute the transient temperature distribution in the glass seal.

```
      ∇GTS[□]∇
    ∇ T←GTS DT
[1]   P←((2÷DT)×CT)-KT
[2]   A←((2÷DT)×CT)+KT
[3]   TI←TI+DT
[4]   P1←(P+.×TA)+2×P
[5]   TA←TB←P1⌹A
[6]   T←TB[(\6);1]
[7]   TN←(HE÷3600×144)×AO×TI÷SK[1]×DK[1]×VB
    ∇
```

APPENDIX B

APL PROGRAMS COMPUTING THE TRANSIENT THERMAL STRESSES

B.1 Main program "STR" to compute the transient thermal stresses at a given radius.

```
      ∇STR[0]∇
      ∇ STR L
[1]   'ENTER THE COEFFICIENTS OF THERMAL  EXPANSION AL (IN/IN/•F)'
[2]   AL←0
[3]   'ENTER THE POISSON RATIOS NU'
[4]   NU←0
[5]   'ENTER THE MODULI OF ELASTICITY E (PSI)'
[6]   E←0
[7]   'ENTER THE RADII R (IN)'
[8]   R←0
[9]   'ENTER THE DENSITIES DK (LB/CU.IN)'
[10]  DK←0
[11]  'ENTER THE SPECIFIC HEATS SK (BTU/LB-•F)'
[12]  SK←0
[13]  'ENTER THE THERMAL CONDUCTIVITY OF THE SEALING MATERIAL KR (BTU/SEC-IN-•F)'
[14]  KR←0
[15]  'ENTER THE OUTSIDE SURFACE AREA OF ONE LEAD OUTSIDE BASE AO (SQ.IN)'
[16]  AO←0
[17]  'ENTER TOTAL OUTSIDE SURFACE AREA OF BASE AB(SQ.IN)'
[18]  AB←0
[19]  'ENTER THE VOLUME OF ONE LEAD VL (CU.IN)'
[20]  VL←0
[21]  'ENTER THE TOTAL VOLUME OF THE BASE VB (CU.IN)'
[22]  VB←0
[23]  'ENTER THE TOTAL NUMBER OF LEADS N'
[24]  N←0
[25]  'ENTER THE INITIAL TEMPERATURE TINITIAL (•F)'
[26]  TA←TB← 6 1 ρ(6ρTINITIAL←0)
[27]  'ENTER THE FINAL TEMPERATURE TFINAL (•F)'
[28]  TFINAL←0
[29]  'ENTER THE EFFECTIVE HEAT TRANSFER COEFFICIENT HE (BTU/HR-SQ.FT-•F)'
[30]  HE←0
[31]  'ENTER THE RADIUS WHERE YOU WANT THE STRESSES RS (IN)'
[32]  RS←0
[33]  'ENTER THE TIME INCREMENT DT (SEC)'
[34]  DT←0
```

```
[35]  'ENTER THE TOTAL NUMBER OF TIME INCREMENTS'
[36]  W←□
[37]  LAM←DG×SG
[38]  TI←0
[39]  F1←F2← 6 1 ⍴0
[40]  ZN←ZS←(W,6)⍴0
[41]  ZT←(W,7)⍴0
[42]  IS←+/RS<⍵R
[43]  JS←1
[44]  W TEMPDIS DT
[45]  TDIF←TFINAL-TINITIAL
[46]  D←1
[47] KK:T←GTS DT
[48]  ZT[JS;]←TI,T
[49]  TOT←(R[3],R[2]) TRAP 5
[50]  STRESS L
[51]  ZS[JS;]←TI,TN,SR[IS],SRN[IS],ST[IS],STN[IS]
[52]  JS←JS+1
[53]  D←D+1
[54]  →KKX\D≤W
[55]  '      TIME          N-D TIME      RAD. STRESS    N-D RAD. STR.    TANG. STRESS    N-D TANG. STR.
[56]  ZS
```

B.2 Programs "STRESS" and "Z" to compute the thermal stresses at each increment of time.

```
      ∇STRESS[□]∇
    ∇ S←STRESS L;Q;G;M;N;P;F1;F2;K;C;KN;ED;E1;C1;A;Y;C2
[1]   Q←1÷NU
[2]   K←G←M←N←P←E1←A←Y←SR←ST←SRN←STN←PA←L⍴0
[3]   J←1
[4]  CL:K[J]←E[J]×Q[J]×AL[J]÷Q[J]-1
[5]   G[J]←E[J]×Q[J]÷2×Q[J]+1
[6]   J←J+1
[7]   →CL×⍳J≤L
[8]   J←2
[9]  CK:M[J]←4×G[J-1]×(Q[J]-1)÷Q[J]×(G[J]-G[J-1])
[10]  N[J]←⁻4×G[J]×(Q[J-1]-1)÷Q[J-1]×(G[J]-G[J-1])
[11]  P[J]←1×G[J]×G[J-1]×(Q[J-1]-Q[J])÷Q[J]×Q[J-1]×(G[J]-G[J-1])
[12]  J←J+1
[13]  →CK×⍳J≤L
[14]  T←(T[6],TOT,T[1])-TINITIAL
[15]  KN←(K[1]×T[1]×R1←(R[1]*2)-(R[2]*2))+(K[2]×T[2]×R2←(R[2]*2)-(R[3]*2))
[16]  KN←KN+K[3]×T[3]×R[3]*2
[17]  ED←(E[1]×R1)+(E[2]×R2)+E[3]×R[3]*2
[18]  J←1
[19] CM:A[J]←E1[J]←((Z R[J])[J])÷R[J]*2
[20]  J←J+1
[21]  →CM×⍳J≤L
[22]  C1←2,(1÷R[1]*2),(3⍴0),(N[2]+X1←8×R1×P[2]÷Q[1]×ED),0
[23]  C1←C1,(2+M[2]+X2←8×R2×P[2]÷Q[2]×ED),(1÷R[2]*2),(X3←8×(R[3]*2)×P[2]÷Q[3]×ED)
[24]  C1←C1,(2+M[2]+X1),(1÷R[2]*2),(M[2]+X2),0,X3
[25]  C1←C1,(X1←X1×P[3]÷P[2]),0,(N[3]+X2←X2×P[3]÷P[2]),0,(2+M[3]+X3←X3×P[3]÷P[2])
[26]  C1←C1,X1,0,(2+N[3]+X2),(1÷R[3]*2),(M[3]+X3)
[27]  C1← 5 5 ⍴C1
[28]  C2←A[1],X1,(X1←A[2]+2×KN×P[2]÷ED),X2,(X2←A[3]+2×KN×P[3]÷ED)
[29]  C2← 5 1 ⍴C2
[30]  C←C2⌹C1
[31]  F1←C[1;1],C[3;1],C[5;1]
[32]  F2←C[2;1],C[4;1],0
[33]  J←1
[34] CN:SR[J]←(2×F1[J])+((F2[J])-((Z RS)[J]))÷RS*2
[35]  SRN[J]←SR[J]÷PA[J]×E[2]×AL[2]×TDIF
[36]  ST[J]←(2×F1[J])-((((F2[J])-((Z RS)[J]))÷RS*2)+K[J]×T[J])
[37]  STN[J]←ST[J]÷PA[J]
[38]  J←J+1
[39]  →CN×⍳J≤L
    ∇


      ∇Z[□]∇
    ∇ YY←Z RS
[1]   Y←3⍴0
[2]   Y[1]←((K[3]×T[3]×R[3]*2)+(K[2]×T[2]×(R[2]*2)-(R[3]*2))+(K[1]×T[1]×(RS*2)-(R[2]*2)))×0.5
[3]   Y[2]←((K[3]×T[3]×R[3]*2)+(K[2]×T[2]×(RS*2)-(R[3]*2)))×0.5
[4]   Y[3]←((K[3]×T[3]×RS*2))×0.5
[5]   YY←Y
    ∇
```

APPENDIX C

APL FUNCTION EXPLAINING HOW THERMAL STRESSES ARE COMPUTED USING THE APL PROGRAMS PRESENTED IN APPENDICES A AND B

C.1 Function that explains the use of STR and illustrates the use of the program with an example.

```
      )COPY 04330000 CLAUDE

SAVED  21.48.50 10/25/78

      STRHOW
THE PROGRAM STR COMPUTES THE TRANSIENT RADIAL AND TANGENTIAL THERMAL STRESSES THAT DEVELOP IN AND AROUND
ONE SEAL OF A MICROELECTRONIC PACKAGE AS THE PACKAGE IS SUBMITTED TO A THERMAL SHOCK TEST,ONE TYPICAL LEAD,
THE SEAL SURROUNDING THE LEAD,AND PART OF THE BASE (OR WALL) TO WHICH THE LEAD IS SEALED ARE MODELED AS 3
CONCENTRIC CYLINDERS,THE PROGRAM EVALUATES THE STRESSES AT A GIVEN RADIAL DISTANCE FROM THE CENTER,FOR EACH
TIME INCREMENT AND IT IS DESIGNED ONLY FOR PACKAGES WITH CIRCULAR LEADS.

ENTER THE VALUES OF THE VARIABLES NEEDED FOR THE COMPUTATION DURING THE EXECUTION OF THE PROGRAM.

AFTER TYPING STR,LEAVE A BLANK SPACE AND TYPE 3.THIS IS NECESSARY BECAUSE 3 CONCENTRIC CYLINDERS ARE ANALYZED.

ENTER THE COEFFICIENTS OF THERMAL EXPANSION,THE POISSON RATIOS,THE MODULI OF ELASTICITY,THE RADII,THE DENSITIES,
AND THE SPECIFIC HEATS CORRESPONDING TO THE 3 CYLINDERS AS 6 DIFFERENT VECTORS,IN EACH VECTOR,THE FIRST TERM
SHOULD BE THE VALUE CORRESPONDING TO THE OUTERMOST CYLINDER,THE SECOND TERM,THE VALUE CORRESPONDING TO THE MIDDLE
CYLINDER AND THE THIRD TERM,THE VALUE CORRESPONDING TO THE INNERMOST CYLINDER.

IF THE RADIUS WHERE THE STRESSES ARE TO BE DETERMINED IS ONE OF THE LEAD-GLASS OR GLASS-BASE INTERFACES
DO NOT ENTER THE EXACT VALUE OF THE RADIUS CORRESPONDING TO ONE OF THESE TWO INTERFACES,DEPENDING ON WHETHER
YOU WANT THE STRESSES IN THE SEALING MATERIAL OR THE METAL,ENTER A SLIGHTLY LARGER OR A SLIGHTLY SMALLER
RADIUS.(E.G.,IF THE LEAD -TO-GLASS INTERFACE IS AT .009IN. FROM THE CENTER,FOR THE STRESSES IN THE
GLASS ENTER .00901 IN.)

THE RESULTING TRANSIENT THERMAL STRESSES CORRESPONDING TO EACH INCREMENT OF TIME ARE PRESENTED IN
DIMENSIONAL AND NON-DIMENSIONAL FORM.

AN EXAMPLE ILLUSTRATING THE USE OF THE PROGRAM IS GIVEN BELOW.

EXAMPLE:A MICROELECTRONIC PACKAGE CONSISTING OF KOVAR LEADS SEALED TO A KOVAR BASE WITH CORNING 7052
GLASS IS SUBJECTED TO THE THERMAL SHOCK TEST CONDITION B OF MIL-STD-883B,THE TEMPERATURE EXTREMES
FOR THIS TEST CONDITION ARE -67°F AND 257°F.THE TRANSIENT THERMAL STRESSES AT THE LEAD-GLASS
INTERFACE WILL BE DETERMINED USING THE PROGRAM STR.
```

```
   STR 3
ENTER THE COEFFICIENTS OF THERMAL  EXPANSION AL (IN/IN/oF)
0:
      3.25E-6 2.56E-6 3.25E-6
ENTER THE POISSON RATIOS NU
0:
      0.3 0.22 0.3
ENTER THE MODULI OF ELASTICITY E (PSI)
0:
      20E6 8.2E6 20E6
ENTER THE RADII R (IN)
0:
      .06 .035 .01
ENTER THE DENSITIES DK (LB/CU.IN)
0:
      .302 .082 .302
ENTER THE SPECIFIC HEATS SK (BTU/LB-oF)
0:
      .105 .23 .105
ENTER THE THERMAL CONDUCTIVITY OF THE SEALING MATERIAL KR (BTU/SEC-IN-oF)
0:
      .0000136629
ENTER THE OUTSIDE SURFACE AREA OF ONE LEAD OUTSIDE BASE AO (SQ.IN)
0:
      .0115925
ENTER TOTAL OUTSIDE SURFACE AREA OF BASE AB(SQ.IN)
0:
      4.2874
ENTER THE VOLUME OF ONE LEAD VL (CU.IN)
0:
      .0000750684
ENTER THE TOTAL VOLUME OF THE BASE VB (CU.IN)
0:
      .15434605
ENTER THE TOTAL NUMBER OF LEADS N
0:
      48
ENTER THE INITIAL TEMPERATURE TINITIAL (oF)
0:
      -67
ENTER THE FINAL TEMPERATURE TFINAL (oF)
0:
      257
ENTER THE EFFECTIVE HEAT TRANSFER COEFFICIENT HE (BTU/HR-SQ.FT-oF)
0:
      210
ENTER THE RADIUS WHERE YOU WANT THE STRESSES RS (IN)
0:
      .01001
ENTER THE TIME INCREMENT DT (SEC)
0:
      .4
ENTER THE TOTAL NUMBER OF TIME INCREMENTS
0:
      20
```

TIME (SEC)	N-D TIME	RAD. STRESS (PSI)	N-D RAD.STR.	TANG.STRESS (PSI)	N-D TANG. STR.
4.000000000E-1	3.837952860E-4	-3.078505738E3	-4.526277115E-1	2.989896814E3	4.395996850E-1
8.000000000E-1	7.675905720E-4	-3.722173502E3	-5.472651401E-1	3.304814247E3	4.861955417E-1
1.200000000E0	1.151385859E-3	-3.589503405E3	-5.277588707E-1	3.582253028E3	5.266928595E-1
1.600000000E0	1.535181144E-3	-3.213389774E3	-4.724594928E-1	3.466356217E3	5.096527390E-1
2.000000000E0	1.918976430E-3	-2.801620853E3	-4.119177769E-1	3.399715067E3	4.998545988E-1
2.400000000E0	2.302771716E-3	-2.409803199E3	-3.543094605E-1	3.276975727E3	4.818084324E-1
2.800000000E0	2.686567002E-3	-2.060271380E3	-3.029183633E-1	3.188348659E3	4.687777382E-1
3.200000000E0	3.070362288E-3	-1.751812696E3	-2.575661828E-1	3.092804648E3	4.547300571E-1
3.600000000E0	3.454157574E-3	-1.483811476E3	-2.181623976E-1	3.020964805E3	4.441675613E-1
4.000000000E0	3.837952860E-3	-1.250083030E3	-1.837976828E-1	2.948569542E3	4.335239031E-1
4.400000000E0	4.221748146E-3	-1.047845926E3	-1.540630890E-1	2.894158057E3	4.255233706E-1
4.800000000E0	4.605543432E-3	-8.718387265E2	-1.281950356E-1	2.839306904E3	4.174586801E-1
5.200000000E0	4.989338718E-3	-7.196387540E2	-1.058073202E-1	2.798673654E3	4.114844535E-1
5.600000000E0	5.373134004E-3	-5.872327637E2	-8.633988193E-2	2.757037099E3	4.053626983E-1
6.000000000E0	5.756929290E-3	-4.727444325E2	-6.950684807E-2	2.726825546E3	4.009207426E-1
6.400000000E0	6.140724576E-3	-3.731536009E2	-5.486416943E-2	2.695166251E3	3.962659277E-1
6.800000000E0	6.524519862E-3	-2.870415496E2	-4.220325403E-2	2.672762911E3	3.929720010E-1
7.200000000E0	6.908315148E-3	-2.121333923E2	-3.118962901E-2	2.648649913E3	3.894267059E-1
7.600000000E0	7.292110434E-3	-1.473669895E2	-2.166712973E-2	2.632080020E3	3.869904615E-1
8.000000000E0	7.675905720E-3	-9.102289599E1	-1.338294894E-2	2.613681829E3	3.842854052E-1

REFERENCES

1. R.W. Thomas, "IC Packages and Hermetically Sealed-In Contaminants," pp. 4-19, NBS Special Publication 400-9, December 1974.

2. G.M. Johnson and L.K. Conaway, "Reliability Evaluation of Hermetic Dual in Line and Flat Microcircuit Packages," McDonnell-Douglas Unclassified Report, Contract NAS8-31446, Oct. 1976-Dec. 1977.

3. H. Poritsky, "Analysis of Thermal Stresses in Sealed Cylinders and the Effect of Viscous Flow During Anneal," Physics 5, 406-411 (1934).

4. B.E. Gatewood, "Thermal Stresses in Long Cylindrical Bodies," Phil. Mag. Ser. 7, 32, 282-301 (1941).

5. M.P. Borom and R.A. Giddings, "Considerations in Designing Glass/Metal Compression Seals to Withstand Thermal Excursions," American Ceramic Society Bulletin, Vol. 55, No. 12, December 1976.

6. MIL-STD-883B, Method 1011, "Test Methods and Procedures for Microelectronics," August 31, 1977.

7. P.J. Schneider, Temperature Response Charts, John Wiley and Sons, Inc. 1963.

8. B.E. Gatewood, "Note on the Thermal Stresses in Long Circular Cylinder of m+1 Concentric Materials," Quarterly App. Math, 6, No. 1, 84-86, (1948).

9. C. Libove, "Rectangular Flat-Pack Lids Under External Pressure: Improved Formulas for Screening and Design," Final Technical Report, RADC-TR-76-291, September 1976, A032490.

10. F. Kreith, Principles of Heat Transfer, Intext Press, Inc., New York, 1973.

11. L.J. Segerlind, Applied Finite Element Analysis, John Wiley and Sons, Inc., New York, 1976.

12. S.P. Timoshenko and J.N. Goodier, Theory of Elasticity, McGraw-Hill, New York, 1970.

MISSION
of
Rome Air Development Center

RADC plans and executes research, development, test and selected acquisition programs in support of Command, Control Communications and Intelligence (C^3I) activities. Technical and engineering support within areas of technical competence is provided to ESD Program Offices (POs) and other ESD elements. The principal technical mission areas are communications, electromagnetic guidance and control, surveillance of ground and aerospace objects, intelligence data collection and handling, information system technology, ionospheric propagation, solid state sciences, microwave physics and electronic reliability, maintainability and compatibility.